Volume 6 JANUARY, 1935 Number 1

PHYSICS

A Journal of General and Applied Physics

Instantaneous Speeds in Air of Explosion Reports at Short Distances from the Source

F. L. PARTLO AND JERRY H. SERVICE, *Department of Mathematics and Physics, Michigan College of Mining and Technology*

(Received May 28, 1934)

In the first series of measurements the source was one No. 6 blasting cap, while in the second series one pound of 50 percent nitroglycerine stick dynamite was used as source. A telephone carbon button microphone was the receiver and was held fixed in location while shots were fired successively at 5, 8, 12.5, 25, 35, 50, 100 and 600 meter distances. A two-element string oscillograph was used for timing, one element recording the instant of firing, the other element recording the arrival of the wave at the microphone. The work was done at time of no perceptible wind; air temperatures were measured carefully; no humidity measurements were made. Travel times could be read reliably to 10^{-4} second and distance measurements were at least correspondingly good. Instantaneous speeds were obtained by plotting time computed minus time observed against distance and measuring slopes of the resulting curve. Since this work was incidental to seismic prospecting, the observations were not quite as numerous as those of von Angerer and Ladenburg. However, the results are similar as regards *abnormally high speeds near the source.* Also, the use of instantaneous speeds appears to show *abnormally low speeds a little farther from the source,* perhaps masked in the work of von Angerer and Ladenburg due to the use by them of average speeds instead of instantaneous speeds.

I. INTRODUCTION

ONE of us, from experience with seismic prospecting, and the other,[1] from experience with echo sounding and sound ranging in water, had long held the opinion that sound waves of finite amplitude are propagated with abnormally high speeds. Since for our experimental work in refraction seismic prospecting we have at hand adequate means of measuring travel times, it was decided to carry out two series of measurements of travel times in air over short distances, one series with one blasting cap as source, the other series with one pound of 50 percent nitroglycerine stick dynamite as source. The results of the measurements, which were carried out in October, 1933, are as stated in this paper. Not much search of the literature for accounts of similar work was made prior to the carrying out of the observations and the computation of the results. Nor has an exhaustive search yet been made. However, the work of von Angerer and Ladenburg[2] is the only published work that has come to our knowledge that was carried out under conditions comparable to those involved in this work of ours. Their observations at short distances were a little more numerous than ours. Our time measurements, because of a larger time scale on the oscillograph records, may have been a little more accurate than theirs. They computed average speeds over various sections of the course; we computed instantaneous speeds *at* various distances from the source. Their results showed abnormally high speeds near the source, decreasing asymptotically to the normal value (for faint sounds) within a comparatively short distance. Our results are consistent with theirs, except that we found abnormally high speeds near the source, *abnormally low speeds a little farther from the source,* then normal speed for greater distances. We cannot but wonder whether von Angerer and Ladenburg would not find these abnormally low speeds also, if they would compute instantaneous, rather than average, speeds from their data.

[1] Jerry H. Service, *The Transmission of Sound through Sea Water,* J. Frank. Inst. **206**, 802 (1928).

[2] E. von Angerer and R. Ladenburg, *Experimentelle Beitraege zur Ausbreitung des Schalles in der freien Atmosphaere,* Ann. d. Physik **66**, 293 (1921).

TABLE I. *Data using one No. 6 blasting cap.*

No.	x (meters)	t°C	v_0 (m/sec.)	x/v_0	T	ΔT	Est.
1	5.005	11.6	337.9	0.0148	0.0079	−0.0069	±2
2	8.007	11.6	337.9	0.0237	0.0165	−0.0072	4
3	12.506	11.6	337.9	0.0370	0.0242	−0.0128	2
4	25.000	11.6	337.9	0.0740	0.0632	−0.0108	2
9	35.305	9.9	336.8	0.1048	0.0928	−0.0120	4
10	50.003	10.8	337.4	0.1482	0.1402	−0.0080	3
14	100.00	9.5	336.6	0.2971	0.2914	−0.0057	2
16	158.44	8.0	335.6	0.4721	0.4705	−0.0016	6
17	600.03	6.0	334.4	1.7943	1.7860	−0.0083	10

TABLE II. *Data using 1 lb. 50 percent nitroglycerine.*

No.	x (meters)	t°C	v_0 (m/sec.)	x/v_0	T	ΔT	Est.
8	5.005	11.1	337.6	0.0148	0.0078	−0.0070	±3
7	8.007	11.0	337.5	0.0237	0.0146	−0.0091	2
6	12.506	11.3	337.7	0.0370	0.0257	−0.0113	2
5	25.000	12.1	338.2	0.0739	0.0596	−0.0143	2
12	35.305	10.3	337.1	0.1047	0.0887	−0.0160	2
11	50.003	10.4	337.1	0.1483	0.1307	−0.0176	3
13	66.187	8.9	336.2	0.1968	0.1838	−0.0130	2
15	100.00	10.0	336.9	0.2968	0.2836	−0.0132	3
18	600.03	5.8	334.3	1.7949	1.7800	−0.0149	6

II. EXPERIMENTAL PROCEDURE

An ordinary telephone transmitter carbon button microphone was used as receiver. It was supported by means of rubber bands at the center of a hoop about 18 inches in diameter so that it faced the line of shot points and was about four feet above the ground. The microphone was connected through a 3-stage vacuum tube amplifier to one element of a General Radio string oscillograph.

Stakes about four feet high were driven into the ground along a straight line through the microphone, at distances approximately 5, 8, 12.5, 25, 35, 50, 100 and 600 meters from the microphone. The distances were then taped with a 100-foot steel tape. The charges were suspended loosely from the tops of the stakes.

The microphone was kept in a fixed location and the charges were fired successively at the various distances. In the first series the charge was a No. 6 electric blasting cap fired at each distance; in the second series the charge was two sticks (approximately one pound total) of 50 percent nitroglycerine powder fired at each distance by means of an electric blasting cap. Instant of firing was recorded on the second element of the string oscillograph by wrapping a wire around the blasting cap, connecting this wire in series with a dry cell and the primary of a transformer, and connecting the secondary of the transformer to the galvanometer string through a 3-stage amplifier alike in all respects to the one used for the microphone. The charges were fired at times when no motion of the air sufficient to move an anemometer was to be noted. Air temperatures near the ground were measured at each shot by means of standardized thermometers. No humidity measurements were made. No barometer readings were made, but barograph records are available at the college for the time of the shots.

Fig. 1 shows some of the records. Travel times were scaled off independently by the two of us and averaged, with the results given in Tables I and II. Our agreement with each other and with

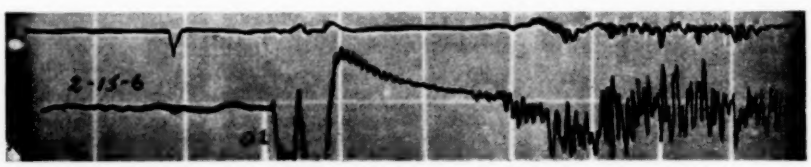

(a)

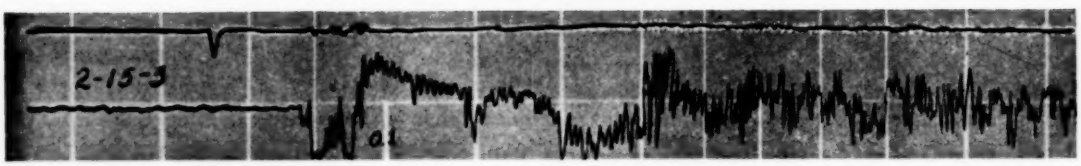

(b)

FIG. 1. (a) Record No. 6. 1 lb. dynamite, 125 meters. Note arrival of echo at 0.151. (b) Record No. 3. 1 blasting cap, 125 meters.

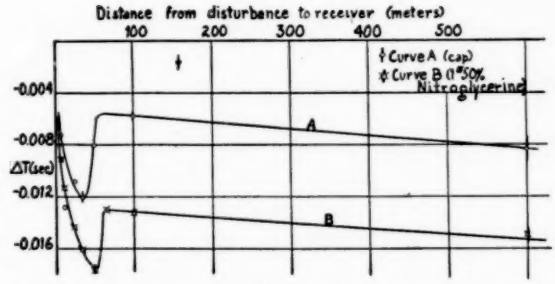

FIG. 2. Experimental relation between ΔT (travel time observed minus travel time computed) and x (distance from disturbance to receiver) Curve A for No. 6 blasting cap and Curve B for one pound 50 percent nitroglycerine powder.

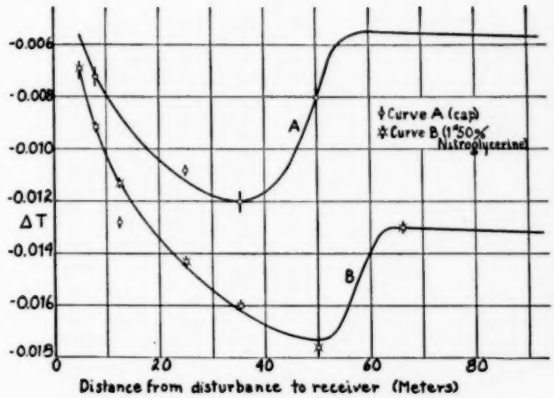

FIG. 3. A portion of Fig. 2 drawn to larger scale.

ourselves at different times indicates that the travel times are probably generally correct to 10^{-4} second. Taking into consideration slight uncertainties on some of the records as to just where on the record the reception of the wave is represented, however, the last columns of Tables I and II give rather pessimistic estimates of the uncertainties of the travel times. The long time marks on the records are one-fiftieth second apart, very nearly, and the short time marks are at one-tenth second intervals, very nearly. The timing apparatus is controlled by a tuning fork and was standardized at several fork temperatures against a Bond break circuit chronometer, which was checked daily (during the standardization) against radio time signals from Arlington. The temperature of the tuning fork of the time marking apparatus was recorded at each shot, as measured by a calibrated thermometer.

Referring to Tables I and II, the first column gives the order of firing; column two, x in meters, records the distance from the charge to the microphone; t_0 is the air temperature between charge and microphone; v_0 is the accepted[3] normal speed of sound in air at temperature t_0 given by the equation $v_0=330.6+0.63t_0$; x/v_0 is self-explanatory, being the normal travel time for distance x; T is the observed travel time in seconds. ΔT is T minus x/v_0, while the last column of each table gives the uncertainty in the fourth decimal place of T and ΔT as already explained.

[3] T. Vautier, *Acoustique—Sur la propogation d'ondes aériennes produites par des étincelles ou des amorces*, Comptes rendus **181**, 1055 (1925).

In Figs. 2 and 3 are shown ΔT plotted as ordinate against x as abscissa, Fig. 3 being merely a large scale reproduction of the part of Fig. 2 that involves the shorter distances and the abnormal speeds.

III. COMPUTATION OF INSTANTANEOUS SPEEDS

Defining x, T and v_0 as above gives,

$$T=x/v_0+\Delta T. \tag{1}$$

Now the instantaneous speed, v, is given by $v=dx/dT$, and by differentiating (1) we have

$$dT/dx=1/v_0+d(\Delta T)/dx, \tag{2}$$

$$\text{whence}\quad v=\frac{1}{1/v_0+\text{slope of }\Delta T=f(x)\text{ curve}}. \tag{3}$$

Three points, at 5, 12.5 and 158 meters, on the A curves of Figs. 2 and 3 were disregarded in drawing the curves, because the authors could not draw smooth curves through these points. No points were disregarded on curves B.

Slopes of the $\Delta T=f(x)$ curves in Fig. 3 were measured by the two of us independently and averaged, with results as recorded in the second columns of Tables III and IV. From these slopes $1/v$ and v were computed with the results given in the third and fourth columns of Tables III and IV and shown graphically in Fig. 4. The values of v_0 given below Tables III and IV are the accepted values for the average air temperatures of first and second series of shots, respectively. In other words, the average of the air temperatures in Table I is 10.1, and likewise for Table II.

TABLE III. *Computed data (blasting caps).*

x (meters)	Slope of $\Delta T = f(x)$ curve	$1/v$	v (m/sec.)
5	-0.658×10^{-3}	2.309×10^{-3}	433.1
7.5	-0.436×10^{-3}	2.531×10^{-3}	395.1
10	-0.337×10^{-3}	2.630×10^{-3}	380.2
15	-0.245×10^{-3}	2.722×10^{-3}	367.4
20	-0.176×10^{-3}	2.791×10^{-3}	358.3
25	-0.144×10^{-3}	2.823×10^{-3}	354.2
30	-0.091×10^{-3}	2.876×10^{-3}	347.7
35	$+0.005\times10^{-3}$	2.972×10^{-3}	336.5
40	$+0.146\times10^{-3}$	3.113×10^{-3}	321.2
50	$+0.52\times10^{-3}$	3.49×10^{-3}	287.
58	-0.005×10^{-3}	2.962×10^{-3}	*337.6

$t = 10°.1C.$ $v_0 = 337.0$ and $1/v_0 = 0.002967$
* 337.6 m/sec. reduced to 0°C = 331.2 m/sec.

TABLE IV. *Computed data (1 lb. 50 percent nitroglycerine).*

x (meters)	Slope of $\Delta T = f(x)$ curve	$1/v$	v (m/sec.)
5	-0.79×10^{-3}	2.18×10^{-3}	459.
7.5	-0.62×10^{-3}	2.35×10^{-3}	426.
10	-0.469×10^{-3}	2.498×10^{-3}	400.3
12.5	-0.383×10^{-3}	2.584×10^{-3}	387.0
15	-0.318×10^{-3}	2.649×10^{-3}	377.5
20	-0.230×10^{-3}	2.737×10^{-3}	365.4
25	-0.193×10^{-3}	2.774×10^{-3}	360.5
30	-0.167×10^{-3}	2.800×10^{-3}	357.1
40	-0.100×10^{-3}	2.867×10^{-3}	348.8
45	-0.064×10^{-3}	2.903×10^{-3}	344.5
50	-0.012×10^{-3}	2.955×10^{-3}	338.4
50.8	0.000×10^{-3}	2.967×10^{-3}	337.0
58	$+0.515\times10^{-3}$	3.482×10^{-3}	287.2
65	-0.004×10^{-3}	2.960×10^{-3}	*337.5

$t = 10°.1C.$ $v_0 = 337.0.$ $1/v_0 = 0.002967$
* 337.5 m/sec. reduced to 0°C = 331.1 m/sec.

Fig. 4 summarizes the results of the experiments. It will be seen that with a No. 6 blasting cap as source the abnormally high speed of 433. m/sec. was found at 5 meters from the source; the speed decreased more or less regularly to a normal value at a distance of 35 meters from the source. *From 35 meters to 58 meters the speed was abnormally low.* At distances greater than 58 meters the speed was about normal.

With the heavier charge (two sticks of dynamite) a higher speed (459 m/sec.) was measured at 5 meters from the source, a somewhat greater distance (50.8 meters) was required for decrease to normal speed, the same minimum abnormally low speed (287 m/sec.) was noted as with the blasting caps, but at 58 meters instead of 50 meters. Normal speed was reached finally with the heavier charge at 65 meters instead of at 58 meters as with the caps.

The authors do not attempt to explain either the abnormally high speeds or the abnormally low speeds found as the results of these experiments. Considering the probable accuracy of the time, distance and slope measurements, and the regularity of the results, it does not seem likely that the results are merely accidental. Possibly the high speeds near the source are *sound speed plus explosion gas speed*, and possibly the low speeds a little farther out are *sound speed minus explosive gas recoil speed.*

It should be stated again that confusion of the air wave with a wave through the earth was guarded against by suspending the charges in the air by light string and by suspending the microphone in the air on rather light rubber bands. Also, those who have done seismic work over comparatively short distances will realize that the arrival of the air wave records itself on the oscillogram in a rather characteristic manner, not at all likely to be confused with the record made by an earth wave that must pass through a foot of light string and a foot or so of light rubber band. If anyone interested should wish to study the oscillograms first-hand they are available for that purpose.

The authors regret that they were not able to carry out more numerous observations before

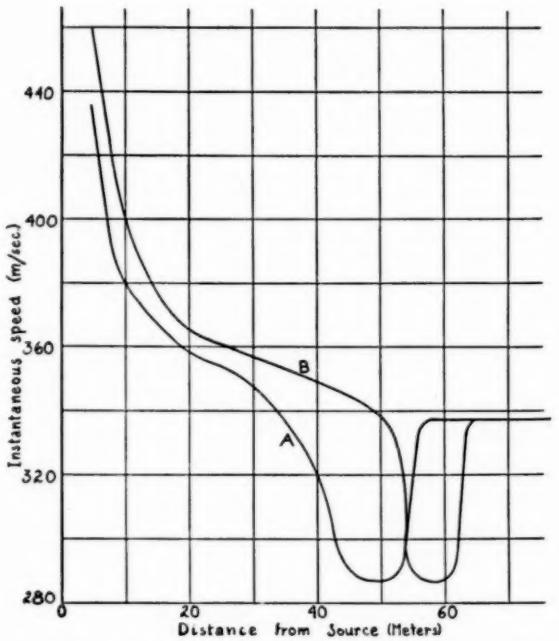

FIG. 4. Instantaneous speed of sound in air relative to the ground with blasting cap (Curve *A*) and one pound 50 percent nitroglycerine powder (Curve *B*) as sources of disturbance.

publication. Since their major research duty is seismic prospecting, it did not seem feasible to spend more field time upon the subject. The work is published in the hope that it may stimulate further work along the same line on the part of other experimenters. It should be stated that previous to the work for which data are here given the authors carried out other similar measurements. The work was not included in this report because it was of a somewhat lower order of accuracy. The absolute values of speed agreed only roughly with those here published; however, similar effects with increasing distances from the source, abnormally high speeds, then speeds somewhat below normal, then normal speed, were found as in the case of the work here reported.

It is interesting to note that extrapolating back to zero distance, Fig. 4, gives speeds at the source of 516 and 544 meters per sec. for cap and dynamite respectively. If the curves of Figs. 2 and 3 were to continue back smoothly from 5 to zero meters, as they must necessarily do in order to arrive at the origin, Fig. 2, the extrapolation is evidently legitimate and the instantaneous speed of the sound relative to the earth would not be less than the above figures. As a matter of fact, the average speeds for 5.005 meters are 633.5 and 641.7 meters per sec. for cap and dynamite respectively, and at 5.005 meters the instantaneous speeds are 433.1 and 459 meters per sec. making the necessary initial speed at least 834 and 825 meters per sec., respectively.

The authors hope to be able to carry out similar measurements in water in the near future.

Shot Effect and Thermal Agitation in an Electron Current Limited by Space Charge

G. L. PEARSON, *Bell Telephone Laboratories, New York*

(Received September 28, 1934)

Experimental evidence is presented which shows that shot effect is decreased by space charge and that the internal impedance of a vacuum tube is subject to thermal agitation.

INTRODUCTION

THE space current in a thermionic vacuum tube is not a steady flow of electricity but is subject to minute irregular fluctuations. The two most fundamental causes for these fluctuations are the random distribution of instants of emission of the individual electrons and the distribution of these electrons in velocity. The random emission produces shot noise which may be reduced by the space charge surrounding the cathode, while the velocity distribution produces thermal noise and is dependent upon the temperature of the cathode.

Although plausible theories of these effects have been given they have never been checked by accurate experiments because of the difficulties involved. By using two electrode tubes capable of producing a large space charge such measurements have now been made and are reported in this paper.

SHOT EFFECT

The theory of the shot effect in the absence of space charge has been studied quite completely both theoretically and experimentally and more recently Llewellyn[1] has extended the theory to cases where partial temperature saturation exists. The general equation developed by him is as follows:

$$\overline{E_s^2} = 2ej\left(\frac{\partial i}{\partial j}\right)^2 \int_0^\infty Z^2 G^2 df. \qquad (1)$$

$\overline{E_s^2}$ is here the mean square shot voltage across the output measuring device, i the space current, j the total current emitted by the cathode, e the electronic charge, Z the impedance of the parallel combination consisting of the internal plate impedance, r_p, of the vacuum tube and the external load impedance z_0, G the voltage amplification between z_0 and the output measuring device, and df the differential of frequency.

Eq. (1) shows that as long as space charge is too small to affect the flow of current, the mean square shot voltage is directly proportional to the space current. As the emission is increased, however, space charge begins to control, and finally limits, the space current so that the value of $\partial i/\partial j$ approaches zero. At the same time the internal plate impedance is reduced and Z is thus decreased. The shot voltage therefore increases less rapidly as space charge becomes effective and finally decreases rapidly toward zero as complete space charge control is reached.

The effect of space charge on shot noise has been demonstrated in a qualitative manner by several workers.[2] A precise experimental verification of Eq. (1) is very difficult because most vacuum tubes are incapable of producing good temperature saturation and even after obtaining saturation an exact measurement of $\partial i/\partial j$ is almost impossible. This latter difficulty is particularly objectionable with thoriated and oxide coated cathodes. Accordingly, in the measurements to be described here, a tube having a pure tungsten filament was used. Although the tube contained three electrodes the grid and plate were tied together in order to simplify the system. The plate voltage was kept as low as possible in order to eliminate extraneous noise due to ionization of the residual gas in the tube. Under these operating conditions the thermal noise in the plate circuit of the tube is so small that it may be neglected.

[1] F. B. Llewellyn, Proc. I.R.E. **18**, 243 (1930).

[2] A. W. Hull and N. H. Williams, Phys. Rev. **25**, 147 (1925); J. B. Johnson, Phys. Rev. **26**, 71 (1925); N. H. Williams and E. W. Thatcher, Phys. Rev. **39**, 474 (1932); and reference 1 above. E. W. Thatcher, Phys. Rev. **40**, 114 (1932) has reported experimental evidence to show that the mean square shot voltage in the presence of space charge is proportional to $j(\partial i/\partial j)^2$. He did not, however, make corrections for Schottky emission in the determination of j.

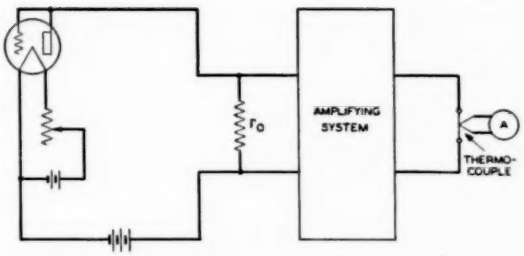

FIG. 1. Noise measuring circuit consisting of experimental tube, coupling circuit, amplifying system, thermocouple and microammeter.

The experimental arrangement is shown diagrammatically in Fig. 1. The amplifying system and the output measuring device are the same as those described in a previous paper.[3] The emission in the experimental tube was varied by changing the filament heating current while the plate voltage remained constant at 9.4 volts. The plate battery was varied to compensate for voltage drop in the load resistance, r_0, which was 1000 ohms. The output deflection (proportional to the mean square voltage fluctuations across r_0) was recorded for widely different space currents. These are given in Table I and also plotted as experimental points in Fig. 2. It is seen that the noise varies qualitatively as previously described except that instead of reaching the value zero it passes through a minimum value, at about 5 milliamperes, and then increases. This latter effect is well known and is almost certainly a fluctuation in the space charge produced by positive ions emitted from the tungsten filament.[3] The experiments can thus distinguish between Eq. (1) and the pure shot effect equation over the range of currents between the values where space charge just becomes perceptible and where the space charge is so dense that it can be affected appreciably by the positive ions.

TABLE I. *Shot noise data.**

i (m.a.)	Z (ohms)	j_0 (m.a.)	$\partial i/\partial j_0$	$\overline{E_s^2}$—Arbitrary units	
				Cal.	Obs.
1.0	*995*	1.0	1.03	27	25
2.0	989	1.9	1.03	51	50
2.5	985	2.4	1.03	65	64
3.0	978	2.9	1.03	77	77
3.3	*969*	3.2	1.03	83	82
3.5	*960*	3.4	1.03	87	85
3.7	*944*	3.6	1.00	83	84
3.8	935	3.7	0.95	75	80
3.9	*906*	3.8	0.90	65	68
4.0	874	4.0	0.85	57	56
4.1	*849*	4.2	0.80	50	45
4.4	760	4.5	0.65	29	32
4.6	690	4.8	0.47	13	28
4.8	620	5.5	0.34	6.4	26
5.0	585	6.2	0.22	2.6	26
5.2	*562*	7.4	0.14	1.2	29
5.5	533	10.5	0.068	0.35	40

* Those values given in italics were interpolated from the measured data.

[3] G. L. Pearson, Physics **5**, 233 (1934).

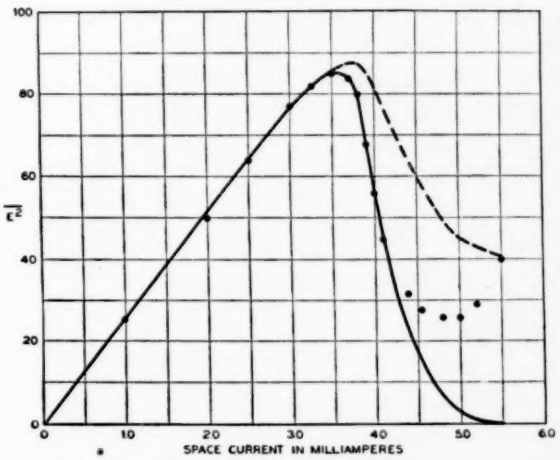

FIG. 2. Shot effect in the presence of space charge. $\overline{E^2}$ is the mean square noise voltage across the output measuring device expressed in arbitrary units. The variation in space current was obtained by changing the cathode temperature, the plate voltage remaining constant. The plotted points represent measured noise, the solid curve was calculated by means of Eq. (1), and the dashed curve calculated according to the relation suggested by Moullin and Ellis.

For each value of i, the total emission of the cathode was determined in the following manner. Keeping the filament temperature constant at that value which gave a fixed space current i when the plate voltage was 9.4 volts, the voltage in the plate circuit was increased and the values of space current recorded. The logarithm of the space current was plotted against the square root of the plate voltage. At the higher voltages where the variation in space current results solely from the "Schottky current" the plot is a straight line.[4] By extrapolation of this line to zero voltage the total emission j_0 at zero field is obtained. Although this j_0 is slightly different from the j in Eq. (1), j_0 will be used in the calculations since it is impossible to determine the field at the cathode

[4] K. T. Compton and I. Langmuir, Rev. Mod. Phys. **2**, 123 (1930).

under operating conditions. The error introduced by this substitution is very small. The space current i was now plotted as a function of j_0 and $\partial i/\partial j_0$ was found by measuring the slope of this curve at the various points. The values of j_0 and $\partial i/\partial j_0$ so obtained are given in Table I. The corresponding values of the internal tube impedance r_p were also measured in the order to determine Z, the impedance of r_p in parallel with r_0, as given in column 2 of Table I. The values of the impedance of the tube used in calculating Z were obtained simply from the slope of the V–i curve, V being the plate voltage, and may be expressed by

$$\frac{1}{r_p}=\left(\frac{\partial i}{\partial V}\right)_j+\frac{\partial i}{\partial j}\frac{dj}{dV}.$$

In Llewellyn's derivation of Eq. (1) it is assumed that

$$1/r_p=(\partial i/\partial V)_j.$$

Using the former value of r_p makes Z at the most one percent too large.

By substituting these quantities in Eq. (1) and assigning to G the value required to make the observed and calculated shot noise identical when the space current is 3 milliamperes, the values of shot noise given in column 5 of Table I were calculated. These are also shown in the solid curve in Fig. 2. The check between theory and experiment is remarkably good over the range in which the comparison is valid.

Thermal Agitation

Thermal agitation in the internal plate impedance of a vacuum tube has been investigated theoretically by a number of workers.[5] It has been deduced that the resistive component of this impedance should produce thermal noise as if it were at the temperature of the cathode and that the total thermal noise of the circuit consisting of the tube impedance in parallel with the load resistance should be given by the expression:

$$\overline{E_T^2}=4kT_0r_0\left(1+\frac{T_fr_p}{T_0r_p}\right)\left(\frac{r_p}{r_0+r_p}\right)^2\int_0^\infty G^2df. \quad (2)$$

$\overline{E_T^2}$ is here the mean square thermal agitation voltage across the output measuring device, k is Boltzmann's gas constant, and T_0 and T_f are, respectively, the temperature of the load resistance and of the cathode expressed in degrees Kelvin.

In order to measure this effect experimentally the noise from other causes such as shot effect, positive ions, etc., must be kept very low. Accordingly the tubes in the measurements described here were worked at high cathode temperatures in order to insure a high degree of space charge at all times and the plate potentials were kept low to prevent ionization from electron impact. Tubes having both oxide coated and thoriated tungsten cathodes were used for the measurements. Pure tungsten cathodes could not be used because of the positive ion emission noted above. Although the tubes contained three electrodes the grid and plate were tied together in order to simplify the system.

The experimental arrangement is the same as that used in the shot measurements, as shown in Fig. 1. With a fixed filament voltage, corresponding to a high filament temperature, the noise was measured as the internal plate impedance was varied by changing the plate voltage. The amplifying system was calibrated by measuring the thermal noise as the load resistance alone was varied, with the experimental tube in position but with zero plate battery so that its impedance was infinite. The noise was the same whether the filament was hot or cold. This gave the linear relationship shown by the dashed line in Fig. 3 where ordinates represent mean square noise voltage across the output measuring device and abscissae represent the resistance of the tube and the load in parallel. From these measurements the value of G was obtained. The load resistance was now fixed at 45,500 ohms and different plate voltages were applied to the tube. With increased voltage the space current increased while the tube impedance and the noise both decreased. The noise data obtained with two different tubes having oxide coated filaments and one tube having a filament of thoriated tungsten are shown in Fig. 3. Curves corresponding to the experimental points were calculated by Eq. (2) letting T_0 be 300 degrees and T_f be for the oxide coated filaments 650 degrees and for the thoriated filament 1200 degrees Kelvin.

It is seen that the experimental points fit the theoretical curves for thermal noise very well if

[5] For example see reference 1.

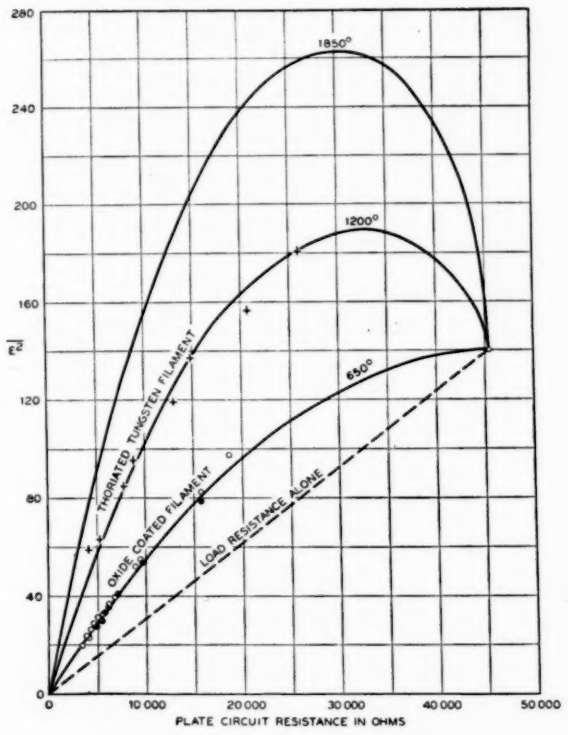

FIG. 3. Thermal noise in the plate circuit of a vacuum tube. The dashed curve represents the thermal noise in the load resistance alone. With the tube in the circuit the experimental points are represented by: + thoriated tungsten; open circle, oxide coated No. 1; and closed circle, oxide coated No. 2. The solid curves were calculated by means of Eq. (2), T_f having the values shown.

the filament temperatures are assumed to be those stated above. In reality it is known that the temperature of the coated filament was about 1100 degrees Kelvin while that of the thoriated filament was approximately 1850 degrees. The curve corresponding to this latter temperature has been calculated and is shown in the upper curve of Fig. 3 for comparison. The cause for this discrepancy between theory and experiment is not understood. Among the various suggestions two may be mentioned.[6] (1) Of the three velocity components of the electrons corresponding to temperature not all are equally effective in producing thermal noise. (2) In the thermodynamic argument[1] which leads to Eq. (2) the circuit including filament, plate, and external load are first supposed to be maintained at the temperature of the cathode. Later the external load is permitted to take any other temperature. In the experimental circuit, however, the plate is more nearly at the lower temperature of the external load than at that of the cathode. Because of the close electrical reaction between the plate and the space charge the latter may be at a lower effective temperature near the plate than near the cathode. Whatever the cause of this discrepancy may be the experiments prove with certainty that the thermal noise in these tubes is even lower than that calculated by Eq. (2).

Discussion of Results

Moullin and Ellis[7] have recently contended that neither of the effects exists which have here been described and measured. They believe that the flow of electrons is random even in the presence of space charge, so that space charge should have no effect on shot noise, the reduction in noise at high space currents being caused solely by the decrease in internal plate impedance of the tube; and that there is no possibility of the electrons in the space current sharing thermal energy with molecules, so that the internal impedance of the tube cannot produce thermal noise. According to the views of Moullin and Ellis the factor $j(\partial i/\partial j)^2$ in Eq. (1) should be replaced by i, the other factors remaining the same.

The dashed curve in Fig. 2 gives the noise calculated in accordance with this relation which denies the existence of the cushioning effect of the space charge. The agreement of the experimental points with the solid curve calculated from Eq. (1) shows that space charge is effective in reducing shot noise. The experiments prove, further, that the impedance of the tube contributes to the total thermal noise of the circuit but that in place of the cathode temperature an even lower temperature must be used. This temperature appears to lie about midway between the temperature of the cathode and room temperature.

In conclusion I wish to express my thanks to Dr. J. B. Johnson for the helpful discussion and criticism given during the course of this work.

[6] The first suggestion was made by Dr. Llewellyn, the second by Dr. Johnson.

[7] E. B. Moullin and H. D. Ellis, I.E.E.J. **74**, 323 (1934). F. B. Llewellyn (I.E.E.J. **75**, 395 (1934)) has discussed this article.

The Potential Distribution Between Parallel Plates and Concentric Cylinders Due to Any Arbitrary Distribution of Space Charge

W. G. CADY, *Wesleyan University*

(Received October 29, 1934)

Equations are derived for the electric potential and field intensity due to a distribution of space charge in a slab of dielectric between two infinite parallel conducting plates. The charge density may be any integrable function of the coordinate perpendicular to the plates. The corresponding solution for concentric cylinders is also given. A number of special cases are discussed, including that of a uniformly distributed charge, and one of sinusoidal distribution. The latter has an application in the theory of the piezoelectric resonator.

IN the author's recent development of the theory of the piezoelectric resonator, which will soon be published, it has been found necessary to take into account the reaction of polarization charges in the crystal upon the performance of the resonator. To this end, general equations have been derived for potential and field intensity due to a distribution of space charge in a slab of dielectric between two infinite parallel conducting plates, the charge density being any arbitrary integrable function of the coordinate perpendicular to the plates. This solution is then applied to the resonator problem. The derivation is given in the present paper, in the hope that the results may be useful in a wider field. Though it has no present bearing on the resonator problem, the corresponding theorem for space charge between concentric cylinders is also included. Special cases of the general problem in its relation to thermionic phenomena and discharge in gases have been discussed by many writers.[1]

I. PARALLEL PLATES

In Fig. 1 the x-axis is perpendicular to the plates, which are located at the origin O, and at X. The slab of dielectric, which has a dielectric constant k, occupies the space from $A(x=a)$ to $B(x=a+e)$. On each side of the dielectric is a gap having $k=1$, devoid of space charge, the gap lengths being a and b, respectively. The space charge in the dielectric, represented by the curve ρ in Fig. 1, may be any arbitrary function of x, but is uniform in all directions perpendicular to the x-axis. The potential is assumed to be zero at O and X. If there is a potential difference between the plates, it can be superposed on the space charge solution. For a one-dimensional problem, Poisson's equation has the form

$$d^2V(x)/dx^2 = -(4\pi/k)\rho(x), \tag{1}$$

where $V(x)$ and $\rho(x)$ are functions of x alone.

The following notation will be used, wherein C_1 and C are constants to be determined from boundary conditions.

$$\int \rho(x)dx \equiv \rho_1(x) + C_1, \tag{2}$$

$$\int \rho_1(x)dx \equiv \rho_2(x) + C_2, \tag{3}$$

$$s \equiv k(a+b)+e, \tag{4}$$

where s may be called the "electrical distance" between the plates. Upon integrating Eq. (1) we have

$$\frac{dV(x)}{dx} = -\frac{4\pi}{k}\{\rho_1(x)+C_1\} = -E(x), \qquad [a<x<(a+e)], \tag{5}$$

$$V(x) = -\frac{4\pi}{k}\{\rho_2(x)+C_1x+C_2\}, \qquad [a<x<(a+e)]. \tag{6}$$

[1] For example, C. D. Child, Phys. Rev. **32**, 492 (1911); I. Langmuir, Phys. Rev. **2**, 450 (1913), also **24**, 49 (1924); W. Schottky, Verh. d. D. Phys. Ges. **16**, 490 (1914), also Jahrb. d. Radioakt. u. Elektronik **12**, 147 (1915); T. C. Fry, Phys. Rev. **17**, 441 (1921); R. Gans, Ann. d. Physik **69**, 385 (1922); I. Langmuir and K. T. Compton, Rev. Mod. Phys. **3**, 191 (1931); A. Trost, Phys. Zeits. **35**, 725 (1934); S. Werner, Zeits. f. Physik **90**, 398 (1934); H. J. Van der Bijl, *The Thermionic Vacuum Tube*, New York 1920, pp. 54–57; J. J. Thomson, *Conduction of Electricity Through Gases*, 3rd ed., Vol. 1, 1928, p. 370 ff; Wien-Harms, Handb. d. Experimentalphysik, 1928, Vol. 13, Part II, pp. 244 ff.

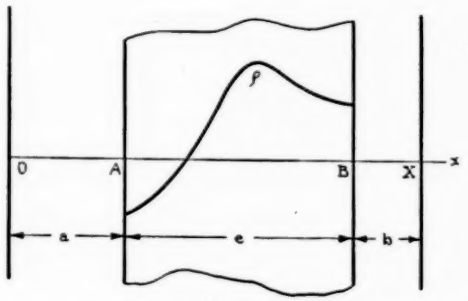

FIG. 1. Space charge distribution in dielectric between parallel plates, with gaps a and b.

These expressions for potential V and field intensity E are valid only in the region occupied by space charge, i.e., from A to B in Fig. 1. The values in the gaps a and b are easily derived as soon as the potentials at A and B have been determined.

C_1 and C_2 are found from the boundary conditions at A and B. At A, where $x=a$, the electric intensity in the gap is $-V(a)/a$, while in the dielectric it is $-V(a)/ka$. In passing, it may be remarked that this recognition of the change in intensity at the surface of the dielectric obviates the necessity of introducing explicitly the polarization surface charge. Upon setting $x=a$ in (5), we have

$$\frac{dV(a)}{dx}=\frac{V(a)}{ka}=-\frac{4\pi}{k}\{\rho_1(a)+C_1\}.$$

From this equation, together with a similar one for the point $x=(a+e)$, and the two equations obtained by substituting a and $(a+e)$ respectively for x in Eq. (6), we can solve for C_1, C_2, $V(a)$, and $V(a+e)$. The expressions for C_1 and C_2 are

$$C_1=-\frac{1}{s}\{\rho_2(a)-ka\rho_1(a)-\rho_2(a+e)-kb\rho_1(a+e)\}, \quad (7)$$

$$C_2=-\frac{1}{s}[(a+e+kb)\{ka\rho_1(a)-\rho_2(a)\}-a(k-1)\{kb\rho_1(a+e)+\rho_2(a+e)\}]. \quad (8)$$

If, in addition to the considerations discussed, the plate at X, Fig. 1, is at a potential V_1, we simply add the corresponding term to Eq. (6).

II. Concentric Cylinders

In Fig. 2 the origin is at O, the axis of the cylinders. The two cylindrical electrodes, of infinite length, both at zero potential, have radii r_1 and r_4. The space charge, distributed uniformly around and in the direction of the axis, is comprised between the clyindrical surfaces of radii r_2 and r_3. It may be expressed as any arbitrary integrable function $\rho(r)$ of the radius. The dielectric constant is assumed to be unity throughout the system.

Poisson's equation for the cylindrical case is

$$\frac{1}{r}\frac{d}{dr}\left(r\frac{dV(r)}{dr}\right)=-4\pi\rho(r). \quad (9)$$

Upon integrating and introducing the notation

$$\int r\rho(r)dr\equiv F_1(r)+C_1,$$

$$\int (1/r)F_1(r)dr\equiv F_2(r)+C_2,$$

we have for the intensity

$$-E(r)=\frac{dV(r)}{dr}=-\frac{4\pi}{r}\{F_1(r)+C_1\} \quad [r_2<r<r_3], \quad (10)$$

and for the potential

$$V(r)=-4\pi\{F_2(r)+C_1\log r+C_2\} \quad [r_2<r<r_3]. \quad (11)$$

The constants are determined by applying to the regions r_1r_2 and r_3r_4, which are devoid of charge, the usual equation for potential difference between infinite concentric cylinders. Remembering that $V(r_1)=V(r_4)=0$, we have $V(r_2)=-r_2E(r_2)$

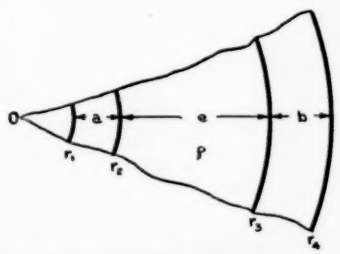

FIG. 2. Partial cross section of concentric cylinders of radii r_1 and r_4, with space charge occupying the region from r_2 to r_3.

$\log r_2/r_1$, and a similar equation for $V(r_3)$. From these equations, and by substituting r_2 and r_3 for r in (10) and (11), we find

$$C_1=\frac{1}{\log (r_4/r_1)}\left\{F_2(r_2)-F_2(r_3)\right.$$
$$\left.-\log\frac{r_2}{r_1}F_1(r_2)-\log\frac{r_4}{r_3}F_1(r_3)\right\}, \quad (12)$$

$$C_2=\log (r_2/r_1)F_1(r_2)-F_2(r_2)-C_1\log r_1. \quad (13)$$

Examples

(1) Parallel plates, gaps $a=b=0$, $k=1$

The space charge may have any distribution $\rho(x)$ perpendicular to the plates. From Eqs. (6), (7), and (8), the potential at any point is

$$V(x)=(4\pi/e)\{x\rho_2(e)+(e-x)\rho_2(0)-e\rho_2(x)\}, \quad (14)$$

where e is now the distance between the plates.

In the special case where ρ is uniform this reduces to the usual parabolic equation

$$V(x)=2\pi\rho x(e-x). \quad (15)$$

If the space charge has the form $\rho(x)=\rho_0+cx$ the solution is

$$V(x)=\tfrac{2}{3}\pi x(e-x)\{3\rho_0+c(e+x)\}. \quad (16)$$

This case is illustrated in Fig. 3, which is drawn on the assumption that $\rho_0=0.5$ e.s.u., $e=1$ cm, and $c=1$. The maximum value of V comes at $x=0.54$ cm.

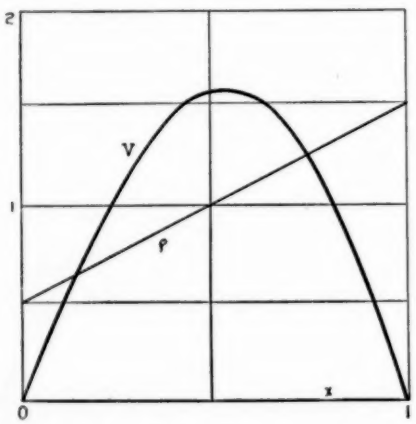

Fig. 3. Linear distribution of space charge between parallel plates, with no gaps.

(2) Parallel plates, sinusoidal distribution of space charge

This case is encountered in the piezoelectric resonator. For illustrative purposes it suffices to assume that we have a plate of piezoelectric crystal AB, Fig. 4, of thickness e and dielectric constant k, of relatively great extent in directions perpendicular to the X-axis, and with gaps of lengths a and b between it and the electrodes, which are at A' and B'. The origin is now at O, Fig. 4, in the center of the dielectric. Owing to its state of instantaneous strain while in vibration in the X-direction, the plate is polarized parallel to X according to the equation $P(x)=P_0\cos \pi x/e$. This polarization, represented by the curve P in Fig. 4, gives rise to a space charge ρ of the form $\rho(x)=-dP(x)/dx=\rho_0\sin \pi x/e$, where $\rho_0=\pi P_0/e$. The quantities $\rho_1(x)$ and $\rho_2(x)$ in Eqs. (2) and (3) are now written

$$\rho_1(x)=-\frac{\rho_0 e}{\pi}\cos\frac{\pi x}{e}, \quad \rho_2(x)=-\frac{\rho_0 e^2}{\pi^2}\sin\frac{\pi x}{e}. \quad (17)$$

By the use of these expressions, and with due regard to the shift in the position of the origin, Eqs. (7) and (8) become $C_1=2\rho_0e^2/\pi^2s$ and $C_2=-k\rho_0e^2(b-a)/\pi^2s$. The potential equation is therefore, from (6),

$$V(x)=\frac{4\rho_0e^2}{\pi k}\left\{\sin\frac{\pi x}{e}-\frac{2x}{s}+\frac{k(b-a)}{s}\right\},$$
$$[a<x<(a+e)]. \quad (18)$$

As is shown by this equation and represented in Fig. 4, the potential function has the form of a sine curve superposed upon a straight line.

The field intensity in the dielectric has the equation

$$E(x)=-\frac{dV(x)}{dx}=-\frac{4\rho_0 e}{k}\left(\cos\frac{\pi x}{e}-\frac{2e}{\pi s}\right). \quad (19)$$

The intensity is, under the conditions shown in Fig. 4, negative except near the bounding faces of the dielectric, where it becomes positive. It passes through zero at points corresponding to maximum and minimum potential. These points $\pm x_m$ are given by the equation $\cos \pi x_m/e=2e/\pi s$.

In Fig. 4 lines are also drawn representing the values of E and V in the gaps a and b. If $a=b$, the potential curve becomes symmetrical, passing through the origin.

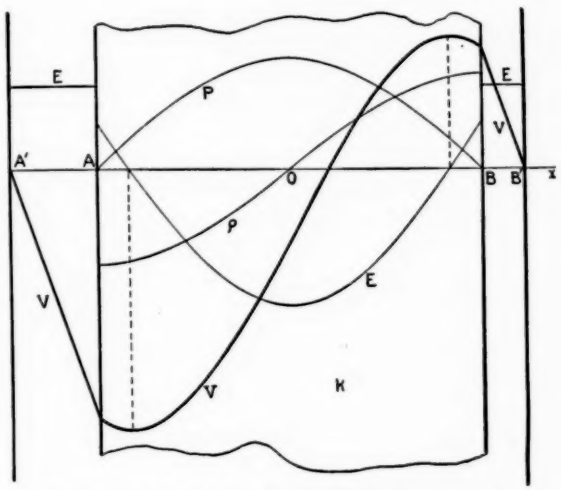

FIG. 4. Sinusoidal distribution of space charge in dielectric between parallel plates.

(3) Concentric cylinders, no region devoid of space charge

In Fig. 2, $a=b=0$, $r_1=r_2$, $r_3=r_4$. The ρ distribution extends from r_1 to r_4. By making these substitutions in (11), (12) and (13), we find for the potential at any point

$$V(r)=\frac{4\pi}{\log\,(r_4/r_1)}\Big[\{F_2(r_4)-F_2(r_1)\}\log r - \log\frac{r_4}{r_1}F_2(r)-\log r_1F_2(r_4)+\log r_4F_2(r_1)\Big]. \quad (20)$$

If, under the same conditions, ρ is uniform between the cylinders, the functions F_1 and F_2 become $F_1(r)=\rho r^2/2$, $F_2(r)=\rho r^2/4$. Hence (20) becomes

$$V(r)=\frac{\pi\rho(r_4^2-r_1^2)}{\log\,(r_4/r_1)}\log r-\pi\rho r^2 + \frac{\pi\rho(r_1^2\log r_4-r_4^2\log r_1).}{\log\,(r_4/r_1)}. \quad (21)$$

This equation has the same form as Eq. (217) of Langmuir and Compton,[1] and in addition it gives the values of their coefficients A and C.

Potential Distributions About an Infinitely Extended Line Electrode on the Surface of a Horizontally Stratified Earth. II

MORRIS MUSKAT, *Gulf Research and Development Corporation, Pittsburgh*

(Received October 5, 1934)

The analytical theory is given for the potentials and gradients to be found on the surface of a horizontally stratified earth in which the current source is an infinitely extended cable or line electrode lying on the surface. Power series expansions in the distance from the electrode are derived for small distances and asymptotic expansions for large distances. Detailed treatments are given for the two layer earth, for all thicknesses of the surface layer, and for the three layer earth in which the thickness of the second layer either equals or is twice as great as that of the surface layer, as well as formal expansions for general many layered earths. Simple closed hyperbolic function expressions are derived for the surface gradients for three layer systems in which the lowest layer is either of infinite or zero conductivity. The solution for the direct interpretation problem in which the continuous vertical conductivity variation may be determined from a knowledge of the surface gradients is briefly outlined, following the method of Slichter and Langer for the case where the current source is a point electrode. The analytical results of the indirect interpretation problem for a stratified earth are illustrated by thirty numerical and graphical examples.

INTRODUCTION

THE problem of electrical prospecting by means of point electrodes has recently been the subject of considerable study both from the point of view of indirect[1] and direct[2] interpretation. While much remains yet to be done in the development of convenient and rapid numerical techniques, especially in the case of the direct interpretation method, the analytical theory of the problem may be considered to be fairly well completed insofar as one assumes a uni-dimensional variation of the conductivity. However, the case of the analogous two dimensional system in which the current or potential source is an infinitely extended cable, and which has been frequently used in ore prospecting, has not been given any detailed treatment. For the stratified earth, several cases have been discussed graphically by means of series of logarithmic terms[3] while integral expressions have been derived by King[1] for the surface gradients for continuous variations of conductivity which are either exponential or parabolic.

Although, as King points out, the theory of the line electrode can be formally derived from that for a point electrode by integration of the results of the latter and will give no essentially new information beyond that of the point electrode,[4] the line electrode gradients may be expressed as series of exponentials rather than Hankel functions and hence are better suited for practical interpretation when one of the layers is of zero or infinite conductivity. In fact, King indicates how to derive from empirical point electrode gradients the corresponding line electrode gradients which are more convenient for analysis in terms of the electrical depth constants.

While most of the analysis will be ultimately expressed here also in terms of the surface gradients, the potentials themselves will diverge if obtained by simple integration of the integral expressions for the point electrode potentials. Furthermore, when none of the layers is of zero or infinite conductivity the point electrode potentials or gradients cannot be expressed as Hankel function series and power series must be used for small distances from the electrode; these will evidently diverge on integration. We shall, therefore, briefly outline the direct derivation of the integral expressions for the potentials of the line electrode system in a two layer earth without the use of the point electrode expressions. The expressions for the 3 layer earth will be

[1] L. V. King, Proc. Roy. Soc. **A139**, 237 (1933), and Phil. Trans. Roy. Soc. **A233**, 327 (1934); M. Muskat, Physics **4**, 129 (1933). This latter paper will be referred to in the text as *I*.

[2] L. B. Slichter, Physics **4**, 307 (1933); A. F. Stevenson, Physics **5**, 114 (1934).

[3] L. J. Peters and J. Bardeen, U. of Wisconsin Engineering Expt. Station Bul. 71, 1930.

[4] On the other hand it should be observed that the two dimensional prospecting problem implies no *physical* simplification as compared to the point electrode system, as in both cases the earth is supposed to be horizontally stratified with uniform conductivities in planes parallel to the earth's surface. The reduction of the analytical problem to one of two dimensions is based on the use of a theoretically infinite cable as the current source rather than a point electrode.

given without derivation and only for the surface gradients, and may be considered as obtained by integration of the point electrode gradients or by independent solutions similar to that given for the two layer earth. Finally, it may be mentioned that although the case of continuous conductivity variation appears to be more general than that of discrete layers of different conductivity, the latter representation probably corresponds more closely to the situations occurring in practice and cannot be obtained from the continuous conductivity variation theory, but must be derived by a separate analysis. This analysis will be given here.

I. A Two Layered Earth

The analytical problem may be formulated as follows: find potential functions Φ_1 and Φ_2 pertaining to regions (1) and (2) (cf. Fig. 1), such that:

$$\left.\begin{aligned} &\Phi_1=\log\{x^2+(y-h)^2\} : \lim\{x^2+(y-h)^2\}\to 0;\\ &\partial\Phi_1/\partial y=0 : y=0;\\ &\Phi_1=\Phi_2;\quad \sigma_1\partial\Phi_1/\partial y=\sigma_2\partial\Phi_2/\partial y : y=\tfrac{1}{2}, \end{aligned}\right\}(1)$$

where the unit of length has been taken as twice the thickness of the upper layer and σ_1, σ_2 denote the conductivities of the two layers.

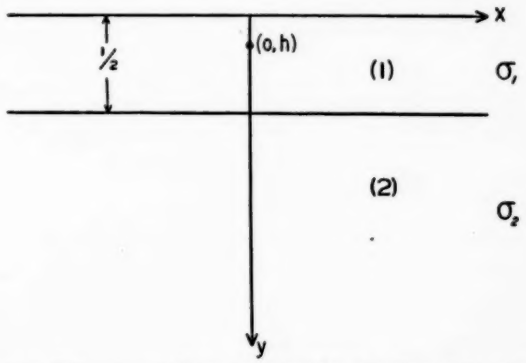

Fig. 1. Diagrammatic representation of a line electrode at $(0, h)$ in a two layer earth.

Although it is not difficult to sum the series of logarithmic terms corresponding to the system of images giving the solution to the Eqs. (1) the direct integral method has the advantage that it may be readily generalized to systems containing any number of parallel layers, and even to those in which the conductivity varies continuously. Here one may begin with an integral representation of the primary source which may be written as:

$$\Phi_0=\log\{x^2+(y-h)^2\}=2\int_0^\infty \frac{d\alpha}{\alpha}\left[e^{-2\alpha}-\cos 2x\alpha\begin{Bmatrix} e^{-2(h-y)\alpha} : y\leqslant h\\ e^{-2(y-h)\alpha} : y\geqslant h\end{Bmatrix}\right]. \tag{2}$$

The perturbation in the potential in the upper medium due to its closure at $y=0$ and the presence of the lower medium at $y=\frac{1}{2}$ may then be expressed as:

$$\Phi_p=2\int_0^\infty \frac{d\alpha}{\alpha}[\Psi_1(\alpha)+\{A_1e^{-2y\alpha}+B_1e^{2y\alpha}\}\cos 2x\alpha] \tag{3}$$

and the total potential in the lower medium as:

$$\Phi_2=2\int_0^\infty (d\alpha/\alpha)[\Psi_2(\alpha)+A_2e^{-(2y-1)\alpha}\cos 2x\alpha], \tag{4}$$

where Ψ_1 and Ψ_2 are introduced to take care of the term $e^{-2\alpha}$ in Φ_0. Applying the boundary conditions of Eqs. (1) to $\Phi_1=\Phi_0+\Phi_p$ and Φ_2 and adjusting Ψ_1 and Ψ_2 so as to insure the convergence of Eqs. (3) and (4) it is found that:

$$\left.\begin{aligned} &\Delta A_1=2(\sigma_1/\sigma_2)\cosh(1-2h)\alpha+2\sinh(1-2h)\alpha;\qquad \Delta B_1=-2(1-\sigma_1/\sigma_2)e^{-\alpha}\cosh 2h\alpha,\\ &\Delta A_2=4\sigma_1/\sigma_2\cosh 2h\alpha;\qquad \Delta=-2\{\cosh\alpha+\sigma_1/\sigma_2\sinh\alpha\},\\ &\Psi_1(\alpha)=(2\sigma_1/\sigma_2-1)e^{-2\alpha};\qquad \Psi_2(\alpha)=2\sigma_1/\sigma_2\cdot e^{-2\alpha}, \end{aligned}\right\}(5)$$

so that denoting by k the quantity: $(\sigma_1-\sigma_2)/(\sigma_1+\sigma_2)$,

$\sigma_1/\sigma_2<1$: $k=-e^{-2\gamma}$:

$$\left.\begin{aligned}\Phi_1&=4\int_0^\infty\frac{d\alpha}{\alpha}\left[\tanh\gamma e^{-2\alpha}-\frac{\cos 2x\alpha}{\cosh(\alpha+\gamma)}\begin{cases}\sinh(\alpha+\gamma-2h\alpha)\cosh 2y\alpha : y\leqslant h\\ \sinh(\alpha+\gamma-2y\alpha)\cosh 2h\alpha : y\geqslant h\end{cases}\right],\\ \Phi_2&=4\int_0^\infty\frac{d\alpha}{\alpha}\left[\tanh\gamma e^{-2\alpha}-\frac{\sinh\gamma\cosh 2h\alpha e^{-(2y-1)\alpha}\cos 2x\alpha}{\cosh(\alpha+\gamma)}\right];\end{aligned}\right\}\tag{6}$$

$\sigma_1/\sigma_2>1$: $k=e^{-2\gamma}$:

$$\left.\begin{aligned}\Phi_1&=4\int_0^\infty\frac{d\alpha}{\alpha}\left[\operatorname{ctnh}\gamma e^{-2\alpha}-\frac{\cos 2x\alpha}{\sinh(\alpha+\gamma)}\begin{cases}\cosh(\alpha+\gamma-2h\alpha)\cosh 2y\alpha : y\leqslant h\\ \cosh(\alpha+\gamma-2y\alpha)\cosh 2h\alpha : y\geqslant h\end{cases}\right],\\ \Phi_2&=4\int_0^\infty\frac{d\alpha}{\alpha}\left[\operatorname{ctnh}\gamma e^{-2\alpha}-\frac{\cosh\gamma\cosh 2h\alpha e^{-(2y-1)\alpha}\cos 2x\alpha}{\sinh(\alpha+\gamma)}\right].\end{aligned}\right\}\tag{7}$$

Although Eqs. (6) and (7) remain valid when $h=0$[5] it is convenient for the practical discussion of the potential distributions to first separate out Φ_0. Restricting, for the sake of brevity, the further treatment to this case of most practical interest where $h=0$ and considering, furthermore, only the surface potentials $\Phi_1(y=0)$, Eqs. (6) and (7) may be transformed to:

$$\sigma_1/\sigma_2<1 : k=-e^{-2\gamma}:\quad \Phi_1(y=0)=\log x-\frac{e^{-\gamma}}{\cosh\gamma}\int_0^\infty\frac{e^{-\alpha}d\alpha}{\alpha}\left[e^{-\alpha}-\frac{\cosh\gamma\cos 2x\alpha}{\cosh(\alpha+\gamma)}\right];\tag{8}$$

$$\sigma_1/\sigma_2>1 : k=e^{-2\gamma}:\qquad \Phi_1(y=0)=\log x+\frac{e^{-\gamma}}{\sinh\gamma}\int_0^\infty\frac{e^{-\alpha}d\alpha}{\alpha}\left[e^{-\alpha}-\frac{\sinh\gamma\cos 2x\alpha}{\sinh(\alpha+\gamma)}\right],\tag{9}$$

where a factor of 4 has been taken out.

Due to the divergence of the separate parts of the integrals in Eqs. (8) and (9) they are unsuited for detailed discussion. As indicated in the introduction we shall, therefore, remove the constant terms of the integrands by differentiation with respect to x; convergent integrals are then obtained which are, in fact, equivalent to Fourier integrals. Although the original problem as stated in Eq. (1) referred to the potential distribution itself, there is no real loss in generality in expressing the solutions in terms of the gradients of the potential as the series to be derived for the gradients may be readily integrated term by term. Differentiating, then, Eqs. (8) and (9) and dropping the subscript in Φ_1, we have for our final integral expressions for the surface gradients:

$\sigma_1/\sigma_2<1$; $k=-e^{-2\gamma}$:

$$\Phi'=1/x-2e^{-\gamma}\int_0^\infty\frac{e^{-\alpha}\sin 2x\alpha\,d\alpha}{\cosh(\alpha+\gamma)};\tag{10}$$

$\sigma_1/\sigma_2>1$; $k=e^{-2\gamma}$:

$$\Phi'=1/x+2e^{-\gamma}\int_0^\infty\frac{e^{-\alpha}\sin 2x\alpha\,d\alpha}{\sinh(\alpha+\gamma)}.\tag{11}$$

A. Expansions for small values of x

By a method analogous to that developed in *I*, the expansions of Eqs. (10) and (11) for small values of x may be readily derived by expanding first $\sinh(\alpha+\gamma)$ and $\cosh(\alpha+\gamma)$ in series of exponentials, then substituting the power series for $\sin 2x\alpha$, and finally integrating term by term. Thus it is found that both for $\sigma_1/\sigma_2>$ and <1:

$$\Phi'=1/x+2\sum_0^\infty(-1)^m x^{2m+1}\sum_1^\infty k^n/n^{2m+2}.\tag{12}$$

[5] The apparent non-vanishing of $\partial\Phi_1/\partial y$ at $y=0$ for $h=0$ is due to the discontinuity of the integral representation of $\partial\Phi_0/\partial y$ (cf. Eq. (2)) and hence of $\partial\Phi_1/\partial y$ at $y=0$. When Φ_0 is first separated out the difficulty disappears.

Here again as in *I*, the radius of convergence of the series may be advanced from the value 1, by summing out the terms with $n=1$, 2, etc. Doing this for the first two, Φ' may be rewritten as:

$$\Phi'=\frac{1}{x}+\frac{2kx}{1+x^2}+\frac{2k^2x}{4+x^2}+2\sum_0^\infty(-1)^m f_m(k)x^{2m+1}, \quad (13)$$

where $f_m(k)=\sum_3^\infty k^n/n^{2m+2}$.

B. Expansions for large values of x

By direct application of the general formula (cf. *I* Eq. (46)):

$$\int_0^\infty f(\alpha)\sin x\alpha\, d\alpha=\sum_0^\infty\frac{(-1)^m f^{2m}(0)}{x^{2m+1}} \quad (14)$$

it follows at once that the asymptotic expansions of the surface gradients are:

$\sigma_1/\sigma_2<1$:

$$\Phi'=2\sum_0^\infty\frac{(-1)^m}{(2x)^{2m+1}}\frac{\partial^{2m}}{\partial\gamma^{2m}}(\tanh\gamma); \quad (15)$$

$\sigma_1/\sigma_2>1$:

$$\Phi'=2\sum_0^\infty\frac{(-1)^m}{(2x)^{2m+1}}\frac{\partial^{2m}}{\partial\gamma^{2m}}(\operatorname{ctnh}\gamma). \quad (16)$$

Carrying out the differentiations for the first four terms it is found that for both σ_1/σ_2 > and <1,

$$\Phi'=\frac{\sigma_1}{\sigma_2 x}\left[1+\frac{1}{2x^2}(1-\sigma_1^2/\sigma_2^2)-\frac{1}{2x^4}(1-\sigma_1^2/\sigma_2^2)(3\sigma_1^2/\sigma_2^2-2)+\frac{1}{4x^6}(1-\sigma_1^2/\sigma_2^2)(17-60\sigma_1^2/\sigma_2^2+45\sigma_1^4/\sigma_2^4)\right.$$
$$\left.-\frac{1}{2x^8}(1-\sigma_1^2/\sigma_2^2)(315\sigma_1^6/\sigma_2^6-360\sigma_1^4/\sigma_2^4+378\sigma_1^2/\sigma_2^2-62)+\cdots\right]. \quad (17)$$

It is of interest to note that except for the numerical factors the variation of Φ' with σ_1/σ_2 is exactly the same as that for the corresponding point electrode system (cf. *I*, Eq. (16)). And as in that problem the asymptotic expansions fail both for $\sigma_2=\infty$ and $\sigma_2=0$, due to the degeneration of the inverse power variation of Φ' into an exponential variation.

Thus for $\sigma_2=\infty$, $\gamma=0$ for Eq. (10) and Φ' becomes:

$$\Phi'=1/x-2\int_0^\infty\frac{e^{-\alpha}\sin 2x\alpha}{\cosh\alpha}d\alpha=\pi\operatorname{csch}\pi x, \quad (18)$$

which evidently behaves as $e^{-\pi x}$ for large x.

Similarly for $\sigma_2=0$, $\gamma=0$ in Eq. (11) and

$$\Phi'=1/x+2\int_0^\infty\frac{e^{-\alpha}\sin 2x\alpha\, d\alpha}{\sinh\alpha}=\pi\operatorname{ctnh}\pi x, \quad (19)$$

which approaches $\pi(1+2e^{-2\pi x})$ for large x. The constant term here, which represents a linear term for Φ, corresponds to the logarithmic term in the asymptotic expansion for the point electrode problem (cf. *I*, Eq. (18)).

The gradient distributions for $\sigma_1/\sigma_2=0$, 0.20, 1.0, 5.0 and ∞ are plotted in Fig. 2, where for convenience $x\Phi'$ has been used as the ordinate rather than Φ' itself. For small x Eq. (13) was found quite satisfactory as was Eq. (15) for large x for $\sigma_1/\sigma_2=\frac{1}{5}$. However, for $\sigma_1/\sigma_2=5$, Eq. (16) was first modified to the form:

$\sigma_1/\sigma_2>1$:

$$\Phi'=2\sin 2x\gamma\, Ci(2x\gamma)-2\cos 2x\gamma\{Si(2x\gamma)-\pi/2\}$$
$$+2\sum_0^\infty m\frac{(-1)^m}{(2x)^{2m+1}}\left\{\frac{\partial^{2m}}{\partial\gamma^{2m}}(\operatorname{ctnh}\gamma)-\frac{\Gamma(2m+1)}{\gamma^{2m+1}}\right\}, \quad (20)$$

which is analogous to *I* (15a). The convergence was then so rapid that with only 3 terms of the series the remainders were less than 0.003 for $x\geqslant 5$.

The curves here for $x\Phi'$ are strikingly similar to those for $x\Phi$ in the case of the point electrode (cf. *I*, Fig. 3). The only differences are that here the approach to the asymptotic values σ_1/σ_2 is somewhat slower than in *I* and that the slopes of the $x\Phi'$ curves vanish at the origin whereas those of $x\Phi$ for the point electrode system have non-vanishing slopes at $x=0$ and hence show no inflections.

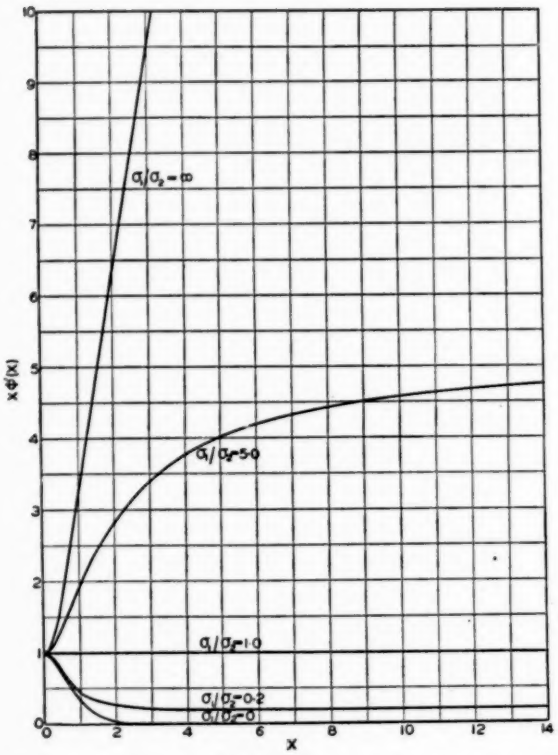

FIG. 2. Surface gradients (Φ') in a two layer earth. σ_1 = conductivity of surface layer; σ_2 = conductivity of lower layer. x = (horizontal distance from line electrode)/(twice the thickness of the surface layer).

II. An Earth with More Than Two Layers

A. General theory

For a general many layered earth, the direct integral method leads to an expression for the surface gradient of the form:

$$\Phi'(x)=1/x+2\int_0^\infty f(\alpha)\sin 2x\alpha\, d\alpha, \qquad (21)$$

where $f(\alpha)\sim e^{-2\alpha}$ for large α, thus insuring the convergence of the integral. For small values of x a power series in x may be derived for $\Phi'-1/x$ by expanding $\sin 2x\alpha$ in a power series. Thus it is found that:

$$\Phi'(x)=\frac{1}{x}+2\sum_0^\infty\frac{(-1)^m(2x)^{2m+1}}{\Gamma(2m+2)}\int_0^\infty\alpha^{2m+1}f(\alpha)d\alpha; \qquad (22)$$

the integrals still remaining may be evaluated by first expanding $f(\alpha)$ in a series of exponentials and then integrating term by term.

For large values of x, a partial fraction expansion of $f(\alpha)$ may be used. Thus $f(\alpha)$ may be expressed as:

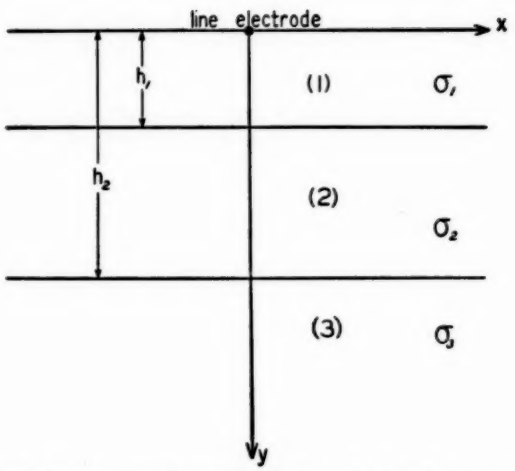

FIG. 3. Diagrammatic representation of a three layer earth.

$$f(\alpha)=f(0)+\sum b_n\{1/(\alpha-\alpha_n)+1/\alpha_n\}, \qquad (23)^6$$

where α_n are the poles (simple) of $f(\alpha)$ and b_n the corresponding residues. Φ' then takes the form:

$$\Phi'(x)=1/x\{1+f(0)+\sum b_n/\alpha_n\}+\sum b_nG_n(-2x\alpha_n), \qquad (24)^7$$

where
$$G(x\alpha_n)=2\int_0^\infty\frac{\sin x\alpha\, d\alpha}{\alpha+\alpha_n}. \qquad (25)$$

To get an asymptotic expansion for Φ' it follows directly from Eq. (21), on applying Eq. (14), or from Eq. (24) on observing that the asymptotic expansion for G is:

$$G(-z)=-2\sum_0^\infty\frac{(-1)^m\Gamma(2m+1)}{(z)^{2m+1}} \qquad (26)$$

that
$$\Phi'=1/x+2\sum_0^\infty\frac{(-1)^mf^{2m}(0)}{(2x)^{2m+1}}. \qquad (27)$$

Furthermore, when the α_n are pure imaginaries the functions G satisfy the relation:

$$G(ix\alpha_n)+G(-ix\alpha_n)=2\pi e^{-x\alpha_n}, \qquad (28)$$

so that if $b(i\alpha_n)=b(-i\alpha_n)$, Eq. (24) becomes:

$$\Phi'(x)=1/x(1+f(0))+2\pi\sum b_ne^{-2x\alpha_n}. \qquad (29)$$

---

[6] When $\alpha=0$ is a pole of $f(\alpha)$ the term b_0/α must first be subtracted from $f(\alpha)$ before the expansion.

[7] Use has been made here of the apparently incorrect result that $\int_0^\infty \sin 2x\alpha\, d\alpha=1/2x$. The difficulty is only apparent, however, and arises from the integral representation of Eq. (2) which leads to the same integral and value for $y=h$, on differentiation of Φ_0. A convergence factor as $e^{-\epsilon\alpha}$ in Eq. (21) before the expansion and integration would evidently lead to Eq. (24) after making ϵ approach zero.

B. The three layer earth

An analysis similar to that given in Part I, shows that for a three layer earth (cf. Fig. (3)) $f(\alpha)$ has the form:

$$f(\alpha)=\frac{2[k_2e^{-2\alpha}+k_3e^{-2\alpha h}]}{1-k_2e^{-2\alpha}+k_3e^{-2\alpha h}(-1+k_2e^{2\alpha})}, \tag{30}$$

where

$$k_2=(\sigma_1-\sigma_2)/(\sigma_1+\sigma_2); \qquad k_3=(\sigma_2-\sigma_3)/(\sigma_2+\sigma_3); \qquad h=h_2/h_1, \tag{31}$$

σ_1, σ_2, σ_3 being the conductivities of the top, intermediate and lowest (infinite) layers, h_1 the depth to the second layer, h_2 the depth to the third layer and α has been so chosen that the unit of length for x in Eq. (21) is $2\,h_1$. As the $f(\alpha)$ here is exactly the same as that for the point electrode problem (cf. *I* (25)), the results of the latter, which depend only on the form of $f(\alpha)$, may be immediately applied here.

Thus for the first two terms in the asymptotic expansion of Eq. (27) for general values of σ_1, σ_2, σ_3 and h we get:

$$x\Phi'(x)=\frac{\sigma_1}{\sigma_3}\left[1-\frac{(\sigma_2^2-\sigma_3^2)\{\sigma_1-\sigma_2+\sigma_2h\}^2+\sigma_3^2(\sigma_1^2-\sigma_2^2)}{2\sigma_2^2\sigma_3^2x^2}+\cdots\right], \tag{32}$$

which is identical with the corresponding expression of *I*(26) except for a factor of 2 in the second term. It follows from Eq. (32) that for very large x, $x\Phi'$ approaches the value σ_1/σ_3 and is independent of σ_2. If $\sigma_1=\sigma_3$, $x\Phi'$ will, therefore, assume the same value for large x as in a homogeneous earth. However, its approach to the limiting value 1 will depend on σ_2, and will be a descent from higher values if $\sigma_2<\sigma_1$ and rise from lower values if $\sigma_2>\sigma_1$.

For small values of x the power series expansion of Eq. (22) may be used to compute $\Phi'(x)$. However, in the evaluation of the integrals $\int_0^\infty \alpha^{2m+1}f(\alpha)d\alpha$ it is convenient to treat separately the cases corresponding to different values of h, as will be seen presently.

Power series expansions for special values of h

$h=2$. When the thickness of the second layer is exactly equal to that of the surface layer ($h=2$), $f(\alpha)$ can be expressed as:

$$f(\alpha)=\frac{k_3e^{-3\alpha}+k_2e^{-\alpha}}{[k_2^2(1-k_3)^2+4k_3]^{\frac{1}{2}}}\left\{\frac{e^{-\gamma_1}}{\sinh(\alpha+\gamma_1)}-\frac{e^{-\gamma_2}}{\sinh(\alpha+\gamma_2)}\right\}, \tag{33}$$

where

$$\begin{aligned} 2k_3e^{2\gamma_1}&=-k_2(1-k_3)+[k_2^2(1-k_3)^2+4k_3]^{\frac{1}{2}}\equiv 2k_3/s_1,\\ 2k_3e^{2\gamma_2}&=-k_2(1-k_3)-[k_2^2(1-k_3)^2+4k_3]^{\frac{1}{2}}\equiv 2k_3/s_2. \end{aligned} \tag{34}$$

Expanding now Eq. (33) in exponentials and integrating Eq. (22) term by term it is found that:

$$\Phi'(x)=1/x+\frac{2}{[k_2^2(1-k_3)^2+4k_3]^{\frac{1}{2}}}\sum_0^\infty(-1)^m x^{2m+1}\sum_1^\infty(s_1^n-s_2^n)\cdot\left(\frac{k_2}{n^{2m+2}}+\frac{k_3}{(n+1)^{2m+2}}\right), \tag{35}$$

the radius of convergence of which can be extended by summing out the terms with $n=1$, 2, etc.

$h=3$. When the second layer is twice as thick as the surface layer, $f(\alpha)$ can be expressed as:

$$f(\alpha)=e^{-\alpha}(k_2+k_3e^{-4\alpha})\left\{\frac{s_1e^{-\gamma_1}/(s_2-s_1)(s_3-s_1)}{\sinh(\alpha+\gamma_1)}+\frac{s_2e^{-\gamma_2}/(s_1-s_2)(s_3-s_2)}{\sinh(\alpha+\gamma_2)}+\frac{s_3e^{-\gamma_3}/(s_1-s_3)(s_2-s_3)}{\sinh(\alpha+\gamma_3)}\right\}, \tag{36}$$

where $s_i=e^{-2\gamma_i}$ and the denominator of $f(\alpha)$ has been factored in the form $\Pi(e^{-2\alpha}-e^{2\gamma_i})$ so that the

γ_i or s_i can be obtained by the solution of a cubic equation. Expanding $f(\alpha)$ as a series of exponentials and integrating Eq. (22) term by term, $\Phi'(x)$ takes the form:

$$\Phi'(x)=1/x+\frac{2}{(s_2-s_1)(s_3-s_1)(s_3-s_2)}\sum_0^\infty(-1)^m x^{2m+1}\sum_1^\infty\left\{\frac{k_2}{n^{2m+2}}+\frac{k_3}{(n+2)^{2m+2}}\right\}$$
$$\cdot\{{s_1}^{n+1}(s_3-s_2)+{s_2}^{n+1}(s_1-s_3)+{s_3}^{n+1}(s_2-s_1)\}. \quad (37)$$

Here, too, a preliminary summation with respect to m of the terms for $n=1, 2, \cdots$ will extend the radius of convergence of the power series.

In a similar manner power series expansions can be derived for systems in which h is any integer or rational fraction, although the degree of the equation to be solved for the s_i would equal h, if it is integral or to the numerator of h if it is a rational fraction. Thus for $h=3/2$, there would again be three s_i just as for $h=3$, which would have to be obtained from the roots of a cubic equation.

Lowest layer of zero conductivity[8]

When the lowest layer is of zero conductivity ($\sigma_3=0$; $k_3=+1$) it may be easily shown that all the poles of $f(\alpha)$ are imaginary and are in fact given by those values α_n which satisfy the equations:

$$[\sinh \alpha_n h]/[\sinh \alpha_n(h-2)]=k_2 \quad (38) \qquad \text{or} \qquad \sinh 2\alpha_n=0, \quad \text{and} \quad \sinh \alpha_n h=0, \quad (38a)$$

the latter of which requires that $h=2p/q$, p and q being integers.

As $\alpha=0$ is a pole of $f(\alpha)$ for $k_3=+1$, the expansion of Eq. (23) must be modified to the form:

$$f(\alpha, k_3=1)=\frac{1+k_2}{(2k_2+h-k_2h)\alpha}-1+\sum b_n\{1/(\alpha-\alpha_n)+1/\alpha_n\}, \quad (39)$$

where
$$b_n=-\frac{\sinh 2\alpha_n(h-1)}{\sinh 2\alpha_n(h-1)-(h-1)\sinh 2\alpha_n} \text{ for Eq. (38)}$$
$$=\frac{1+k_2e^{-2\alpha_n}}{h+(2-h)k_2e^{-2\alpha_n}} \text{ for Eq. (38a).} \quad (40)$$

Hence, as $b(i\alpha_n)=b(-i\alpha_n)$

$$\Phi'(x)=\frac{\pi(1+k_2)}{2k_2+h-k_2h}+2\pi\sum b_n e^{2ix\alpha_n}, \quad (41)$$

where only the positive imaginary values of α_n are to be included in the sum.

Thus for $h=2$ the above equations give:

$$\alpha_n=n\pi i/2 : b_n=(1+(-1)^n k_2)/2.$$

Hence
$$\Phi'(h=2; \sigma_3=0)=\frac{\pi}{2}\{\text{ctnh } \pi x/2+k_2 \tanh \pi x/2\}. \quad (42)$$

For $h=3$:

$$\alpha_n=n\pi i; \qquad b_n=\frac{1+k_2}{3-k_2}; \qquad \alpha_n=\pm\frac{i}{2}\cos^{-1}(k_2-1)/2+n\pi i; \qquad b_n=(1-k_2)/(3-k_2)$$

and
$$\Phi'(h=3, \sigma_3=0)=\frac{\pi}{3-k_2}\{(1+k_2)\text{ ctnh } \pi x+2(1-k_2)\cosh(\pi-\theta)x \text{ csch } \pi x\}, \quad (43)$$

where $\cos\theta=(k_2-1)/2$.

[8] It should be noted that while the results presented here for lowest layers of zero and infinite conductivity are derived from expressions referring to a three layer earth, thus implying that these lowest layers are of infinite thickness, they remain valid even when the third layer of zero or infinite conductivity is of *finite* thickness. For such strata shield those above them from those below, and regardless of the stratification of the medium below these strata, the surface potentials and gradients will be the same as if they were of infinite thickness.

For $h=4$, Eqs. (38), (38a) and (40) give:

$$\alpha_n=n\pi i/2; \qquad b_n=\frac{1+(-1)^n k_2}{2(2-(-1)^n k_2)}; \qquad \alpha_n=\pm\frac{i}{2}\cos^{-1} k_2/2+n\pi i; \qquad b_n=\frac{1-k_2^2}{4-k_2^2},$$

so that

$$\Phi'(h=4,\ \sigma_3=0)=\frac{\pi(1+k_2)}{2(2-k_2)}\operatorname{ctnh}\ \pi x+\frac{\pi(1-k_2)}{2(2+k_2)}\operatorname{csch}\ \pi x+\frac{2\pi(1-k_2^2)}{4-k_2^2}\cosh\ (\pi-\theta)x\ \operatorname{csch}\ \pi x, \quad (44)$$

where $\theta=\cos^{-1} k_2/2$.

It may be observed that the expressions of Eqs. (42), (43) and (44) reduce to that of Eq. (19) for the corresponding two layer earth when k_2 is set equal to 0 or 1. When $k_2=-1$, they reduce to Eq. (18) for a 2 layer earth with a lower layer of infinite conductivity.

Lowest layer of infinite conductivity

When the lowest layer is of infinite conductivity ($\sigma_3=\infty$, $k_3=-1$) the poles of $f(\alpha)$ are again imaginary, being given by the equations:

$$[\cosh\ \alpha_n h]/[\cosh\ \alpha_n(h-2)]=k_2 \quad (45)$$

or

$$\sinh\ 2\alpha_n=0, \quad \text{and} \quad \cosh\ \alpha_n h=0. \quad (45a)$$

Here, $\alpha=0$ is no longer a pole of $f(\alpha)$—except in the trivial case $k_2=1$, which reduces the problem to a two layer earth with the lower layer of zero conductivity—, and $f(\alpha)$ can be expanded as:

$$f(\alpha)=-1+\sum b_n\{1/(\alpha-\alpha_n)+1/\alpha_n\}, \quad (46)$$

where $b_n=\dfrac{\sinh\ 2\alpha_n(h-1)}{\sinh\ 2\alpha_n(h-1)+(h-1)\sinh\ 2\alpha_n}$, for Eq. (45) $=\dfrac{1+k_2e^{-2\alpha_n}}{h+(2-h)k_2e^{-2\alpha_n}}$ for Eq. (45a). (47)

As here, too, $b(i\alpha_n)=b(-i\alpha_n)$, we get: $\Phi'(x)=2\pi\sum b_n e^{2ix\alpha_n}$, (48)

where the sum extends only over the positive imaginary values of α_n.

Applying these results to $h=2$ we find:

$$\alpha_n=\pm\frac{i}{2}\cos^{-1} k_2+n\pi i; \qquad b_n=\tfrac{1}{2},$$

so that $\Phi'(h=2,\ \sigma_3=\infty)=\pi\cosh\ (\pi-\theta)x\ \operatorname{csch}\ \pi x; \qquad \cos\theta=k_2.$ (49)

For $h=3$: $\alpha_n=\pm\dfrac{i}{2}\cos^{-1}(1+k_2)/2+n\pi i; \qquad b_n=\dfrac{1+k_2}{3+k_2}; \qquad \alpha_n=(2n+1)\pi i/2; \qquad b_n=\dfrac{1-k_2}{3+k_2}$

and $$\Phi'(h=3,\ \sigma_3=\infty)=\frac{\pi(1-k_2)}{3+k_2}\operatorname{csch}\ \pi x+\frac{2\pi(1+k_2)}{3+k_2}\cosh\ (\pi-\theta)x\ \operatorname{csch}\ \pi x, \quad (50)$$

where $\cos\theta=(1+k_2)/2$.

Finally, for $h=4$: $\alpha_n=\pm\dfrac{i}{2}\cos^{-1}\left\{\dfrac{k_2+(k_2^2+8)^{\frac{1}{2}}}{4}\right\}+n\pi i : b_n=\dfrac{3k_2+(k_2^2+8)^{\frac{1}{2}}}{4(k_2^2+8)^{\frac{1}{2}}},$

$$\alpha_n=\pm\frac{i}{2}\cos^{-1}\left\{\frac{k_2-(k_2^2+8)^{\frac{1}{2}}}{4}\right\}+n\pi i\ ; b_n=\frac{-3k_2+(k_2^2+8)^{\frac{1}{2}}}{4(k_2^2+8)^{\frac{1}{2}}},$$

and

$$\Phi'(h=4,\ \sigma_3=\infty)=\frac{\pi\ \mathrm{csch}\ \pi x}{2(k_2^2+8)^{\frac{1}{2}}}\{(3k_2+(k_2^2+8)^{\frac{1}{2}})\cosh(\pi-\theta_1)x+(-3k_2+(k_2^2+8)^{\frac{1}{2}})\cosh(\pi-\theta_2)x\},\quad(51)$$

where $$\theta_1=\cos^{-1}\left\{\frac{k_2+(k_2^2+8)^{\frac{1}{2}}}{4}\right\};\qquad \theta_2=\cos^{-1}\left\{\frac{k_2-(k_2^2+8)^{\frac{1}{2}}}{4}\right\}.$$

Here, too, the Eqs. (49), (50) and (51) reduce to the appropriate 2 layer earth expressions of Eqs. (18) and (19). For $k_2=1$, they reduce to the value of Eq. (19) for a 2 layer earth with a lower layer of zero conductivity and for $k_2=0,\ -1$ to that of Eq. (18), or its equivalent, for a 2 layer earth with a lower layer of infinitely high conductivity.

In a similar manner the surface gradients for other values of h may be obtained by first solving Eqs. (38) and (45) for the α_n, determining the b_n by Eqs. (40) and (47) and finally $\Phi'(x)$ by Eqs. (41) and (48). For rational values of h the series of Eqs. (41) and (48) will always be summable as groups of geometric series; when h is not rational the series will still converge rapidly even though they may not be summable in closed form.

The same methods as used here can evidently be also extended to the case of systems with more than 3 layers. While it may be more difficult to prove, it will undoubtedly be found that the corresponding $f(\alpha)$ will again have only imaginary singularities when one of the layers has a vanishing or infinite conductivity, and hence give rise to surface gradients which vanish exponentially if there is present a layer of infinite conductivity, or which exponentially approach constancy if one of the layers has a vanishing conductivity. Eq. (24) will be valid in any case, except for the correction indicated in the footnote when $f(0)=\infty$.

The analytical results derived above are illustrated in Figs. 4, 5, 6, 7 and 8. In Fig. 4 the surface gradients multiplied by the distance from the current source are plotted against the latter for three layer earths for which $\sigma_1=\sigma_3$ and $\sigma_1/\sigma_2=\frac{1}{5}$, 5, with $h_2/h_1=2$. For small x, Eq. (35) was used with the terms for $n=1,\ 2,\ 3,\ 4$ summed out separately, s_1, s_2 being real for $\sigma_2=5\sigma_1$ and complex for $\sigma_1=5\sigma_2$. For large x the extension of Eq. (32) was quite satisfactory for $\sigma_1=5\sigma_2$. In the case of $\sigma_2=5\sigma_1$, how-

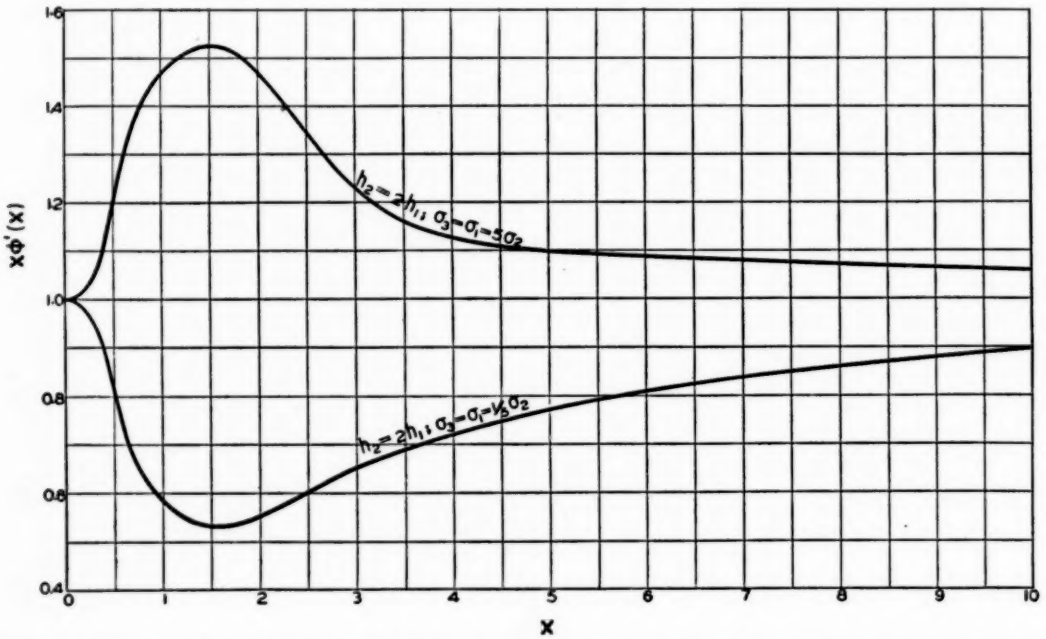

FIG. 4. Surface gradients for the case of a slab of thickness equal to that of the top layer, immersed in an otherwise homogeneous earth. Notation same as in Fig. 3.

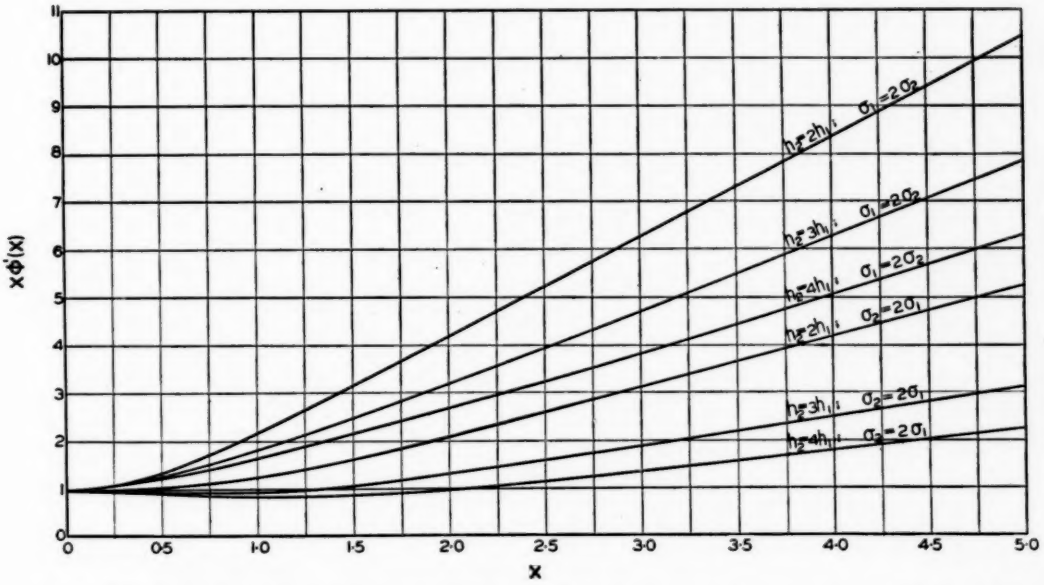

FIG. 5. Surface gradients for a three layer earth in which the lowest layer has a zero conductivity and the conductivity ratios of the two upper layers are 1 : 2 and 2 : 1. h_1 = thickness of surface layer; $h_2 - h_1$ = thickness of second layer; x = (horizontal distance from electrode)/$2h_1$.

ever, the analog of Eq. (20):

$$x\Phi' = \frac{k_2(1-1/s_1)}{[k_2^2(1-k_3)^2+4k_3]^{\frac{1}{2}}}\left[\sum_0^\infty m\frac{(-1)^m}{(2x)^{2m}}\frac{\partial^{2m}}{\partial\gamma_1^{2m}}\left\{\operatorname{ctnh}\gamma_1-\frac{1}{\gamma_1}\right\}+2x\left\{\sin 2x\gamma_1 Ci(2x\gamma_1)\right.\right.$$

$$\left.\left.+\cos 2x\gamma_1(\pi/2-Si(2x\gamma_1))\right\}\right]-\frac{k_2(1-1/s_2)}{[k_2^2(1-k_3)^2+4k_3]^{\frac{1}{2}}}\sum_0^\infty\frac{(-1)^m}{(2x)^{2m}}\frac{\partial^{2m}}{\partial\gamma_2^{2m}}(\operatorname{ctnh}\gamma_2) \quad (52)$$

was found very satisfactory, s_1, s_2, γ_1 and γ_2 being defined by Eqs. (34). Curves of $x\Phi'$ for 3 layer earths with lowest layer of zero or infinite conductivity and $h=2$, 3, 4 and $\sigma_1/\sigma_2=\frac{1}{5}$, $\frac{1}{2}$, 2, 5, are given in Figs. 5–8. Those for $\sigma_3=\infty$ are very similar to the corresponding ones for $x\Phi$ for the point electrode (cf. Figs. 8 and 9 in *I*) except that here the $x\Phi'$ curves have horizontal tangents at $x=0$. In the case of $\sigma_3=0$ the values of $x\Phi'$ are all positive and approach the asymptotic forms:

$$x\Phi'(\sigma_3=0)\to\frac{\pi x}{1+(h-1)\sigma_2/\sigma_1}; \qquad h=h_2/h_1, \quad (53)$$

while the Φ for the point electrode decrease monotonically and approach $-\infty$ logarithmically. Here, too, as will also be true in the general case,—as follows from Eq. (21)—the curves for $x\Phi'$ have vanishing slopes for $x=0$.

III. Direct Interpretation Problem for Continuously Varying Conductivities

To complete the discussion of the problem of the infinitely extended line electrode we shall briefly outline, following Slichter's[2] analysis for the point electrode, the solution to the direct interpretation problem. Thus for the general continuously varying conductivity σ_y and uniform horizontal conductivity σ_x, the fundamental solutions for the potential distribution are of the form:

$$\Phi(x, y)=Y_1(y, \alpha)\begin{Bmatrix}\cos\\ \sin\end{Bmatrix}\alpha x, \quad (54)$$

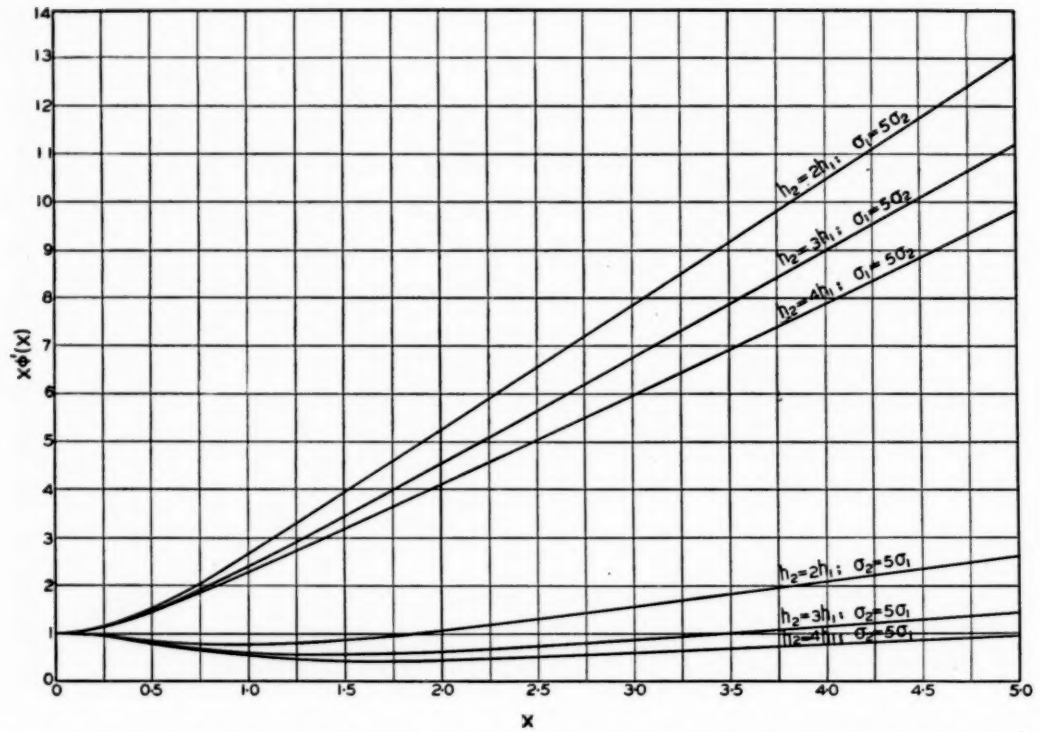

FIG. 6. Surface gradients for a three layer earth in which the lowest layer has a zero conductivity and the conductivity ratios of the two upper layers are 1 : 5 and 5 : 1.

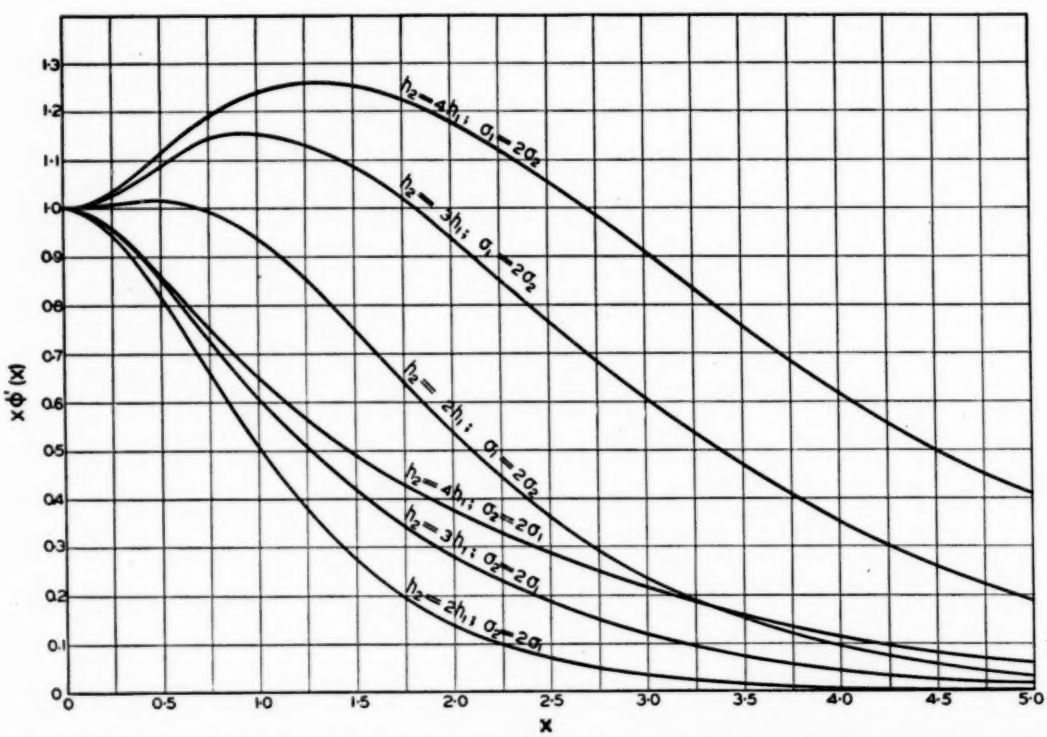

FIG. 7. Surface gradients for a three layer earth in which the lowest layer has an infinite conductivity and the conductivity ratios of the two upper layers are 1 : 2 and 2 : 1.

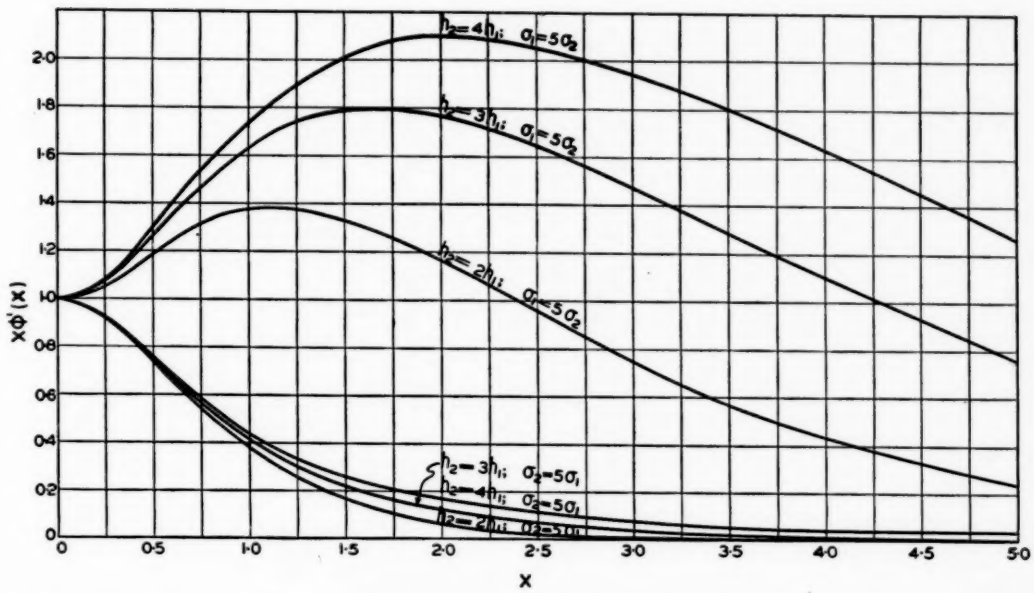

FIG. 8. Surface gradients for a three layer earth in which the lowest layer has an infinite conductivity and the conductivity ratios of the two upper layers are 1 : 5 and 5 : 1.

where Y_1 is the solution vanishing at infinity which satisfies the equation:

$$Y_1''+(\sigma_y'/\sigma_y)\,Y_1'-(\sigma_x/\sigma_y)\alpha^2 Y_1=0. \tag{55}$$

Replacing now the cable by an infinite flat strip of width $2a$ at the center of which the potential is Φ_0, and which is the source of a current of strength C per unit length, the potential distribution will be:

$$\Phi=\Phi_0+\frac{C}{\pi a\sigma_y(0)}\int_0^\infty \frac{\sin a\alpha}{\alpha}\left[\frac{Y_1(0,\alpha)}{\dot{Y}_1(0,\alpha)}-\frac{\cos x\alpha\, Y_1(y,\alpha)}{\dot{Y}_1(0,\alpha)}\right]d\alpha. \tag{56}$$

The surface gradients are, therefore:

$$\Phi'(x)=\frac{C}{\pi a\sigma_y(0)}\int_0^\infty \frac{\sin a\alpha\, Y_1(0,\alpha)\sin x\alpha}{\dot{Y}_1(0,\alpha)}d\alpha, \tag{57}$$

which, being a Fourier integral, may be inverted as:

$$k(\alpha)\equiv-\frac{\alpha Y_1(0,\alpha)}{\dot{Y}_1(0,\alpha)}=\frac{-2a\alpha\sigma_y}{C\sin a\alpha}\int_0^\infty \Phi'(x)\sin\alpha x\,dx. \tag{58}$$

Thus here, the "kernel" $k(\alpha)$—in Slichter's notation—can be found by integrating the surface gradients $\Phi'(x)$ as a Fourier integral, whereas for the point electrode the determination of $k(\alpha)$ required a Bessel function integration over the surface potential itself. Knowing $k(\alpha)$, the conductivity $\sigma_y(y)$ is then given by the Slichter-Langer theory in the form:

$$\sigma_y(y)=\sigma_0 e^{-2\int_0^y \alpha_1(y)\,dy}, \tag{59}$$

where $\alpha_1(y)$ is to be considered as formed by a Taylor expansion with coefficients $\alpha_1^{(n)}(0)$ given by:

$$\alpha_1(0)=a_1; \qquad \alpha_1'(0)=-a_1^2+2a_2; \qquad \frac{\alpha_1''(0)}{2!}=a_1^3-2a_1a_2+2a_3, \qquad \text{etc.} \tag{60}$$

and the a's are to be obtained by expanding $k(\alpha)$ in the form:

$$k(\alpha)=1+a_1/\alpha+a_2/\alpha^2+\cdots. \tag{60a}$$

The writer is indebted to Mr. M. W. Meres for the numerical and graphical work of this paper and to the executives of the Gulf Research and Development Corporation for permission to publish it.

A Note on Mixed Boundary Value Problems in Logarithmic Potential Theory

MORRIS MUSKAT, *Gulf Research and Development Corporation, Pittsburgh*

(Received July 30, 1934)

A method is given for solving logarithmic potential problems in which the potential is preassigned over part of the boundary and the normal derivative over the remainder. A "mixed" Green's function is defined such that it vanishes over part of the boundary of interest and its normal derivative vanishes over the remainder, and the solution for the logarithmic potential is expressed in terms of this function and the boundary conditions by means of Green's theorem. Taking the case of the infinite quadrant as the "prototype" region the solutions for other regions such as the infinite half plane, infinite and semi-infinite strips, and the circle are obtained by mapping them on the infinite quadrant; these are illustrated by several specific examples.

ALTHOUGH methods of treatment are available for the solution of mixed boundary value logarithmic potential problems in which the normal derivative vanishes over part of the boundary and the potential has constant values over the remaining parts of the boundary[1] no detailed discussion seems to have been given[2] of the corresponding problems in which the normal derivatives and potentials are preassigned arbitrarily. Thus even the simple case in which the potential is specified over the right half of the x axis and the normal derivative over the left half, does not seem to be solvable by the methods given in the standard texts. In the following, a method will be given for treating such problems, when restricted to two dimensions.

The principle of the method is simply based upon a combination of the theories of Green's functions and conjugate function transformations both of which have found wide applications in the discussion of the Dirichlet and Neumann potential problems. The Green's function used here will, however, be a "mixed" function rather than those employed heretofore. It is by the introduction of this type of function that the simple results obtainable by the method of conjugate functions alone[1] can be generalized, as will be seen presently.

Thus from the Green's theorems for two dimensions it is readily shown that the potential function $v(x, y)$ within a contour Γ may be expressed in terms of the boundary values of v and its normal derivative by the equation:

$$2\pi v(x, y)=\int_\Gamma\left[v(x', y')\frac{\partial G(x, y; x', y')}{\partial n}-G(x, y; x', y')\frac{\partial v(x', y')}{\partial n}\right]ds, \quad (1)$$

where (x', y') represents a point on Γ, n is the exterior normal and G is a function of the point pair (x', y') and (x, y) and harmonic in each except at the point $(x, y)=(x', y')$ where it has a logarithmic singularity.

If now the countour Γ be separated into two parts Γ_1 and Γ_2 and G is chosen so that:

$$G=0, \text{ on } \Gamma_1; \quad \partial G/\partial n=0, \text{ on } \Gamma_2, \quad (2)$$

G may be defined as the "mixed" Green's function for the contour Γ divided into Γ_1 and Γ_2. Eq. (1) becomes then:

$$v(x, y)=\frac{1}{2\pi}\int_{\Gamma_1} v\frac{\partial G}{\partial n}ds-\frac{1}{2\pi}\int_{\Gamma_2} G\frac{\partial v}{\partial n}ds, \quad (3)^2$$

so that if G has been found, the value of v at

[1] J. Jeans, *Electricity and Magnetism*, p. 352, 5th ed.

[2] The writer is indebted to Professor H. Bateman for calling to his attention a series of papers on the present problem by Carl Neumann in the *Leipziger Berichte*, Math. Phys. Klasse **61**, 156 (1909). In the first paper of this series Neumann outlines two methods for the treatment of the mixed boundary value problem; one of these consists in the reduction of the general case to that in which $\partial v/\partial n$ is a constant on Γ_2; the other is essentially identical with that given here, and Neumann sets up an equation equivalent to Eq. (3). However, he gives no applications or discussion of his equivalent of Eq. (3), although in the later papers of the series he develops his first method at great length after interpreting the reduced problem as that of finding the charge distribution on the segment Γ_2, taken as a conductor, induced by an appropriately chosen external charge distribution. While several cases of the reduced problem are solved by Neumann by this latter method, the analysis required is not only much more complex than that invclved in the method developed here, but moreover, the process of "reducing" the original problem requires the preliminary solution of the "Neumann" problem for the contour Γ with $\partial v/\partial n$ having the value 0 on Γ_1 and its original value on Γ_2.

(x, y) may be computed from a knowledge of v on Γ_1 and of $\partial v/\partial n$ on Γ_2.

Γ_1 and Γ_2 may, of course, be themselves composed of several segments and Eq. (3) will still remain valid. Furthermore, the contour may be finite, or infinite and bound infinite regions. The rigorous proof of these features as well as further properties of G, such as its symmetry in (x, y) and (x', y'), may be carried through by the methods already developed for the study of the ordinary Green's functions, and will not be reproduced here.

The problem that remains is the determination of G. This will be accomplished by first setting up G for simple regions and then treating more complicated systems by mapping them on the "prototype" regions by means of conjugate function transformations.

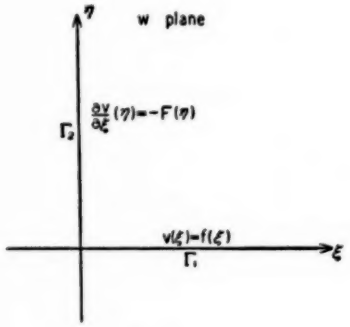

FIG. 1.

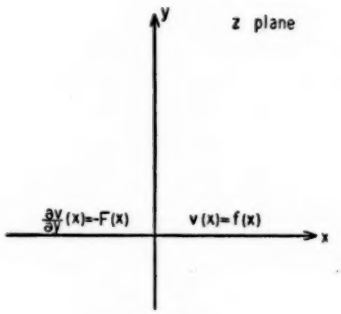

FIG. 2.

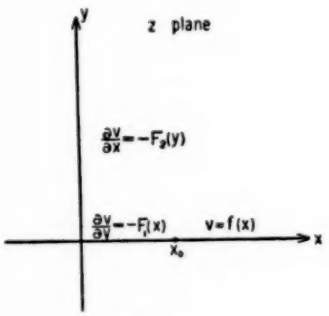

FIG. 3.

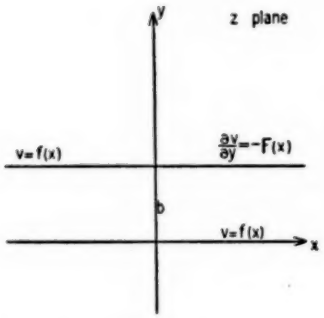

FIG. 4.

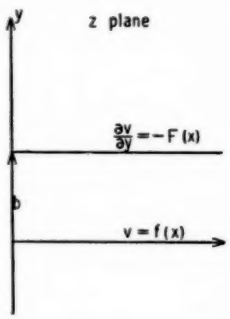

FIG. 5.

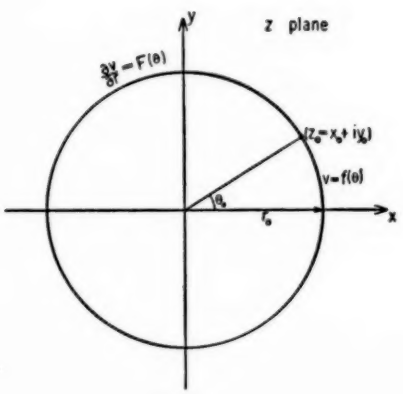

FIG. 6.

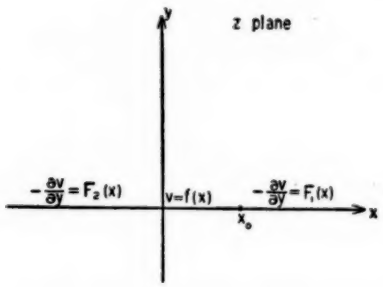

FIG. 7.

A. Γ_1 and Γ_2 Are Single Segments

(1) The infinite quadrant

The prototype for regions in which Γ_1 and Γ_2 are each composed of single segments will be taken as the infinite quadrant for which G can be found by a simple superposition of two source and two sink potentials.

Denoting the plane for the infinite quadrant as the "w plane" where $w=\xi+i\eta$ and taking for Γ_1, Γ_2 the positive ξ and η axes (cf. Fig. 1) we have here at once:

$$G=\tfrac{1}{2}\log\frac{\{(\xi_0-\xi)^2+(\eta_0-\eta)^2\}\{(\xi_0+\xi)^2+(\eta_0-\eta)^2\}}{\{(\xi_0-\xi)^2+(\eta_0+\eta)^2\}\{(\xi_0+\xi)^2+(\eta_0+\eta)^2\}}, \tag{4}$$

so that:

$$v(\xi,\eta)=\frac{\eta}{\pi}\int_0^\infty f(\xi_0)\left\{\frac{1}{(\xi_0-\xi)^2+\eta^2}+\frac{1}{(\xi_0+\xi)^2+\eta^2}\right\}d\xi_0-\frac{1}{2\pi}\int_0^\infty F(\eta_0)\log\frac{\xi^2+(\eta_0-\eta)^2}{\xi^2+(\eta_0+\eta)^2}d\eta_0, \tag{5}$$

where here and below $f(\xi)$ and $F(\eta)$ denote the values of v and $\partial v/\partial n$ on Γ_1 and Γ_2.

If: $$F(\eta_0)=0; \qquad f(\xi_0)=v_0, \tag{6}$$

Eq. (5) gives at once $$v=v_0, \tag{7}$$

which is here but a special case of the general proposition, easily proved by Eq. (1) and obvious physically, that if the potential is constant over part of the boundary of any region, and if the normal derivative vanishes over the remainder, the potential must be constant everywhere within the region.

(2) Infinite half plane (Fig. 2)

Choosing the origin at the division between Γ_1 and Γ_2 we have for the general boundary conditions:

$$v=f(x)\ :\ y=0,\quad x>0; \qquad -\partial v/\partial y=F(x),\quad y=0,\quad x<0. \tag{8}$$

We now transform to the w plane of Fig. (1) by means of:

$$z=x+iy=w^2=(\xi+i\eta)^2, \tag{9}$$

so that: $$\Gamma_1: y=0,\quad x>0\rightarrow\eta=0; \qquad \Gamma_2: y=0,\quad x<0\rightarrow\xi=0; \qquad f(x)\rightarrow f(\xi^2);$$
$$F(x)\rightarrow 2\eta F(-\eta^2). \tag{10}$$

Putting these in Eq. (5), evaluating the integrals and returning to the z plane by means of Eq. (9), the result will be the solution to the original problem of Eq. (8). Furthermore, on inserting Eqs. (9) into the G of Eq. (4), the Green's function for the half plane will be obtained in terms of (x, y).

As a first example we shall take the case:

$$f(x)=v_0; \quad F(x)\begin{matrix}=u_0\ :\ x>-a^2\\ =0\ \ :\ x<-a^2\end{matrix}\Big\}. \tag{11}$$

Then:

$$v(\xi,\eta)=\frac{\eta v_0}{\pi}\int_0^\infty\left\{\frac{1}{(\xi_0-\xi)^2+\eta^2}+\frac{1}{(\xi_0+\xi)^2+\eta^2}\right\}d\xi_0-\frac{u_0}{\pi}\int_0^a\eta_0\log\frac{\xi^2+(\eta_0-\eta)^2}{\xi^2+(\eta_0+\eta)^2}d\eta_0$$
$$=v_0+\frac{u_0}{2\pi}\left[4a\eta+(\xi^2+a^2-\eta^2)\log\frac{\xi^2+(a+\eta)^2}{\xi^2+(a-\eta)^2}-4\eta\xi\tan^{-1}\frac{2a\xi}{\xi^2+\eta^2-a^2}\right]. \tag{12}$$

On returning to the z plane by means of Eq. (9) the solution v will be obtained, explicitly in terms of (x, y). Thus for the negative x axis ($\xi=0$) we find:

$$v(x<0,\ y=0)=v_0+\frac{u_0}{2\pi}\left[4a\sqrt{-x}+(a^2+x)\log\left(\frac{a+\sqrt{-x}}{a-\sqrt{-x}}\right)^2\right]. \tag{13}$$

As another example we may consider the case:

$$f(x)=v_0; \qquad F(x)=u_0/x. \tag{14}$$

The solution for v then takes the form:

$$v(\xi,\ \eta)=\frac{\eta v_0}{\pi}\int_0^\infty\left\{\frac{1}{(\xi_0-\xi)^2+\eta^2}+\frac{1}{(\xi_0+\xi)^2+\eta^2}\right\}d\xi_0+\frac{u_0}{\pi}\int_0^\infty\frac{1}{\eta_0}\log\frac{\xi^2+(\eta_0-\eta)^2}{\xi^2+(\eta_0+\eta)^2}d\eta_0$$

$$=v_0-u_0\pi+2u_0\tan^{-1}\xi/\eta=v_0-u_0\theta, \tag{15}$$

where θ is the polar angle.

This result can be readily checked by elementary means, as the system is simply the conjugate of that of a perfect radial potential distribution in which the equipotentials are circles about the origin and the streamlines or line of forces are the radii vectors.

(3) Infinite quadrant with v or $\partial v/\partial n$ given over parts of both axes

This system (cf. Fig. 3) may be transformed to the normal quadrant distribution by the relation:

$$w^2=(\xi+i\eta)^2=(x+iy)^2-x_0^2, \tag{16}$$

so that the region where F is given goes into the $+\eta$ axis and the boundary where f is known goes into the $+\xi$ axis. The resulting distribution will be given by:

$$v(\xi,\ \eta)=\frac{\eta}{\pi}\int_0^\infty f\{(\xi_0^2+x_0^2)^{\frac{1}{2}}\}\left\{\frac{1}{(\xi_0-\xi)^2+\eta^2}+\frac{1}{(\xi_0+\xi)^2+\eta^2}\right\}d\xi_0-\frac{1}{2\pi}\int_0^{x_0}\frac{\eta_0}{(x_0^2-\eta_0^2)^{\frac{1}{2}}}F_1\{(x_0^2-\eta_0^2)^{\frac{1}{2}}\}\log$$

$$\times\frac{\xi^2+(\eta_0-\eta)^2}{\xi^2+(\eta_0+\eta)^2}d\eta_0-\frac{1}{2\pi}\int_{x_0}^\infty\frac{\eta_0}{(\eta_0^2-x_0^2)^{\frac{1}{2}}}F_2\{(\eta_0^2-x_0^2)^{\frac{1}{2}}\}\log\frac{\xi^2+(\eta_0-\eta)^2}{\xi^2+(\eta_0+\eta)^2}d\eta_0 \tag{17}$$

where the meanings of F_1 and F_2 are indicated in Fig. 3.

(4) Infinite strip

If $\partial v/\partial y$ is given over the whole of $y=b$, the Green's function may be given directly in terms of (x, y) as:

$$G=\tfrac{1}{2}\log\frac{\{\cosh\pi(x-x_0)/2b-\cos\pi(y-y_0)/2b\}\{\cosh\pi(x-x_0)/2b+\cos\pi(y+y_0)/2b\}}{\{\cosh\pi(x-x_0)/2b-\cos\pi(y+y_0)/2b\}\{\cosh\pi(x-x_0)/2b+\cos\pi(y-y_0)/2b\}}. \tag{18}$$

When, however, $\partial v/\partial y$ is given over only part of $y=b$, the y axis may be set so as to go through the division point (cf. Fig. 4) and then the system can be mapped on the quadrant of Fig. 1 by the transformation:

$$(\xi+i\eta)^2=e^{\pi z/b}+1, \tag{19}$$

the region of $x<0$, $y=b$, being mapped on the segment $\eta=0$, $0\leqslant\xi\leqslant1$. Furthermore, for $\xi=0$:

$$\partial v/\partial\xi=(-2b\eta/\pi(\eta^2+1))(\partial v/\partial y). \tag{20}$$

As an example we shall take the case:

$$v=v_1; \qquad y=0; \qquad v=v_2: y=b, \quad x<0; \qquad \partial v/\partial y=0, \quad y=b, \quad x>0. \tag{21}$$

Eq. (5) gives:

$$v(\xi,\eta)=\frac{\eta v_1}{\pi}\int_1^\infty\left\{\frac{1}{(\xi_0-\xi)^2+\eta^2}+\frac{1}{(\xi_0+\xi)^2+\eta^2}\right\}d\xi_0+\frac{\eta v_2}{\pi}\int_0^1\left\{\frac{1}{(\xi_0-\xi)^2+\eta^2}+\frac{1}{(\xi_0+\xi)^2+\eta^2}\right\}d\xi_0$$

$$=v_1+\frac{v_2-v_1}{\pi}\tan^{-1}\frac{2\eta}{\eta^2+\xi^2-1}$$

$$=v_1+[(v_2-v_1)/\pi]\cos^{-1}\{|((e^{-\pi x/b}+\cos\pi y/b)^2+\sin^2\pi y/b)^{\frac{1}{2}}|-e^{-\pi x/b}\}. \tag{22}$$

(5) Semi-infinite strip (cf. Fig. 5)

If v is given only along $y=0$ for $x\geqslant x_0$ the transformation to the w plane of Fig. 1 is made by:

$$(\xi+i\eta)^2=\cosh\pi(x+iy)/b-\cosh\pi x_0/b. \tag{23}$$

If v is given for all $x>0$, $y=0$, and $x=0$, $0\leqslant y\leqslant y_0$, then:

$$(\xi+i\eta)^2=\cosh\pi(x+iy)/b-\cos\pi y_0/b. \tag{24}$$

Finally, if v is preassigned over the whole boundary except for $y=b$, $x>x_0$, the transformation equation is:

$$(\xi+i\eta)^2=\cosh\pi(x+iy)/b+\cosh\pi x_0/b. \tag{25}$$

The rest of the procedure is exactly similar to that given for the other cases.

If x_0 or y_0 in Eqs. (23) or (24) is zero the Green's function may be obtained directly in terms of (x, y) by adding to the G of Eq. (18) a term exactly the same as given there except for a change in the sign in x_0; and if x_0 in Eq. (25) is zero the above term should be subtracted from that in Eq. (18) to get G directly in terms of (x, y).

As the problem of the closed rectangle would require elliptic integral transformations except when the point of separation between Γ_1 and Γ_2 coincides with one of the corners, and as the resulting integrals as in Eq. (5) would be in general intractable except by graphical treatment, this case will not be analyzed further.

(6) Circle (cf. Fig. 6)

The general boundary conditions may be written as:

$$v=f(\theta):0\leqslant\theta\leqslant\theta_0:\partial v/\partial r=F(\theta);\qquad\theta_0\leqslant\theta\leqslant 2\pi. \tag{26}$$

The transformation to the infinite quadrant is accomplished by setting:

$$(\xi+i\eta)^2=i(z_0+z)/(z_0-z)-\operatorname{ctn}\theta_0/2, \tag{27}$$

which, in polar coordinates, is equivalent to:

$$\xi^2-\eta^2=\frac{2rr_0\sin(\theta_0-\theta)}{r_0^2+r^2-2rr_0\cos(\theta_0-\theta)}-\operatorname{ctn}\theta_0/2;\qquad 2\xi\eta=\frac{r_0^2-r^2}{r_0^2+r^2-2rr_0\cos(\theta_0-\theta)}, \tag{27a}$$

so that:

$$\left(\frac{\partial v}{\partial\xi}\right)_{\xi=0}=\frac{-4r_0\eta}{\eta^4-2\eta^2\operatorname{ctn}\theta_0/2+\csc^2\theta_0/2}\left(\frac{\partial v}{\partial r}\right)_{r=r_0}. \tag{27b}$$

As an example we shall take the case: $f(\theta)=v_0$; $\quad F(\theta)=u_0$. (28)

We then get:

$$v(\xi,\eta)=v_0-\frac{2r_0u_0}{\pi}\int_0^{\infty}\frac{\eta_0}{\eta_0^4-2\eta_0^2\operatorname{ctn}\theta_0/2+\csc^2\theta_0/2}\log\frac{\xi^2+(\eta_0-\eta)^2}{\xi^2+(\eta_0+\eta)^2}d\eta_0$$

$$=v_0-\frac{2r_0u_0}{\beta^2-\alpha^2}\left[\tan^{-1}\frac{\eta^2+\xi^2-\beta^2}{2\eta\beta}-\tan^{-1}\frac{\eta^2+\xi^2-\alpha^2}{2\eta\alpha}+\tan^{-1}\frac{2\eta\xi}{\eta^2+\alpha^2-\xi^2}-\tan^{-1}\frac{2\eta\xi}{\eta^2+\beta^2-\xi^2}\right], \tag{29}$$

where:
$$\eta_0^4-2\eta_0^2\operatorname{ctn}\theta_0/2+\csc^2\theta_0/2=(\eta_0^2+\alpha^2)(\eta_0^2+\beta^2). \tag{29a}$$

B. Either Γ_1 or Γ_2 Consists of Two Separate Segments

It will suffice for the present purpose to exhibit the transformation for the treatment of the single case of the infinite half plane, as all the others presented in Section A may be readily reduced to this problem.

Thus if, as indicated in Fig. 7, the region: $0\leqslant x\leqslant x_0$ is that in which v is given whereas $\partial v/\partial y$ is preassigned over the remainder of the x axis we may again transform to the w plane quadrant of Fig. 1 by the transormation:

$$(\xi+i\eta)^2=z/(x_0-z), \tag{30}$$

the region $x>x_0$ mapping onto the η axis with $1\leqslant\eta\leqslant\infty$ and the negative x axis mapping on the rest of the positive η axis. The procedure now may be carried through in exactly the same manner as for the cases of Section A.

When both Γ_1 and Γ_2 consist of two separate segments, the infinite quadrant prototype of the w plane must be replaced by a finite rectangle. The given boundary may be mapped on the rectangle by means of an elliptic function transformation and then, as before, one may apply the Green's function for this simpler system, namely:

$$G(\xi,\eta)$$
$$=\tfrac{1}{2}\sum_{-\infty}^{+\infty}\log\frac{\{\cosh\pi(\xi-2na-\xi_0)/b-\cos\pi(\eta-\eta_0)/b\}\{\cosh\pi(\xi-2na+\xi_0)/b-\cos\pi(\eta-\eta_0)/b\}}{\{\cosh\pi(\xi-2na-\xi_0)/b-\cos\pi(\eta+\eta_0)/b\}\{\cosh\pi(\xi-2na+\xi_0)/b-\cos\pi(\eta+\eta_0)/b\}}, \tag{31}$$

where it has been supposed that the segments Γ_1 are mapped on to: $0\leqslant\xi\leqslant a$, $\eta=0, b$, and the segments Γ_2 to : $0\leqslant\eta\leqslant b$, $\xi=0, a$.

Insofar as the boundary of any given geometrical region can be mapped on one of the simpler types treated above, and its parts Γ_1 and Γ_2 do not contain more segments than permit a reasonably direct development of the Green's function for the appropriate prototype boundary, the above method will give the solutions to the "mixed" problems for those regions. Furthermore, it may be observed that with obvious changes Eq. (3) may also be applied to three dimensional systems, although its application to three dimensional problems suffers from the difficulty that there is no three dimensional analog of the conjugate function transformations, so that different Green's functions have to be obtained explicitly for each different type of boundary.

In addition to those problems occurring in electrical conduction in which the boundary values of the potential or its normal derivatives are usually constants, the mixed boundary value problem arises in the treatment of the irrotational motion of bodies in ideal liquids, in which the normal derivative is specified over the surface of the moving body and the potential itself at infinity. Heat conduction systems may also involve the mixed boundary value problem of the type treated here, if the surface radiation is arbitrarily specified and does not obey the Newtonian law of cooling. Finally, as suggested by Professor Bateman, it is likely that mixed boundary value problems in plane elastic theory, though governed by the biharmonic equation, may be reduced to equivalent problems in the logarithmic potential. The writer plans to return to this question at a later time.

The writer wishes to thank Professor H. Bateman for reading the original manuscript of this paper and for his many helpful suggestions, and Dr. P. D. Foote of this Laboratory for the permission to publish it.

On Electric Charges of Disperse Systems Which Are the Seats of Physico-Chemical Reactions

N. RASHEVSKY, *Department of Physiology, University of Chicago*

(Received August 14, 1934)

In a number of previous papers a mathematical study was made of small drops, which either absorb or produce some substances by virtue of physico-chemical reactions. This creates in the drop and in the surrounding medium gradients of concentrations of corresponding substances. In this note it is pointed out that when the reacting substances are ionized, these gradients will result in the appearance of electric charges and electric fields. An estimation shows that they are quite comparable with electric charges, produced by other factors in disperse systems. The fundamental property of the charges here considered is that they disappear as soon as the reactions cease. Their importance in biological systems is pointed out.

THE question of electric charges of disperse systems has been a matter of much study. A variety of factors are involved in their production, such as the Donnan equilibria, the selective adsorption of ions, etc. All those factors are however of *static* nature. We wish to point out here another factor, of a *dynamic* nature, which must be present whenever physico-chemical reactions take place within a small liquid particle and when these reactions involve ionized substances. In a number of previous papers,[1] we have studied such systems and seen, that those reactions produce gradients of concentrations both within and without the system. Those gradients are determined by the rate of reaction, the diffusion constants and the permeability of the drop-surface. If the substances involved are ions, then the gradients of concentrations of ions of different nature will be different, and this will result in the appearance of free electric charges, though of course the sum total of all charges in the system will be zero.

Consider the simplest case, that of two kinds of monovalent ions of opposite sign, present in equal amounts per unit volume in the surrounding medium at an infinite distance from the drop. And let the numbers of ions of both kinds, which disappear per unit time per cm³ due to the reactions, be the same. For no charges can be *created* by the reactions themselves. The appearance of electric charges will produce an electric field, given for a case of spherical symmetry by $d\varphi/dr$, φ being the electrostatic potential. This field will affect the diffusion process of the ions. If c_+ denotes the number of positive ions per cm³ and α_+ their mobility then instead of the ordinary diffusion equation we have, in polar coordinates, for a quasi-stationary state, as studied before:

$$D_+^i\left(\frac{d^2c_+^i}{dr^2}+\frac{2}{r}\frac{dc_+^i}{dr}\right)+\alpha_+^i\epsilon\frac{d\varphi}{dr}\left(\frac{dc_+^i}{dr}+2c_+^i/r\right)-q=0, \quad (1)$$

for the inside of the drop, and

$$D_+^e\left(\frac{d^2c_+^e}{dr^2}+\frac{2}{r}\frac{dc_+^e}{dr}\right)+\alpha_+^e\epsilon\frac{d\varphi}{dr}\left(\frac{dc_+^e}{dr}+c_+^e\right)=0, \quad (2)$$

for the outside, and corresponding equations for c_-, the concentrations of negative ions.

Further we have Poisson's equation:

$$(d^2\varphi/dr^2)+2(d\varphi/dr)/r=-(4\pi\epsilon/K)(c_+-c_-), \quad (3)$$

ϵ being the electronic charge, K the dielectric constant of the medium (it will in general be different one inside and outside of the drop).

At the boundary, for $r=r_0$, we have:

$$D_+\frac{dc_+^i}{dr}=\left(h-\epsilon\frac{d\varphi}{dr}\right)(c_+^e-c_+^i)=D_+^e\frac{dc_+^e}{dr}, \quad (4)$$

which, together with similar expressions for c_-^i and c_-^e, and with the requirement of continuity of φ and $d\varphi/dr$ at $r=r_0$, determines the problem completely.

The treatment of this problem presents even in this simplest case very great difficulties because of the non-linearity of the differential equations. We shall here restrict ourselves only to a rough evaluation of the charges, which may thus be produced, by considering the case

[1] N. Rashevsky, Physics **1**, 143 (1931), **2**, 303 (1932).

of $D_+^i = D_+^e = D_-^i = D_-^e = \infty$ and by neglecting the effects of the electric field on the diffusion process. We then have a uniform concentration of ions both inside and outside of the drop, and only a discontinuity at the surface. The concentrations c_+ and c_- inside are now determined by the condition that for a quasi-stationary state the amounts diffusing through the surface are equal to the amounts destroyed by the reactions. Hence:

$$\text{and} \qquad \begin{aligned} 4\pi r_0^2 h_+(c_0 - c_+) &= 4\pi r_0^3 q/3, \\ 4\pi r_0^2 h_-(c_0 - c_-) &= 4\pi r_0^3 q/3, \end{aligned} \tag{5}$$

since we assumed $c_+^0 = c_-^0 = c_0$, and $q_+ = q_- = q$.

Eqs. (5) give:

$$c_+ = c_0 - qr_0/3h_+, \quad c_- = c_0 - qr_0/3h_-. \tag{6}$$

Hence the total charge of the drop:

$$E = \frac{4}{3}\pi r_0^3 \epsilon (c_+ - c_-) = \frac{4}{9}\pi r_0^4 q \epsilon \left(\frac{1}{h_+} - \frac{1}{h_-}\right). \tag{7}$$

One point must be discussed in connection with this argument. We assumed the outside concentrations of both ions the same, and the rates of their absorption equal. Yet we find, after the quasi-stationary state is reached, an excess of one of the ions inside, without any change outside. The apparent paradoxon is due to our assumption of an infinite supply of both kinds of ions in the outside medium, so that drawing a finite amount from it does not change c_0. Actually there is an equal but opposite charge $-E$ in the surrounding medium.

Unfortunately there are almost no data available in the biological literature, which would give us h in absolute units. At any rate there is good reason to believe, that for most ions $h < 10^{-4}$ cm·min.$^{-1}$. For 4×10^{-4} cm·min.$^{-1}$ is a plausible value for oxygen,[2] and the cell membrane is very highly permeable for the latter. Taking $q \sim 10^{-6}$ g·cm^{-3}·min.$^{-1} \sim 10^{16}$ ions·cm^{-3}·min.$^{-1}$, and assuming that h_+ differs *only* by 1 percent from h_-, we find for a cell with $r_0 \sim 10^{-3}$, and $h \sim 10^{-5}$ cm·min.$^{-1}$, a total charge of the order of $10^7\epsilon$. Under other conditions it may be much larger. A colloidal particle has usually a charge of about 10^{12} ions per cm^2 of surface,[3] which for $r_0 \sim 10^{-3}$ cm would give for the total charge about $10^7\epsilon$ also.

We thus see, that the dynamic charges considered here are *at least* of the same order of magnitude as the ordinary *static* charges of colloids. Their peculiar property is that they vanish with vanishing q, that is when the reactions for some reasons stop.

This may have a particular bearing on charges of living cells, which are definitely connected with the *life* of the latter. If $h_+ > h_-$ then the cell will be positive and a local increase of both h_+ and h_-, that is a local increase of general permeability will produce a local *negativity*. More detailed considerations of the biological implications of the above will be given elsewhere.

---

[2] N. Rashevsky, Protoplasma **20**, 125 (1933).
[3] A. Gyemant, *Grundzuge der Kolloidphysik*, Vieweg, (1925).

The Mechanism of Division of Small Liquid Systems Which Are the Seats of Physico-Chemical Reactions

II. Instability of Two-Phase Systems

N. RASHEVSKY, *Department of Physiology, University of Chicago*

(Received October 19, 1934)

In continuation of a previous paper, the same mathematical method is applied to a system, consisting of two spherical concentric drops, under the assumption, that a reaction takes place only in the outer larger drop, but not in the inner one. It is found, however, that even in that case the inner drop may become unstable for infinitesimal deformations, and spontaneously elongate.

IN a previous paper[1] we have investigated the mechanical stability of a drop under the action of such forces as result from the presence of concentration gradients, which gradients in their turn are produced by physico-chemical reactions, taking place inside the drop. We propose now to extend this investigation to more complex systems, consisting of two phases. In this paper we shall confine ourselves to the particular case of a system, consisting of two concentric spherical drops, of which only the external one is the seat of reactions, and we shall study the mechanical stability of the inner drop in such a system. On one hand this is one of the simplest cases of a two-phase system. On the other hand, as will be discussed elsewhere, this particular problem has some very interesting biological aspects.

The mathematical method used will be the same as before. We consider first an undeformed system. Let R_1 and R_2 be the radii of the inner and the outer drops, respectively. Let D_0, D_i and D_e denote the coefficient of diffusion in the inner drop, the outer drop and the surrounding medium, correspondingly. Let h_1 be the permeability of the surface of the inner drop, h_2—that of the outer; and let q be the rate of reaction per cm³ per minute, in the outer drop. Finally let c_0 be the concentration at infinite distance from the system.

We shall confine ourselves to the action of osmotic forces only. Other forces discussed in our previous paper[1] and depending on concentration gradients, are easily taken into account in the same manner as before.

Denoting by c_1, c_2 and c_3 the concentrations in the inner and outer phase and in the surrounding medium correspondingly, for a deformed drop we have to consider the sum of the osmotic potential RTc_1/M and of the osmotic pressure $RT(c_2-c_1)M$ at the surface of the inner drop. But this sum is equal to RTc_2/M. Hence we need concern ourselves only with values of c_2 at the surface of the inner phase.

For the case of spherical symmetry we have the differential equations:

$$\nabla^2 c^0=0; \quad D_i\nabla^2 c_i-q=0; \quad \nabla^2 c_e=0, \tag{1}$$

with the boundary conditions:

$$\begin{aligned}&\text{for } r=R_1: D_i(dc_i/dr)=h_1(c_i-c^0)=D_0(dc^0/dr),\\ &\text{for } r=R_2: D_i(dc_i/dr)=h_2(c_e-c_i)=D_e(dc_e/dr),\end{aligned} \tag{2}$$

where c^0, c_i and c_e stand for concentrations in the inner and outer phase, and the surrounding medium correspondingly.

This set of equations is satisfied by:

$$\begin{aligned}c^0&=c_0+\frac{qR_2}{3h_2}+\frac{q(R_2^2-R_1^2)}{6D_i}-\frac{qR_1^2}{3D_i}-\frac{qR_1^3(D_i-R_2h_2)}{3D_iR_2^2h_2}+\frac{q(R_2^3-R_1^3)}{3D_eR_2},\\ c_1&=c_0+\frac{qR_2}{3h_2}+\frac{q(R_2^2-r^2)}{6D_i}-\frac{qR_1^3}{3D_ir}-\frac{qR_1^3(D_i-R_2h_2)}{3D_iR_2^2h_2}+\frac{q(R_2^3-R_1^3)}{3D_eR_2},\\ c_e&=c_0+\frac{q(R_2^3-R_1^3)}{3D_e}\frac{1}{r}.\end{aligned} \tag{3}$$

[1] Rashevsky, Physics **5**, 374 (1934).

We consider a deformation of the inner drop given by

$$R=R_1+\Delta; \quad \Delta=\Delta_0\cos 2\theta. \tag{4}$$

At the deformed boundary we have, neglecting all higher powers of Δ:

$$\begin{aligned} &[c_i]_{R_1+\Delta}=[c_i]_{R_1}; \quad [dc_i/dr]_{R_1+\Delta}=-q\Delta/D_i; \\ &[c_i-c^0]_{R_1+\Delta}=0; \qquad [dc^0/dr]_{R_1+\Delta}=0. \end{aligned} \tag{5}$$

Hence:

$$\begin{aligned} &[D_0(dc^0/dr)-h_1(c_i-c^0)]_{R_1+\Delta}=0, \\ &[D_i(dc_i/dr)-h_1(c_i-c^0)]_{R_1+\Delta}=-q\Delta. \end{aligned} \tag{6}$$

If therefore we represent again,[1] the solution for the deformed drop by

$$c_1=c^0+c_1^*; \quad c_2=c_i+c_2^*; \quad c_3=c_e+c_3^*, \tag{7}$$

and require that

$$\nabla^2 c_1=0; \quad D_i\nabla^2 c_2-q=0; \quad \nabla^2 c_3=0,$$

and that moreover we have

$$\begin{aligned} &D_0(dc_1/dr)=h_1(c_2-c_1)=D_i(dc_2/dr) \\ &D_i(dc_2/dr)=h_2(c_3-c_2)=D_e(dc_3/dr) \end{aligned}$$

at the boundary of the inner and the outer drop, correspondingly, we find that c_1^*, c_2^* and c_3^* must satisfy the following differential equations and boundary conditions.

$$\nabla^2 c_1^*=0; \quad \nabla^2 c_2^*=0; \quad \nabla^2 c_3^*=0. \tag{8}$$

At the boundary of the inner drop:

$$\begin{aligned} &D_0(dc_1^*/dr)-h_1(c_2^*-c_1^*)=0, \\ &D_i(dc_2^*/dr)-h_1(c_2^*-c_1^*)=q\Delta. \end{aligned} \tag{9}$$

At the boundary of the outer drop:

$$\begin{aligned} &D_i(dc_2^*/dr)-h_2(c_3^*-c_2^*)=0, \\ &D_e(dc_3^*/dr)-h_2(c_3^*-c_2^*)=0. \end{aligned} \tag{10}$$

We use again dc/dr instead of $dc/d\nu$ (ν—normal), for they differ only by terms of the order of Δ^2.

Eqs. (8) are satisfied[1] by:

$$\begin{aligned} c_2^*&=\sum_0^\infty a_n r^n P_n(\theta), \\ c_2^*&=\sum_0^\infty (b_n r^n+p_n r^{-n-1})P_n(\theta), \\ c_3^*&=\sum_0^\infty s_n r^{-n-1}P_n(\theta). \end{aligned} \tag{11}$$

Introducing this into (9) and (10) and remembering (4), we find:

$$\sum_0^\infty \mathfrak{A}_n P_n(\theta)=0; \quad \sum_0^\infty \mathfrak{B}_n P_r(\theta)=q\Delta_0\cos 2\theta; \quad \sum_0^\infty \mathfrak{C}_n P_n(\theta)=0; \quad \sum_0^\infty \mathfrak{D}_n P_n(\theta)=0, \tag{12}$$

with

$$\begin{aligned} \mathfrak{A}_n&=D_0 n a_n R_1^{n-1}-h_1(b_n R_1^n+p_n R_1^{-n-1}-a_n R_1^n), \\ \mathfrak{B}_n&=D_i n b_n R_1^{n-1}-D_i(n+1)p_n R_1^{-n-2}-h_1(b_n R_1^n+p_n R_1^{-n-1}-a_n R_1^n), \\ \mathfrak{C}_n&=D_i n b_n R_2^{n-1}-D_i(n+1)p_n R_2^{-n-2}-h_2(s_n R_2^{-n-1}-b_n R_2^n-p_n R_2^{-n-1}), \\ \mathfrak{D}_n&=-D_e(n+1)s_n R_2^{-n-2}-h_2(s_n R_2^{-n-1}-b_n R_2^n-p_n R_2^{-n-1}). \end{aligned} \tag{13}$$

The first, third and fourth of Eqs. (12) give

$$\mathfrak{A}_n=\mathfrak{C}_n=\mathfrak{D}_n=0, \tag{14}$$

while the second gives after a simple calculation:

$$\mathfrak{B}_0=-q\Delta_0/3; \quad \mathfrak{B}_2=4q\Delta_0/3, \tag{15}$$

all other $\mathfrak{B}_n$ being equal to zero.

Hence only a_0, b_0, p_0, s_0, a_2, b_2, p_2 and s_2 are different from zero. Since we are interested only in the variation of the concentration *along the surface* of the inner drop, we need to know only the values with the subscript 2, for the 0-th terms of (11) do not contain θ. We find four linear equations for the determination of a_2, b_2, p_2 and s_2 by putting $n=2$ into (13) and introducing that into (12). But since we are interested only in the value of c_2, we need to know only b_2 and p_2.

After somewhat elaborate, but quite elementary calculations, we find:

$$b_2 = -cE/(AE+BD); \quad p_2 = CD/(AE+BD) \quad (16)$$

with

$$\begin{aligned} A &= 2[(D_i - D_0)h_1R_1^3 + 2D_0D_iR_1^2]; \\ B &= (3D_i + 2D_0)h_1R_1^{-2} + 6D_0D_iR_1^{-3}; \\ C &= -4q\Delta_0(2D_0R_1 + h_1R_1^2)/3; \\ D &= (3D_e - 2D_i)h_2R_2^{-2} - 6D_iD_eR_2^{-3}; \\ E &= 3[(D_e - D_i)h_2R_2^{-7} - 3D_iD_eR_0^{-8}]. \end{aligned} \quad (17)$$

The use of those exact expressions is very inconvenient. We observe, however, that with D_i, D_e and D_0 being of the order of magnitude of $10^{-5}-10^{-6}$ cm^2·min.$^{-1}$; with h_1 and h_2 of the order of 10^{-4} cm·min.$^{-1}$ $q \sim 10^{-4}$ g·cm^{-3}·min.$^{-1}$ and R_1 and $R_2 \sim 10^{-3}$ cm^2) the first terms of A, B, D and E are very small as compared with the second ones. While in C the reverse holds true. Neglecting the small terms and putting $R_2 = \alpha R_1$, we find upon substitution of (17) into (16) the very simple expressions:

$$b_2 = 2q\Delta_0/3D_i\alpha^5R_1; \quad p_2 = -4q\Delta_0R_1^4/9D_i. \quad (18)$$

The approximation is good however only when $\alpha^5 \gg 1$.

Introducing this into the second Eq. (11) in which we put $r = R_1$, we find for the coefficient of $P_2(\theta)$ the expression:

$$(2qR_1\Delta_0/3D_i\alpha^5) - (4qR_1\Delta_0/9D_i). \quad (19)$$

For $\alpha^5 > 1.5$ this expression is negative for positive q, and positive for $q<0$. A positive coefficient of $P_2(\theta)$ means that for $\theta = \pi/2$, that is at the equator, c_1^* is smaller than for $\theta = 0$, that is at the poles. And since, according to (5), c_i has the same value along the deformed surface, a positive sign of (19) means a larger value of c_1 at the poles than at the equator, in other words it means a stable equilibrium for a spherical shape. For $q>0$ the sign of (19) is negative, and the drop is unstable under the action of osmotic forces. Taking into consideration also the capillary forces, which always act in the direction of stabilization and which vary like Δ_0/R_1^2,[2] we find[1] that for small R_1 the capillary forces prevail and the drop will be stable even for $q>0$; but for larger R_1 the osmotic forces, which vary according to (19) like Δ_0R_1, will prevail and the drop will become unstable and may eventually spontaneously divide. In a similar way like before we find for the critical value of the radius:

$$R_1^* = [36\gamma MD_i\alpha^5/RTq(2\alpha^5-3)]^{\frac{1}{4}}, \quad (20)$$

R being the gas constant, T the absolute temperature, M the molecular weight of the reacting substance and γ the surface tension of the inner interface.

We find here, so far as the osmotic forces are concerned, a close analogy to the previously studied simpler case. A spontaneous division of the inner phase of a two-phase system can be caused by osmotic forces created only by substances which are *produced in the system*. The interesting and important point of this investigation is however, that reactions, going on in the external phase only, can produce a division of the inner phase, though the latter may be chemically inert and even impermeable to the reacting substances. For our formulae (18) and (19) do not contain either D_0 or h_1 and hold therefore with the same approximation for $D_0 = h_1 = 0$. The biological importance and implications of this result shall be discussed elsewhere.

The approximation used in deriving (18) is no good as soon as R_1 approaches 10^{-2} cm. For such large drops the more complex expression (17) must be used.

---

[2] N. Rashevsky, Protoplasma **16**, 387 (1932); **20**, 125 (1933); Physics **2**, 303 (1932).

The Flexure Problem for Rectangular Beams with Slits

DWIGHT F. GUNDER, *University of Wisconsin and Colorado State College*

(Received October 1, 1934)

Experimental and approximate theoretical studies, made at the United States Forest Products Laboratory, Madison, Wisconsin, show that the mean shearing stress in the neutral plane of a rectangular beam with symmetrical horizontal slits or checks extending along its lateral faces is less than that given by the usual engineering formulas; that is, there is a definite "two-beam" action which relieves the shearing stress in the portion of the beam weakened by the slits. This paper presents an exact solution of the flexure problem for a beam of such section and confirms the main features of the distribution of shearing stress found in the earlier investigation. The solution of the flexure problem requires the solution of Laplace's equation within the plane region coincident with a cross section of the beam, subject to certain boundary conditions. This solution is obtained by using the Schwartz-Christoffel transformation of a polygon onto a half-plane and solving the transformed boundary value problem. The exact solution is set up as an infinite series. To simplify the calculations two approximate solutions are also obtained, one of which is used in treating a numerical example.

INTRODUCTION

AN experimental and approximate theoretical study[1] made at the United States Forest Products Laboratory (Madison, Wisconsin) indicated that the mean vertical shearing stress was less across the weakened section of a rectangular beam with symmetrically placed slits at the horizontal central line than that stress given by the usual engineering formulas. The following paper gives a more complete mathematical derivation of this result, presenting a method for calculating the shearing stress anywhere in the section of such a beam.

THE FLEXURE PROBLEM

In the analysis of the elastic behavior of a beam, two types of stress must be determined. One is the tensile or compressive stress due to the bending moment at the section, the other is the shearing stress due to the relative sliding of adjacent fibers. For metal beams the second of these stresses is comparatively small and can ordinarily be neglected in discussing the failure of the beam, whereas, for wooden beams of certain sections such as the one to be considered here, this is not the case.

As is customary, the problem will be solved for a uniform cantilever type of beam with cross section of the shape under consideration. This problem, called the flexure problem, was first solved by Saint Venant[2] who gave the method for computing the tensile and compressive stresses for beams of any section and obtained also the equations for determining the shearing stresses. The determination of these shearing stresses, which requires the solution of Laplace's equation $\nabla^2\psi=0$ subject to the condition

$$\psi=\phi=\tfrac{1}{2}\int_S y^2dx-\frac{\mu\sigma}{3E}x^3+C_0 \qquad (1)$$

on the boundary S of the section has not been accomplished except for a few special sections such as the rectangle, circle, et cetera.[3] Recently W. M. Shepherd[4] gave the solution for beams of circular section with one or more radial slits extending inward from the boundary of the section. In (1) μ, σ and E are the usual constants of the material, C_0 is an arbitrary constant, and the coordinate system is indicated on Fig. 1.[5] In terms of the function ψ, the shearing stresses can readily be shown to be,

$$X_z=\frac{W}{EI}\frac{\partial\psi}{\partial y}, \quad Y_z=-\frac{W}{EI}\left[\frac{\partial\psi}{\partial x}-\frac{y^2}{2}+\mu\sigma x^2\right]. \qquad (2)$$

[1] J. A. Newlin, G. E. Heck and H. W. March, *New Method of Calculating Longitudinal Shear in Wooden Beams*. U. S. Forest Products Laboratory, Madison, Wisconsin. Engineering News Record **110**, 594–596 (1933).

[2] Saint Venant, J. de Math. (Liouville), Ser. 2 **1**, 1856.

[3] A. E. H. Love, *Theory of Elasticity*, pp. 335–338, 4th Ed., 1927.

[4] Shepherd, Proc. Roy. Soc. London **A138**, 607–634 (1932).

[5] The equation $\phi_0=(W/\mu I)[\theta-x^3/6]$, where θ is conjugate to ψ, defines the relation between the function ψ of this paper and the function ϕ_0 of Love's general theory. See also, Griffith and Taylor, Tech. Rep. British Advisory Committee for Aeronautics **3**, 963–969 (1917–18). Reference 3, page 331, Eq. (4). It should be noted that due to the symmetry of the section the twist τ vanishes.

Method of Solution

The method which will be used in solving this problem consists of mapping the section onto a half-plane and solving the related boundary value problem.

The Schwartz[6]-Christoffel[7] transformation,

$$z = C_1 \int^{\zeta} \prod_{i=1}^{i=n} (\zeta - a_i)^{\alpha_i - 1} d\zeta + C_2, \qquad (3)$$

transforms any polygon in the z-plane into the upper half of the ζ-plane, the boundary of the polygon transforming into the real axis of the plane. In (3) the a_i are the points on the real axis of the ζ-plane into which the consecutive vertices of the polygon transform, the $\pi\alpha_i$ being the corresponding internal angles of the polygon. By determining the constants of (3) for the section at hand and resolving the transformation into its real and imaginary parts x and y, the boundary function ϕ can be transformed into its value along the ξ-axis.

It is further known that the solution of the two-dimensional Laplace equation over the upper half-plane subject to the boundary condition that ψ is to be equal to ϕ along the ξ-axis is given by,

$$\psi(\rho, \alpha) = \frac{1}{\pi} \int_{-\infty}^{\infty} \frac{\rho \sin \alpha \phi(\xi) d\xi}{\xi^2 - 2\xi\rho \cos \alpha + \rho^2}, \qquad (4)$$

where (ρ, α) are the polar, and (ξ, η) the rectangular coordinates of a point in the half-plane. A restriction which is satisfied here, and one which is sufficient to assure the validity of (4) is that $\phi(\xi)$ be representable by a Fourier integral. After transformation ϕ is readily seen to be a function of ξ only and its direct substitution into (4) determines ψ. Finally, using this value and the relations (4) and (2), the values of X_z and Y_z can be found immediately.

The boundary function (1) is determined only by the fact that the stress at a point on the boundary must be in the direction of the boundary at that point. From the symmetry of the section, it is evident that the x-component of the shearing stress vanishes at the vertical central line, hence either half of the section may be chosen for transformation; for definiteness let it be the right half.

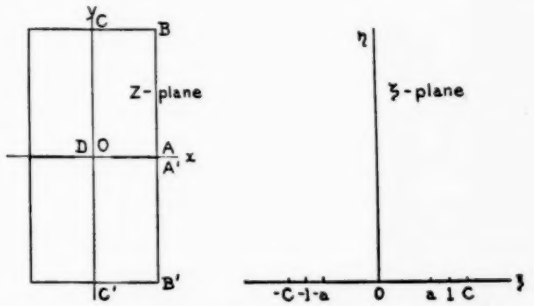

FIG. 1. Beam section before and after transformation.

Since the transformation (3) allows the arbitrary choice of the points corresponding to any three vertices, respect for proper order being maintained, let the points O, B, D (Fig. 1) be transformed into 0, 1, ∞, respectively, on the ξ-axis of the ζ-plane. The transformed coordinates a and c, of A and C will be dependent on the dimensions of the beam, i.e., on the width $2m$, the depth $2n$, and the thickness of the web $2d$. The expressions for a and c are obtained by writing Eq. (8) in its inverted form in terms of theta functions and obtaining from the initial conditions two relations involving only a, c, m, n and d. Following this the two values a and c are readily found from these relations which are $a^2R_0 - a(c_1+1) + R_0c_1 = 0$, and $c^2(c_1^2-1) = c_1^2 - a^2$, where $c_1^2(1-k) = 1+k$ and $R_0 = \mathrm{sn}\,[(m-d)/\tau^2 M, k']$.

After determining C_2 by proper choice of the lower limit ($\zeta = 0$, $z = d$) and replacing C_1 by a more convenient but still arbitrary constant $-\tau^2 i$, Eq. (3) becomes

$$z - d = -\tau^2 i \int_0^{\zeta} \frac{\zeta d\zeta}{[(\zeta^2 - a^2)(\zeta^2 - 1)(\zeta^2 - c^2)]^{\frac{1}{2}}}, \qquad (5)$$

where the singularities of the integrand are to be avoided in the usual manner by enclosing them in infinitesimal circles and choosing the upper halves of these circles as the path of integration.

As is seen by the aid of Fig. 1, the boundary function ϕ is reduced to (C_0 chosen as $n^2m/2$)$\phi = -\mu\sigma x^3/3E + n^2 m/2$ along OAB, to $\phi = -\mu\sigma x^3/3E + n^2 x/2$ along BC and to $\phi = 0$ along CD, similar values holding for $OA'B'C'D$. At this point it is desirable to consider the relative importance of the different terms of ϕ. With the

[6] Schwartz, *Gesammelte Werke*, Vol. II, pp. 65–83.

[7] Christoffel, Annali di Matematica Pura ed Applicata, (2) **1**, 95–103 (1867); **4**, 1–9 (1871).

largest value of $\mu\sigma/3E$ encountered, the term $\mu\sigma x^3/3E$ is never more than approximately five percent of the value of ϕ at any point of the boundary and is much less than this for all beams of common occurrence. It is thus seen that for practical purposes this term may be neglected, the boundary conditions reducing to $\phi=n^2m/2$ along OAB, to $\phi=n^2x/2$ along BC and to $\phi=0$ along CD.

After introduction of the values of ϕ obtained from (5) by resolving it into real and imaginary parts, Eq. (4) becomes,

$$\psi(\rho,\alpha)=\frac{n^2m}{2\pi}\int_0^1 \rho\Omega\sin\alpha d\xi + \frac{n^2}{2\pi}\int_1^c x\rho\Omega\sin\alpha d\xi, \quad (6)$$

where the integrals for symmetric intervals about $\xi=0$ have been combined and where $\Omega=(\xi^2-2\xi\rho\cos\alpha+\rho^2)^{-1}+(\xi^2+2\xi\rho\cos\alpha+\rho^2)^{-1}$. The substitution,

$$t=\frac{\gamma-\zeta^2}{k(\zeta^2-\delta)}, \text{ where } \begin{cases}\gamma=c^2-[(c^2-a^2)(c^2-1)]^{\frac{1}{2}}\\ \delta=c^2+[(c^2-a^2)(c^2-1)]^{\frac{1}{2}}\\ k=\dfrac{(c^2-a^2)^{\frac{1}{2}}-(c^2-1)^{\frac{1}{2}}}{(c^2-a^2)^{\frac{1}{2}}+(c^2-1)^{\frac{1}{2}}}\end{cases} \quad (7)$$

reduces (5) to

$$z-d=-\tau^2Mi\int_{t_0}^{t}\frac{dt}{[(t^2-1)(k^2t^2-1)]^{\frac{1}{2}}},$$

$$\text{where } \begin{cases}\tau^2M=\dfrac{1}{[c^2-a^2]^{\frac{1}{2}}+[c^2-1]^{\frac{1}{2}}}\\ t_0=-\dfrac{\gamma}{k\delta}.\end{cases} \quad (8)$$

Comparison of particular values of z, t, and ζ corresponding to the vertices of the section gives,

$$2\tau^2MK=n, \quad \tau^2MK'=m, \quad (9)$$

K and K' being the complete elliptic integrals with moduli k and $k'=(1-k^2)^{\frac{1}{2}}$, respectively. Equating real and imaginary parts after the transformation (8), it is seen that on BC

$$x=m-\tau^2M\int_1^{t\le 1/k}\frac{dt}{[(t^2-1)(1-k^2t^2)]^{\frac{1}{2}}}, \quad y=n. \quad (10)$$

Also by proper manipulation, Eq. (6) can be reduced to,

$$\psi(\rho,\alpha)=\frac{n^2\tau^2i}{2\pi}\int_1^c\frac{\xi\tan^{-1}2\xi\rho\sin\alpha/(\rho^2-\xi^2)}{[(\xi^2-a^2)(\xi^2-1)(\xi^2-c^2)]^{\frac{1}{2}}}d\xi, \quad (11)$$

which is the formal solution of the boundary value problem at hand. In order to complete the solution of the flexure problem it is necessary to invert the transformation (5) and to thus compute $\partial\psi/\partial x$ and $\partial\psi/\partial y$ and hence, by direct substitution into (2), the shearing stresses X_z and Y_z.

Due to the difficulties which arise in integrating (11) even after the integrand has been broken up into a series, two simpler methods are given here[8] to aid in obtaining practical results.

First method of approximation

Investigation shows that the constant c (see above), is always near unity in value. Further, the function ϕ is monotone decreasing in the interval $1\leqslant\xi\leqslant c$ and a straight line approximation for ϕ in this interval is found to be very satisfactory. Using this the integral is readily evaluated and yields,

$$\psi(\rho,\alpha)=\frac{n^2m}{2\pi}\Bigg[\tan^{-1}\frac{2\rho\sin\alpha}{\rho^2-1}-\frac{\sin\alpha}{2(c-1)}\log_e\frac{(c^2+\rho^2)^2-4c^2\rho^2\cos^2\alpha}{(1+\rho^2)^2-4\rho^2\cos^2\alpha}+\frac{c}{c-1}\Bigg\{\tan^{-1}\frac{2c\rho\sin\alpha}{\rho^2-c^2}-\tan^{-1}\frac{2\rho\sin\alpha}{\rho^2-1}\Bigg\}+\frac{\cos\alpha}{c-1}\Bigg\{\tan^{-1}\frac{\rho^2\sin 2\alpha}{c^2-\rho^2\cos 2\alpha}-\tan^{-1}\frac{\rho^2\sin 2\alpha}{1-\rho^2\cos 2\alpha}\Bigg\}\Bigg]. \quad (12)$$

Second method of approximation

A second method which yields a simpler value for ψ consists in obtaining two solutions, one with $\phi=n^2m/2$ in $1\leqslant\xi\leqslant c$ and one with $\phi=0$ in this same interval, and using the mean of these

[8] For a more detailed discussion of these solutions see the writer's thesis (University of Wisconsin Library).

values for ψ. The above two values of ϕ are, respectively, its maximum and minimum values in the interval and the results are accurate for points in the neighborhood of the slits, the error in the resultant shearing stress being not more than five percent. The value of ψ obtained by this method is,

$$\psi=(\psi_0+\psi_2)/2, \tag{13}$$

where, $$\psi_0=\frac{n^2m}{2\pi}\tan^{-1}\frac{2\rho\sin\alpha}{\rho^2-1}, \quad \text{and} \quad \psi_2=\frac{n^2m}{2\pi}\tan^{-1}\frac{2c\rho\sin\alpha}{\rho^2-c^2}.$$

Inversion of the Transformation

By resolving into real and imaginary parts, Eq. (5) or its equivalent form (8), is to be solved for ρ and α in terms of x and y. This solution will be expressed parametrically. Eq. (8) can be rewritten after change of the lower limit, in the form

$$\int_0^t \frac{dt}{[(1-t^2)(1-k^2t^2)]^{\frac{1}{2}}}=\frac{2K}{n}\left(y-\frac{n}{2}\right)+\frac{iK'}{m}(m-x), \tag{14}$$

which after inversion becomes,

$$t=\frac{\gamma-\zeta^2}{k(\zeta^2-\delta)}=sn\left[\frac{K}{n}(2y-n)+\frac{iK'}{m}(m-x),\ k\right]=sn(u+iv) \tag{15}$$

defining the new variables u and v. The left hand member is resolved into real and imaginary parts by ordinary algebraic methods while the right hand member is similarly treated by using the addition formula for the sn function. The equating of these parts gives in terms of ρ and α,

$$\begin{aligned}\frac{-\rho^4+(\delta+\gamma)\rho^2\cos 2\alpha-\gamma\delta}{k[\delta^2-2\delta\rho^2\cos 2\alpha+\rho^4]}&=\frac{sn(u,k)dn(v,k')}{1-sn^2(v,k')dn^2(u,k)},\\ \frac{\rho^2(\delta-\gamma)\sin 2\alpha}{k[\delta^2-2\delta\rho^2\cos 2\alpha+\rho^4]}&=i\frac{sn(v,k')cn(v,k')cn(u,k)dn(u,k).}{1-sn^2(v,k')dn^2(u,k)}.\end{aligned} \tag{16}$$

Solution of these yields (left hand members called U and V)

$$\tan 2\alpha=\frac{kV(\delta-\gamma)}{k^2(U^2+V^2)\delta+k(\delta+\gamma)U+\gamma}, \qquad \rho^2=\frac{kV\delta}{kV\cos 2\alpha+(1+kU)\sin 2\alpha} \tag{17}$$

which are the required expressions in parametric form. The solutions (17), when taken with any one of the values of ψ, (10), (12) or (13), give a complete solution of the flexure problem for this section.

Since the values of the shearing stresses are in terms of the partial derivatives of ψ the following additional formulas are necessary for computation, the notation $\partial/\partial x,\ y$ indicating two formulas, one with x and one with y appearing throughout.

$$\frac{\partial U}{\partial x}=\frac{\partial V}{\partial y}=\frac{K'sn(u,k)sn(v,k')cn(v,k')}{m[1-sn^2(v,k')dn^2(u,k)]^2}[k'^2-dn^2(u,k)\{1+dn^2(v,k')\}],$$

$$\frac{\partial U}{\partial y}=\frac{-\partial V}{\partial x}=\frac{K'dn(v,k')cn(u,k)dn(u,k)}{m[1-sn^2(v,k')dn^2(u,k)]^2}[cn^2(v,k')-k^2sn^2(u,k)sn^2(v,k')],$$

$$\frac{\partial\alpha}{\partial x,\ y}=\frac{\frac{k(\delta-\gamma)}{2}\left[\{k^2\delta(U^2+V^2)+kU(\delta+\gamma)+\gamma-2k^2\delta V^2\}\frac{\partial V}{\partial x,\ y}-\{2k^2\delta U+k(\delta+\gamma)\}V\frac{\partial U}{\partial x,\ y}\right]}{k^2(\delta-\gamma)^2V^2+[k^2\delta(U^2+V^2)+k(\delta+\gamma)U+\gamma]^2},$$

$$\frac{\partial \rho}{\partial x, y}=\frac{k\delta\left[(1+kU)\sin 2\alpha\frac{\partial V}{\partial x, y}-2V\{(1+kU)\cos 2\alpha-kV\sin 2\alpha\}\frac{\partial \alpha}{\partial x, y}-kV\sin 2\alpha\frac{\partial U}{\partial x, y}\right]}{2\rho[kV\cos 2\alpha+(1+kU)\sin 2\alpha]^2},$$

$$\frac{\partial \psi_0}{\partial x, y}=\frac{n^2 m\pi^{-1}}{(\rho^2-1)^2+4\rho^2\sin^2\alpha}\left[\rho(\rho^2-1)\cos\alpha\frac{\partial \alpha}{\partial x, y}-(\rho^2+1)\sin\alpha\frac{\partial \rho}{\partial x, y}\right],$$

$$\frac{\partial \psi_2}{\partial x, y}=\frac{n^2 mc\pi^{-1}}{(\rho^2-c^2)^2+4c^2\rho^2\sin^2\alpha}\left[\rho(\rho^2-c^2)\cos\alpha\frac{\partial \alpha}{\partial x, y}-(\rho^2+c^2)\sin\alpha\frac{\partial \rho}{\partial x, y}\right]$$

$$\frac{\partial \psi}{\partial x, y}=\frac{1}{2}\left[\frac{\partial \psi_0}{\partial x, y}+\frac{\partial \psi_2}{\partial x, y}\right], \text{ and } X_z \text{ and } Y_z \text{ from Eqs. (2).}$$

The indeterminate forms of the above formulas which arise at certain boundary points of the section are readily evaluated by elementary methods.

Conclusions

The above formulas have been used to compute the shearing stresses in a test piece whose dimensions were, $m=1.25$, $n=2.25$, and $d=0.25$, whence the values, $k=0.6216$, $k'=0.7833$, $a=0.9524$, $c=1.0026$, $\gamma=0.9825$, $\delta=1.0281$, were determined.

Fig. 2 shows the distribution of shearing stress and the direction of this stress in the vicinity of the slits as calculated by the foregoing formulas. Those values omitted in the upper half of the figure have not been calculated since they do not affect the following discussions. The average maximum possible error, including that resulting from the omission of $\mu\sigma x^3/3E$ from the boundary function is not more than two percent. It is to be noted that this is probably much larger than the actual error.

A very interesting phenomenon, which was discussed on the basis of experimental results combined with an approximate theoretical treatment by Newlin, Heck and March,[1] is shown in Fig. 3. This shows the vertical components of the shearing stress averaged over the width of the beam as this mean stress varies from the central line through the slits to the top of the beam. The graph very clearly proves the fact that, contrary to general belief, the mean vertical shear over the entire width of the beam is less at the central line through the slits than it is just above or just below this line. In other words, when the checks are deep, the beam tends to act, not as one beam but more as two beams. This result confirms the work of the paper just quoted which found a pronounced "two-beam" action. This action was even greater than that indicated by the present treatment due to the fact that wood is not perfectly elastic in shear but is somewhat plastic with the result that the shear distortion in the plane of the slits before failure is greater than that which would occur in a perfectly elastic material. Calculations show that this two-beam action does not appear until the thickness of the web is reduced to less than half the width of the beam.

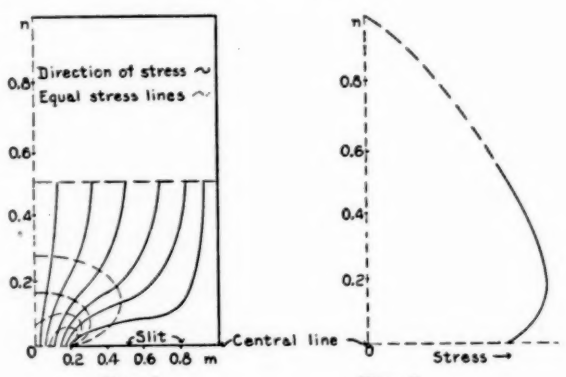

Fig. 2.

Fig. 3.

Fig. 2. Stress distribution in quarter section of beam.
Fig. 3. Mean vertical shearing stresses showing two-beam action.

A Determination of the Refractive Index of Vitreous Silica and the Calibration of Silica Refraction Thermometers Between 18° and −200°C

J. B. AUSTIN AND R. H. H. PIERCE, JR., *Research Laboratory, United States Steel Corporation, Kearny, N. J.*

(Received October 18, 1934)

The variation with temperature of the refractive index of fused silica for the helium line 5877.2A has been determined between 18° and −200°C and the results have been applied to the calibration of vitreous silica refraction thermometers at low temperatures. These data have been correlated with measurements at high temperatures. It is found that the refractive index between −200°C and 1000°C can be represented by the equation $n=1.45657+0.001553\ t/100 +0.00219\ e^{-0.33t/100}$.

INTRODUCTION

A METHOD for calibrating vitreous silica refraction thermometers at high temperatures by means of a calculation based on the temperature variation of their refractive index has already been described.[1] The present paper gives the results of a determination of the refractive index of fused silica at low temperatures and extends the range of the calibration equation to −200°C. The method employed was in principle the same as that used at high temperatures, namely, observation of the passage of interference fringes across a polished plate, in this case thermometer 311, when the temperature was changed by a definite number of degrees. The apparatus is shown in Fig. 1. The fused silica plate R was placed in a cavity in a small copper block C in which there was imbedded the junction of a copper-constantan thermocouple. The block itself rested on the bottom of a Pyrex tube P the upper end of which was closed by an optically flat window W sealed on with stopcock grease. This tube had two side arms, one leading to a vacuum pump capable of reducing the pressure to 0.002 mm Hg or better, the other providing an entrance, through a vacuum wax seal, for the thermocouple. The use of a vacuum in P served the double purpose of preventing the condensation of moisture on the surfaces of the plate and window, and of permitting the direct measurement of the change in absolute index of refraction, that is the index of refraction of the plate relative to vacuum, thus eliminating the correction for the change in refractive index of air with temperature. It also reduced the rate of cooling to a convenient value—approximately 3 degrees a minute with the refrigerants employed, so that satisfactory measurements could be obtained by the simple procedure of immersing tube P in the refrigerating bath and following the change in temperature of the plate with the thermocouple. On the other hand, the vacuum made it necessary to use great care in measuring the temperature because of the conduction of heat along the wires. For example, in some preliminary observations in which the silica plate rested on top of the junction of the thermocouple at the bottom of the tube, the inflow of heat along the wires was so much greater than the loss of heat across the vacuum to the silica that with the tube immersed in liquid air the thermocouple readings were high by almost 100°C. The sudden admission of air reduced the observed temperature to very near its true value almost instantaneously. Errors from this source appeared, however, to be eliminated by the use of the copper block and by wrapping the thermocouple around the block before bringing it to the side arm, thus insuring that at least 7 cm of the thermocouple were at the same temperature as the junction.

The e.m.f. of the thermocouple was measured with a potentiometer with a sensitivity of five microvolts. The couple itself was calibrated by the Bureau of Standards immediately after the completion of the measurements; and as an additional check on the overall accuracy of the temperature measurements with the thermocouple carefully purified mercury was substituted for the silica plate in the copper block and the melting point was determined from a heating curve. A flat lasting four minutes was obtained

[1] Austin, Physics **3**, 240 (1932).

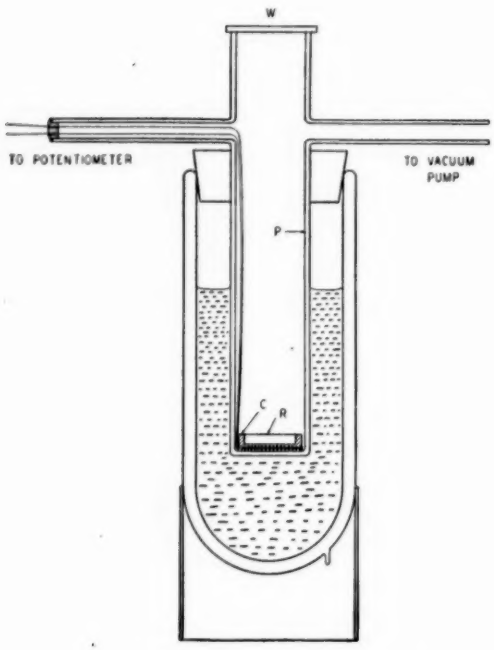

FIG. 1. Cross section of apparatus.

at −39.93°C, which is in satisfactory agreement with the value −39.87°C given in *International Critical Tables* (Vol. I, p. 53). It also confirms to some extent our belief that the thermocouple wire was reasonably homogeneous and indicates that the unavoidable differences in thermal gradient in the couple during calibration and during use did not appreciably influence the readings.

In making a determination the silica plate, copper block and thermocouple were set in place, tube P was sealed and evacuated, and the Dewar flask, containing the refrigerant was raised around it. The passage of the fringes on the plate was then observed and the temperature corresponding to each was recorded. Three refrigerants were used: an ice bath, an ether-CO_2 mixture, and liquid air, and observations were made over the temperature range obtainable with each of them. Since the initial temperature, that of the room, was different for each determination all readings were corrected to the reference temperature 18°C, an adjustment which is easily made since the number of fringes passing per degree at room temperature is accurately known for the silica plate employed.

The final values, taken from a smooth curve which is the average of the several sets of data, are represented within 0.1 fringe by the equation:

$$\Delta N = 2.6 - 0.131t - 1.90\times10^{-4}t^2, \qquad (1)$$

where ΔN is the number of fringes passing between 18° and t°C. From this empirical equation a similar expression can be obtained by dividing (1) by the thickness of the plate, 0.465 cm, thus

$$\Delta N = (L)(5.59 - 0.281t - 4.09\times10^{-4}t^2), \qquad (2)$$

which, as in the case of the equation previously given for high temperatures,[1] we believe holds for any well-annealed thermometer used with the wavelength 5877.2A. A more general equation applicable to any wavelength is obtained by multiplying (2) by $\lambda_v/2$ or 2.9386×10^{-5}, or

$$\Delta N = (2L)/\lambda_v(16.45 - 0.828t - 12.0 \times10^{-4}t^2)\times10^{-5}. \qquad (3)$$

It should be noted that as the temperature is lowered vitreous silica becomes less and less sensitive as an indicator of temperature; thus, for thermometer 311, the limit of accuracy of observation, 0.1 fringe, corresponds to 0.6°C at room temperature and to approximately 2°C at −200°C. Such a lack of precision is a definite disadvantage in many cases and, just as with most thermocouples at low temperatures, places a real limit to the usefulness of this method. If high precision is not required, however, this method provides a convenient and simple means of following temperature changes at low temperatures in any system or apparatus which can be provided with a suitable window; and it is possible that a plate of some kind of glass with a higher sensitivity at low temperatures might be more suitable than silica as a thermometer.

It is also possible to obtain from Eq. (1) an expression for the change in refractive index of silica in this temperature range by means of the relation

$$\Delta n = \Delta N\lambda_v/2L - \alpha t n_1, \qquad (3a)$$

where Δn is the change in refractive index between 18° and t°C, λ_v is the wavelength of the light used in vacuum, 5877.2A, α is the coefficient of thermal expansion of vitreous silica

and n_1 is the refractive index at 18°C.[2] Values for λ_ν, L and ΔN having already been given it is necessary only to evaluate α and n_1, which need not be done with great accuracy since the quantity $(\alpha t n_1)$ is but a small correction term. A review of the data collected by Sosman[3] shows that α can be represented with sufficient accuracy over the range 18° to −200°C by the equation

$$\alpha = 10^{-6}(0.4 + 2.67 \times 10^{-3} t), \qquad (4)$$

while n_1 can be taken as 1.459. Substituting these values in (3a) we obtain

$$\Delta n = 10^{-5}(16.45 - 0.886t - 15.90 \times 10^{-4} t^2) \qquad (5)$$

for the change in n between 18°C and −200°C.

The values represented by Eq. (5) can be used to calculate the index of refraction at any temperature within the range specified if the absolute index of vitreous silica at 18°C for the wavelength 5877.2A is known. No direct determinations of this quantity appear to have been made with the requisite accuracy the only datum in the literature, that of Rinne,[4] being given to but five significant figures; but a value can be derived without difficulty by interpolation in the table of most probable values for 18°C at various frequencies as selected by Sosman.[5] The absolute index so derived is 1.45896, which, used with Eq. (5), yields the values for 0°C and lower found in Table I. The data for higher temperatures given in the table are calculated from Δn as given in the paper already cited[1] and are included to give an idea of the variation of n over the range −200°C to 1000°C. The data in this table can be satisfactorily represented by the equation

$$n = 1.45657 + 0.001553t/100 + 0.00219e^{-0.33t/100},$$

as shown by the comparison in the table between the observed and computed values.

The data in the table give no indication of a minimum in the refractive index such as is found in the density and such as would be expected if the equation of Gladstone and Dale,[6] namely, $(n-1)/d = \text{constant} = (n-1)v$, where d is the density and v is the specific volume, were strictly valid in this temperature range. The temperature of minimum density seems to vary somewhat with the sample, or at least there is a considerable discrepancy in the temperature reported by the several investigators who have observed it, so that it is difficult to predict the magnitude of the effect upon $n-1$ between the possible minimum and our lowest temperature, which was approximately −200°C. An average of the existing data for the density gives, however, a decrease between −150° and −200°C of close to 5 parts in 20,000. Since the constant in the Gladstone and Dale equation is about 0.208, the corresponding change in n should be about 5 parts per 100,000, which is equivalent to the reversal of a whole fringe and should have been easily observable. Inasmuch as no reversal was observed, the minimum, if it does exist at all, is not a pronounced one and the increase in n between the temperature of the possible minimum in our silica and −200°C is less than 5 parts per million; or it is possible that the temperature of the minimum may be close to −200°C. Values of the Gladstone and Dale constant for the wavelength 5877.2A have been calculated for the whole temperature range with results given in Table II. The constant shows a variation of only 3 percent over a temperature range of 1100°C indicating that the equation holds to a reasonable degree of accuracy for the change of refractive index of vitreous silica with temperature.

TABLE I. *The influence of temperature on the refractive index of vitreous silica for 5877.2A relative to vacuum.*

t°C	$n_{obs.}$*	$n_{calc.}$+	$n_{obs.}-n_{calc.}\times 10^5$	t°C	$n_{obs.}$*	$n_{calc.}$+	$n_{obs.}-n_{calc.}\times 10^5$
−200	1.45765	1.45770	−5	500	1.46475	1.46475	0
−150	1.45782			550	1.46546		
−100	1.45808	1.45807	+1	600	1.46619	1.46619	0
− 50	1.45840			650	1.46691		
0	1.45880	1.45876	4	700	1.46764	1.46766	−2
50	1.45923			750	1.46840		
100	1.45971	1.45970	1	800	1.46914	1.46915	−1
150	1.46023			850	1.46990		
200	1.46079	1.46081	−2	900	1.47070	1.47066	4
250	1.46137			950	1.47144		
300	1.46201	1.46204	−3				
350	1.46268						
400	1.46335	1.46337	−2				
450	1.46404						

*based on $n_{18} = 1.45896$
+ from equation $n = 1.45657 + 0.001553\ t/100 + 0.00219\ e^{-0.33t/100}$

[2] In the discussion of the high temperature calibration (reference 1, p. 247) Eq. (3a) is erroneously printed as $\Delta n = \lambda_\nu / 2L(\Delta N + \alpha t n_1)$. The above form is correct.

[3] Sosman, *The Properties of Silica*—Chemical Catalog Co., New York, 1927.

[4] Rinne, Neues Jahrb. Mineral. Beil. **39**, 388 (1914).

[5] Reference 3, p. 591.

[6] Gladstone and Dale, Phil. Trans. p. 337 (1863).

TABLE II. *Temperature variation of the Gladstone and Dale constant* $(k=(n-1)v)$ *for vitreous silica.*

t°C	$n-1$+	$v10^3$*	k
−200	0.45765	454.0	0.2078
−100	.45808	453.9	.2079
0	.45880	454.0	.2082
100	.45971	454.0	.2087
200	.46079	454.1	.2092
300	.46201	454.1	.2098
400	.46335	454.2	.2104
500	.46475	454.3	.2111
600	.46619	454.4	.2118
700	.46764	454.4	.2124
800	.46914	454.5	.2132
900	.47070	454.6	.2140

+ taken from Table I.
* taken from Sosman, reference 3, p. 361.

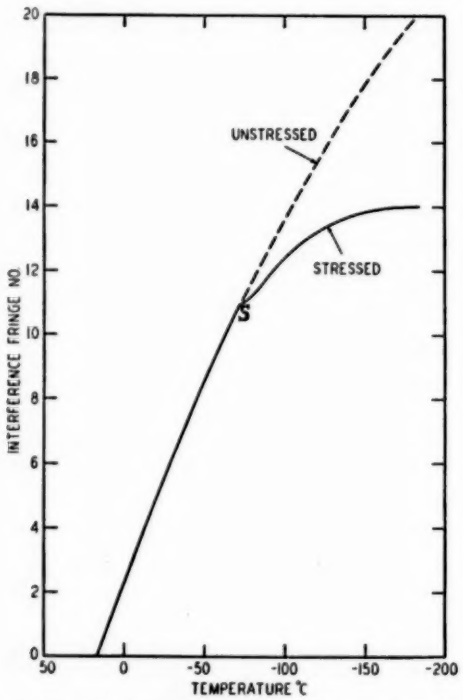

FIG. 2. Curves showing the effect of stressing the silica plate. Stress due to contraction of copper plate began at point *S*.

If, instead of taking n_{18} equal to 1.45896 as in Table I, we adopt Rinne's determination, $n_{18}=1.4592$, a check on the consistency of his measurements at −64° and −160°C can be easily obtained. Thus, it is found that rounded values of n derived from Eq. (5) lead to $n_{-64}=1.4586$ and $n_{-160}=1.4581$, which are in exact agreement with Rinne's data, showing that the change of n with temperature was the same in both cases.

It is interesting to note in passing that in the first measurements in which the copper block was used, the cavity contracted more than had been allowed for and consequently began to squeeze the silica plate. The effect on the interference fringes was immediately evident as is shown by Fig. 2 in which the solid line represents the observations for this run and the dashed curve is for the unstressed silica. In order to remove any strain which might have resulted from this treatment the silica plate was annealed at high temperatures before being used again.

SUMMARY

The change in refractive index of vitreous silica has been determined in the range 18° to −200°C by means of an interference method. The results are applied to the calibration of vitreous silica refraction thermometers in this temperature region. The number of fringes ΔN passing the reference mark on such a thermometer when the temperature is changed from 18° to t°C is given by the equation $\Delta N=2(L)/\lambda_v(16.45-0.828t-12.0\times10^{-4}t^2)\times10^{-5}$ where L is the thickness of the plate in cm and λ_v is the wavelength in vacuum of the light used. No minimum appears in the index of refraction at low temperature.

Magnetic Susceptibility of Some Alloys of "Gamma-Brass" Structure

CYRIL STANLEY SMITH*

(Received September 26, 1934)

The change of diamagnetic susceptibility with composition of a number of phases of gamma-brass structure (Cu–Zn, Cu–Cd, Ag–Zn, Ag–Cd) has been determined. In each case when the phase makes its first appearance with low electron ratio, it is not strongly diamagnetic, but the increase in diamagnetism is approximately lineally dependent on the number of free electrons, and the strongest diamagnetism occurs at the limit of the gamma-phase with the highest electron ratio possible for the structure.

THE recent theoretical treatment by H. Jones[1] renders particularly interesting physical measurements on that peculiar series of alloys of complex cubic structure known, from the first phase of the type examined, as "gamma-brass" structures.**

Phases of gamma-brass structure occur frequently in alloys, but only at or around compositions corresponding to a ratio of 21 valence electrons to 13 atoms, i.e., at compositions approximating Ag_5Zn_8, Cu_9Al_4, $Cu_{31}Sn_8$, Fe_5Zn_{21}, etc., the transition elements being considered as zero valent. This was pointed out by Westgren and Phragmen[2] and Westgren and Ekman[3] who extended the Hume-Rothery rule[4] to the gamma-alloys. The structure of all the phases is cubic. The unit cube contains 52 atoms and results from the removal of the center and corner atoms from a cubical group of 27 body-centered cubes and slight distortion of the remaining ones. The exact distribution of the different atoms in the different sets of equivalent positions varies with the particular alloy considered. The principal crystallographic determinations have been by Bradley and Thewlis,[5] Bradley and Gregory,[6] and Bernal.[7]

The results of Endo[8] on a large series of carefully heat treated alloys, including, however, only two systems with a phase of gamma-brass structure, permitted Bernal[9] to make the generalization that the strong diamagnetism is a structural property and depends on the presence in the large unit cell of electron orbits including several atoms.

The earlier measurements of Greulich reported by Weber[10] showed a marked maximum in the diamagnetic susceptibility of cast copper-zinc alloys at about 32.8 percent copper, which was attributed to the compound $CuZn_2$.

The measurements of Spencer and John[11] and of Clifford,[11a] although they include systems in which phases of gamma-brass structure are present, are of little value in the present connection. As has so often been emphasized, it is useless to perform physical measurements on alloys unless they have been heat treated to reach equilibrium. A cast alloy or one that has been annealed for too short a time represents a quite indeterminate mixture of phases of irregular and variable composition, but suitable heat treatment will convert this to a structure in both chemical and physical equilibrium (except for grain size) and it is only on such material

* Research Laboratory, The American Brass Co., Waterbury, Conn., U. S. A. Work performed in The University Chemical Laboratories, Cambridge, England.

** These are often referred to as "gamma structures," a name that is apt to be misleading since many phases that are called gamma in the metallurgist's nomenclature, are of totally different structures. This led Jones[1] to mistake the gamma-phase in the copper-cadmium system for the phase of gamma-brass structure, which in this system is the delta-phase.

[1] H. Jones, Proc. Roy. Soc. **A144**, 225 (1934).

[2] A. Westgren and G. Phragmen, Trans. Faraday Soc. **25**, 379 (1929).

[3] A. Westgren and W. Ekman, K. Vetenskapakad. Arkiv. Kemi. etc. **B10**, No. 11 (1930).
W. Ekman, Zeitz f. physik. Chemie **B12**, 57 (1931).

[4] W. Hume-Rothery, J. Inst. Metals **35**, 295 (1926).

[5] A. J. Bradley and J. Thewlis, Proc. Roy. Soc. **A112**, 678 (1926).

[6] A. J. Bradley and C. H. Gregory, Phil. Mag. **12**, 143 (1931).

[7] J. D. Bernal, Nature **122**, 54 (1928).

[8] H. Endo, Sci. Rep. Tohoku Imp. Univ. **14**, 479 (1925).

[9] J. D. Bernal, Trans. Faraday Soc. **25**, 367 (1929).

[10] R. H. Weber (and K. Greulich), Ann. d. Physik **62**, 666 (1920).

[11] J. F. Spencer and M. E. John, Proc. Roy. Soc. **A116**, 61 (1927).

[11a] O. C. Clifford, Phys. Rev. **26**, 424 (1908).

that physical measurements should be made. None of the earlier workers have been primarily interested in gamma-phase, and their measurements on alloys were not sufficiently close to permit the behavior within the phase boundaries to be definitely established.

The present investigation, prompted by Bernal's discussion of the subject, was aimed primarily at determining the manner in which the susceptibility varies as the composition changes across the field of homogeneity. The systems copper-zinc, copper-cadmium, silver-zinc and silver-cadmium were selected. Of these, measurements have previously been reported only on the copper-zinc system.

Preparation of Alloys

The copper-zinc alloys for the present work were made from pure cathode copper and a commercial grade of 99.99+ percent zinc. The other alloys were made from special zinc or cadmium that had been redistilled from material containing 0.003 percent iron. Analysis of two of the copper-zinc alloys showed the presence of 0.0065 and 0.0054 percent iron (alloys 31 and 41, respectively—Table I). A silver-zinc alloy (No. 50—Table IV) contained 0.0012 percent, a copper-cadmium alloy (No. 61—Table III), 0.0002 percent, and a silver-cadmium alloy (No. 67—Table V) contained 0.0003 percent iron. The silver used was of specially high purity but was not analyzed. Alloys of the desired composition were made by first melting under a cover of powdered graphite or a flux consisting of LiCl and KCl the required quantity of the pure metals with intermediate alloys containing about 60 percent zinc or cadmium. The resulting ingots were reduced to coarse powder and then remelted under oxygen-free dry hydrogen* in vertical silica tubes, 0.55 cm bore, with the bottom end sealed. With an oxyhydrogen flame the silica tube was then melted off and sealed about 2 cm above the top of the specimen, the tube still being filled with hydrogen at atmospheric pressure. The specimens had an average grain diameter of about 3 to 5 mm.

The cast alloys, sealed in their silica tubes, were annealed for a long time to produce equilibrium structures and then were either quenched, air-cooled or very slowly cooled in the furnace. The last method was first used with the copper-zinc alloys and resulted in iron precipitation, so the other series were cooled more rapidly. Quenching was not possible with the copper-cadmium alloys on account of the extreme fragility of the alloys, but the silver alloys, which have the greatest mechanical strength of the series, could be quenched. The tubes containing the heat treated alloys were broken open with care and a sample for analysis† chipped off from each end of the bar. This was done with a single sharp blow with a hammer and chisel which, after a little practice, gave a clean flat fracture without damaging the bar as a whole.

Measurement of Susceptibility

The magnetic volume susceptibility was determined at 16 to 20°C by the Gouy method, by weighing small bars (0.55×4 cm) of the alloys with the lower end in a homogeneous magnetic field. The magnet, for the loan of which the author wishes to thank Dr. Cockroft of the Cavendish Laboratory, gave a maximum field strength of 18,500 gauss in a gap of about 0.8×0.8×1 cm. The specimen was suspended by a fine nonmagnetic wire from a balance sensitive to 0.05 mg and protected from draughts by a tubular brass box with the necessary glass windows, the sides of the box being pierced with conical holes to fit closely around the poles of

* Shimizu[12] has shown that vacuum melted alloys differ in susceptibility from alloys melted in contact with air. Goetz and Focke[13] did not find this effect in single crystals of bismuth alloys. It is obviously impossible to melt alloys containing zinc or cadmium in vacuum, and hydrogen was selected as the least harmful of the available gases to prevent too great volatilization. The volatility of cadmium and zinc result in a blanket of metal vapor which prevents much absorption of hydrogen,—indeed it is impossible to get blowholes due to hydrogen in brass, although hydrogen is a frequent cause of unsoundness in commercial castings of deoxidized copper alloys.

[12] Y. Shimizu, Sci. Rep. Tohoku Imp. Univ. **21**, 826 (1932).

[13] A. Goetz and A. B. Focke, Phys. Rev. **45**, 170 (1934).

† The determination of copper was done by electrolysis, using a rotating cathode in a sulphuric-nitric acid solution of about 1 g of alloy. Silver was determined by titration with thiocyanate. Zinc or cadmium was taken by difference. In most cases there was a slight difference between the composition of top and bottom of the bar due to the distillation of volatile constituent, but this amounted to less than 0.2 percent in the copper-zinc system, 0.4 percent in the silver-cadmium system and 0.1 percent in the other systems. The reported composition is the average of the top and bottom samples.

the magnet. The box was extended to the base of the balance case, which was mounted on a sturdy shelf above the magnet and was furnished with means for fine adjustment for centering the specimen in the gap. The specimen was contained in a thin glass tube, and rested on two small projections made by pushing a point into the walls of the tube while hot. The top end of the tube had ears for attaching the suspension wire and at the bottom, 8 cm below the gap, was blown a small bulb which contained about 30 g mercury, the weight of which prevented the specimen from being thrown out of the field when strongly diamagnetic specimens were used. A correction for the specimen tube blank, amounting to less than 6 mg, was made to all readings.

The weakest point in the method was the determination of field strength. This was done by measuring the force acting on a column of water (the susceptibility of which was assumed to be -0.72×10^{-6}) in a tube, with a cemented flat bottom, of internal diameter approximating that of the specimen. Since the specimens used were rather short (3 to 5 cm) the upper ends did not reach a point where the field strength was negligible and curves of $(H^2-H_0^2)^{\frac{1}{2}}$ *vs.* magnet current were obtained for several specimen lengths. The true value of H was obtained by the use of a long column of water. The susceptibility calculations were made directly from the change of weight in the specimen and the change of weight of a column of water of the same length for the same current. Thus

$$\kappa\cdot10^6=-0\cdot72Fd_w^2/F_wd^2,$$

where κ is the magnetic volume susceptibility; F and F_w the forces acting on the specimen and on the column of water of the same length and of diameter d and d_w, respectively, for the same current. F_w was read for each experiment from a large scale calibration curve. The current for the magnet (<15 amp., 110 volts) was obtained from a large battery of accumulators and was measured by determining the potential drop across a standard resistance with a Leeds and Northrup potentiometer.

In all cases κ was determined on each end of each specimen and at least five different field strengths varying from 10,000 to 18,000 gauss.

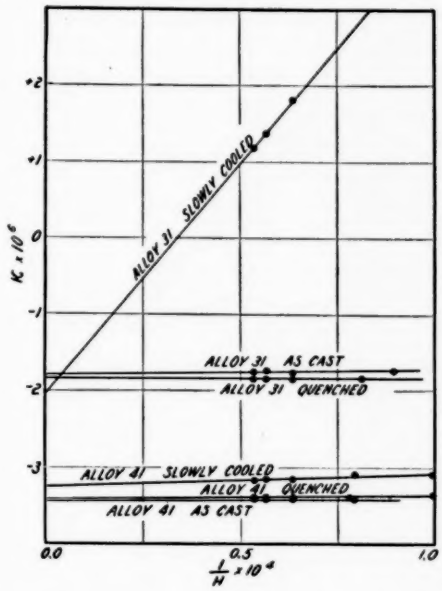

FIG. 1. Effect of heat treatment on magnetic susceptibility of some copper-zinc alloys.

TABLE I. *Magnetic susceptibility of some copper-zinc alloys in the cast condition.*

Alloy No.	Composition (% Cu) Weight	Atomic	$\kappa(\times10^6)$
26	38.32	38.99	−2.84
27	39.09	39.76	−2.70
28	40.96	41.64	−2.72
31	41.32	42.00	−1.79
35	35.62	36.27	−5.03
39	30.46	31.06	−5.27
41	25.33	25.87	−3.44

The resulting values of κ plotted against $1/H$ gave straight lines and permitted κ_∞ to be determined, this figure being uninfluenced by ferromagnetic impurities.

The density determinations were made by weighing in air and water, and the mass susceptibility, χ, calculated in the usual way.

EFFECT OF HEAT TREATMENT ON COPPER-ZINC ALLOYS

In most cases the curves of κ *vs.* $1/H$ were straight and almost horizontal, but the curves of the slowly cooled copper-zinc alloys which contained precipitated iron were steeply inclined. These showed the effect of heat treatment in an interesting way. The main series was annealed at 650°C and 300°C and very slowly cooled, a heat treatment intended to result in a state

closely approximating equilibrium at room temperature. This was satisfactory for the pure gamma-alloys, but those alloys containing the beta-phase were found to be paramagnetic and to have a susceptibility which varied enormously with field strength, an effect obviously due to the precipitation of free iron. The alloys not containing beta were diamagnetic and were uninfluenced by field strength, hence it is obvious that iron is almost entirely insoluble in beta at low temperatures but is soluble in the gamma-phase. This is to be expected since the iron-zinc system itself has a phase of gamma-brass structure and this should be at least partially isomorphous with other gamma-phases. The small amount of iron in beta can be rendered magnetically harmless by quenching from a temperature where it is in solution. Quenching from 600°C (and probably cooling at any rate other than an extremely slow one) holds the iron in solution. Fig. 1 shows clearly the effect of heat treatment on the susceptibility of two copper-zinc alloys, alloy 31 being in the beta +gamma-range and alloy 41 in the gamma-range.

The results for the cast alloys (Table I) show no regular change with composition since they are not in equilibrium. Equally valueless are those measurements on the slowly cooled copper-zinc alloys which contained iron precipitation which rendered the extrapolation to infinite field strength very uncertain. On account of greater purity and more rapid cooling, the alloys of the other systems studied were not paramagnetic and were practically uninfluenced by field strength. For all but the paramagnetic copper-zinc alloys the values of κ_∞ are believed to be accurate to 0.01×10^{-6}.

Results

The results of the susceptibility measurements are given in Tables II to V and are plotted in Figs. 2 to 5 against electron ratio, the latter being the ratio of valence electrons to atoms, i.e., $(Aa+Bb)/(A+B)$ where A and B are the atomic percentages* of elements of valency a and b. The theoretical composition of the gamma-phases corresponds to an electron ratio 1.62. This is not a critical point, but only the point where the structure is most symmetrical.

It is immediately apparent from Figs. 2 to 5 that the susceptibility of all the gamma-phases considered varies in the same way. Very little change in susceptibility occurs across the beta +gamma range, the susceptibility being of about the same order of magnitude as for the elements themselves. As the electron ratio increases across the range of the homogeneous gamma-phase the alloys become more strongly diamagnetic, and on the appearance of the next phase diamagnetism decreases once more, proportionately to the

TABLE II. *Magnetic susceptibility of gamma-phase in copper-zinc system.*

Alloy No.	Composition (%Cu) Weight	Atomic	Mag. Vol. Suscept. $-\kappa$ ($\times10^6$) Annealed+	Quenched* from 600°C	Density ρ, g/cc, 20°C	Mass Suscept. $-\kappa/\rho$ ($\times10^6$) Annealed	Quenched
29	46.65	47.36	(2.01)	1.71	8.19	(0.246)	0.209
30	43.60	44.30	(2.40)	1.73	8.11	(0.296)	0.213
31	41.30	41.98	(2.01)	1.84	8.08	(0.249)	0.228
32	40.36	41.04	(1.27)	2.13	8.06	(0.159)	0.264
33	39.39	40.06	(2.01)	2.54	8.05	0.249	0.316
34	37.19	37.84	4.04	—	8.02	0.503	—
35	35.44	36.17	5.03	—	8.00	0.629	—
36	33.30	33.92	6.16	6.10	7.95	0.775	0.767
37	32.29	32.90	5.85	5.74	7.87	0.743	0.728
38	31.18	31.78	5.64	5.71*	7.88	0.715	0.725
39	30.37	30.97	5.31	5.65*	7.87	0.675	0.717
40	28.30	28.88	4.70	4.58*	7.79	0.604	0.589
41	25.26	25.80	3.42	3.25*	7.83	0.437	0.415
42	38.08	38.74	3.37	—	8.02	0.420	—

+ Alloys 29, 30, 36, 38 and 41 annealed 96 hrs. at 675°C, slowly cooled to and held 48 hr. at 500°C; slowly cooled to and held 120 hr. at 300°C; slowly cooled to room temperatures.
Alloys 31 to 35, 37, 39 and 42 annealed 52 hr. at 675°C, slowly cooled to and held 96 hr. at 300°C; slowly cooled to room temperatures.
Figures in ( ) are for alloys paramagnetic in weak fields due to free iron precipitation. The extrapolation to infinite field strength is rather uncertain.
*a Alloys marked * were annealed 141 hr. at 650°C and quenched in cold water; all other quenched alloys were annealed 5.2 hr. at 600°C before quenching.

TABLE III. *Magnetic susceptibility of delta-phase, copper-cadmium system (gamma-brass structure).*

Alloy No.	Composition (%Cu) Weight	Atomic	Mag. Vol. Suscept. $-\kappa$ ($\times10^6$) Annealed+	Density ρ, g/cc, 20°C	Mass Suscept. $-\kappa/\rho$ ($\times10^6$) Annealed
56	34.25	47.95	2.23	9.04	0.247
57	32.18	45.62	2.51	9.02	0.278
58	30.18	43.33	2.67	9.04	0.296
59	28.09	40.86	2.82	9.08	0.311
60	26.16	38.52	3.35	8.87	0.378
61	24.30	36.21	3.98	8.63	0.461
62	22.22	33.56	5.19	8.76	0.592
63	20.93	31.94	5.27	8.89	0.594

+Annealed 268 hr. at 375°C, air-cooled.

* For tables for the rapid interconversion of atomic and weight percentages in any binary system see Smith.[14]

[14] C. S. Smith, Trans. Am. Inst. Min. Met. Eng. Contribution No. 60 (1933).

TABLE IV. *Magnetic susceptibility of gamma-phase, silver-zinc system.*

Alloy No.	Composition (%Ag) Weight	Atomic	Mag. Vol. Suscept. $-\kappa$ ($\times 10^6$) Annealed*	Density ρ, g/cc, 20°C	Mass Suscept. $-\kappa/\rho$ ($\times 10^6$) Annealed
47	56.93	44.48	3.14	8.87	0.354
48	54.99	42.55	2.89	8.76	0.330
49	53.93	41.50	2.84	8.75	0.325
50	51.00	38.68	3.64	8.67	0.419
43	50.94	38.62	3.54	8.65	0.409
51	50.47	38.18	3.65	8.64	0.422
52	49.11	36.90	4.02	8.61	0.467
53	48.13	36.00	3.60	8.60	0.419
54	46.74	34.72	2.88	8.53	0.338

* Annealed 65 hr. at 600°C, 96 hr. at 400°C, quenched.

TABLE V. *Magnetic susceptibility of gamma-phase, silver-cadmium system.*

Alloy No.	Composition (%Ag) Weight	Atomic	Mag. Vol. Suscept. $-\kappa$ ($\times 10^6$) Annealed*	Density ρ, g/cc, 20°C	Mass Suscept. $-\kappa/\rho$ ($\times 10^6$) Annealed
64	35.20	36.15	3.32	9.60	0.346
65	37.30	38.26	4.28	9.61	0.445
66	35.43	36.38	3.53	9.64	0.367
67	39.62	40.62	3.12	9.65	0.323
68	40.67	41.66	2.88	9.73	0.296
69	41.78	42.78	2.78	9.75	0.285
70	42.80	43.82	2.56	9.68	0.265
71	43.22	44.24	2.38	9.73	0.245

* Annealed 239 hr. at 450°C, quenched in water at 18°C.

amount of the latter. The diamagnetic susceptibility of the gamma-phase at the limiting composition corresponding to the lowest electron ratio is not much greater than that of the beta-phase (in the case of the silver-zinc system it is actually smaller), but there is a rapid increase with increasing number of electrons right up to the point where the epsilon phase appears. There are insufficient points to establish the type of curve exactly, but in each case they lie on a straight line within the accuracy of the measurements. These facts fit in perfectly with the theory of Jones.[1]

The copper-zinc gamma-phase shows the strongest diamagnetism and the silver alloys the least. This is largely due to the fact that the gamma-structure remains stable to higher electron ratios in the copper systems, and if it were possible to extend the limit of stability of the structure to still higher electron ratios, the diamagnetism would undoubtedly become greater.

The intersection of the different branches of the curves provide a means of determining with some accuracy the composition limits of the gamma-phases. The limits derived from Figs. 2 to 5 compare favorably with those determined by metallographic or crystal structure determinations, although there are minor differences as can be seen in Table VI. A correction to the equilibrium diagrams cannot be made with certainty on the basis of the present results, however, since it is by no means certain that quenching retains the alloys in equilibrium, and

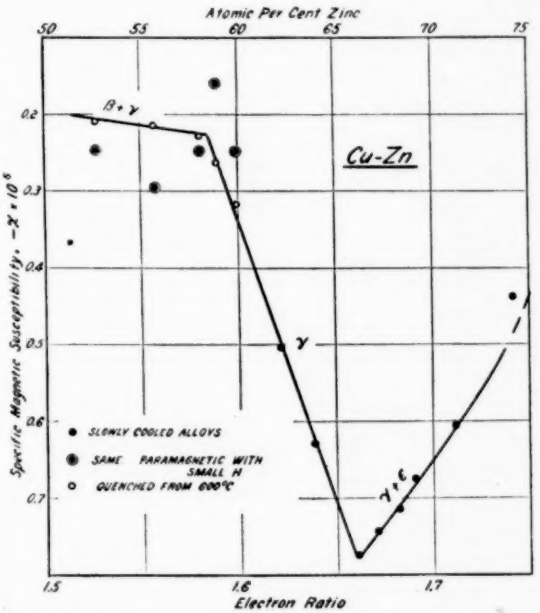

FIG. 2. The magnetic susceptibility of the gamma-phase in the copper-zinc system.

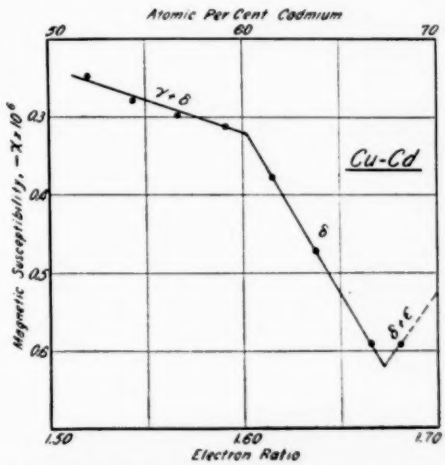

FIG. 3. Magnetic susceptibility of the delta-phase (gamma-brass structure) in the copper-cadmium system.

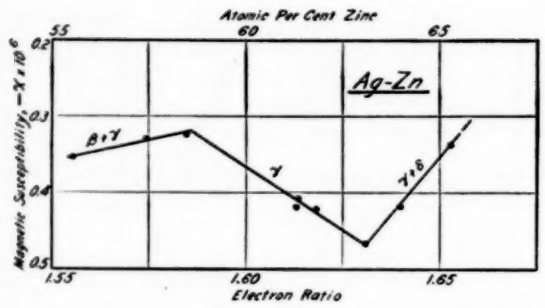

FIG. 4. Magnetic susceptibility of the gamma-phase in the silver-zinc system.

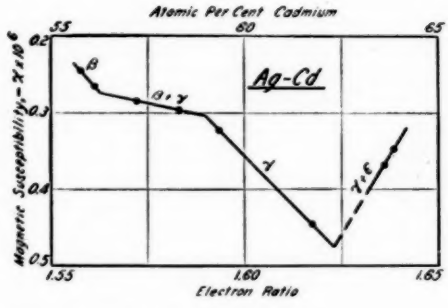

FIG. 5. Magnetic susceptibility of the gamma-phase in the silver-cadmium system.

TABLE VI. *"Gamma"-phase concentration limits.*

System	Atomic Percent Zinc or Cadmium From Figs. 2–6	From Literature	Authority
CuZn	58.4–66.0	59.5–67.7 (380°)	Owen and Pickup[17]
		57.8–67.1 (400°)	Bauer and Hansen[18]
CuCd (δ-phase)	60.1–67.2	57.4–63.9 (375°)	Jenkins and Hanson[19]
AgZn	58.7–63.2	57.5–63.1 (380°)	Owen and Pickup[20]
AgCd	59.0–62.3	57.6–61.5 (450°)	Durrant[21]

partial transformation might easily occur that would be undetected by any physical measurements. Susceptibility measurements actually made at high temperature, would provide an ideal method for the study of metallic equilibria and transformations.

It was unfortunately not possible to determine the electrical conductivity of the alloys used for the magnetic measurements. The results of Puschin and Rjaschsky[15] and Richards and Evans[16] on the copper-zinc and copper-cadmium alloys, respectively, show, as would be expected, that both the conductivity and temperature coefficient increase with increasing electron ratio.

[15] N. Puschin and W. Rjaschsky, Zeits. f. anorg. Chemie **82**, 50 (1913).
[16] W. Richards and E. S. Evans, Phil. Mag. **13**, 201 (1932).

ACKNOWLEDGMENTS

The author wishes to express his thanks particularly to Dr. R. S. Hutton, Goldsmith Professor of Metallurgy at the University of Cambridge, in whose laboratory this work was done, for his frequent help and encouragement.

The Ag-Cd alloys were remelted from ingots kindly provided by Dr. P. J. Durrant.

[17] E. A. Owen and L. Pickup, Proc. Roy. Soc. **A140**, 179 (1933).
[18] O. Bauer and M. Hansen, *Der Aufbau der CuZn legierungen*, Berlin (1927).
[19] C. H. M. Jenkins and D. Hanson, J. Inst. Metals **31**, 257 (1924).
[20] E. A. Owen and L. Pickup, Proc. Roy. Soc. **A140**, 344 (1933).
[21] P. J. Durrant, J. Inst. Metals **56**, 1935 (Advance Copy).